Modeling Of Two Electrophoretic Separation Techniques And Factors Affecting Mobility Measurement And Resolution.

MODELING OF TWO ELECTROPHORETIC SEPARATION TECHNIQUES AND FACTORS AFFECTING MOBILITY MEASUREMENT AND RESOLUTION

by

Paul Henry Krumrine III

A Dissertation

Presented to the Graduate Committee

of Lehigh University

in Candidacy for the Degree of

Doctor of Philosophy

in

Chemical Engineering

Lehigh University

1978

Approved and recommended for acceptance as a dissertation in partial fulfillment of the requirements for the degree of Doctor of Philosophy

July 1, 1978
(date)

F. J. Micale
Professor in Charge

Accepted _____
(date)

Special committee directing
the doctoral work of
Paul H. Krumrine III

F. J. Micale
Dr. F. J. Micale, Chairman

Mohamed S. El-Aasser
Dr. Mohamed S. El-Aasser

Gary Poehlein
Dr. Gary W. Poehlein

John W. Vanderhoff
Dr. John W. Vanderhoff

Leonard A. Wenzel
Dr. Leonard A. Wenzel

ACKNOWLEDGEMENTS

The author would like to express special thanks to Professor Fortunato J. Micale for his patient help and advice during the course of this research. Also, thanks are due to Dr. John W. Vanderhoff for the technical knowledge and advice provided, and to Dr. Mohamed S. El-Aasser, Dr. Gary W. Poehlein, and Dr. Leonard A. Wenzel for serving on the special committee. Thanks also to the many others on the Sinclair Laboratory staff who assisted with various details of this work.

Grateful acknowledgement is made to the National Aeronautics and Space Administration and the Emulsion Polymers Institute for financial support of this research.

Also, special thanks are due to Susie who assisted in the typing and correcting of this thesis, and to the author's parents whose moral and material support over many years, has made all this possible.

TABLE OF CONTENTS

LIST OF TABLES

LIST OF FIGURES

LIST OF SYMBOLS

a	FFE channel Radius (cm)
a_c	particle radius (cm)
A	cross-sectional area of CPE channel (cm^2)
A_h	Hamaker constant (ergs)
d	half of the channel thickness (cm)
e	electronic charge (coulombs)
E	applied potential gradient (volts/cm)
F	curtain flow rate (cm^3/min)
H	electrode length (cm)
H_o	surface-to-surface distance between particles (cm)
k	Boltzmann's constant (ergs/^oK)
n	ion concentration (ions/cm^3)
r	radial distance in FFE channel (cm)
r_c	center-to-center distance of two particles (cm)
R	ratio of sample width to channel width
R_w	ratio of dielectric constants and viscosities as a function of temperature at the wall
R_z	ratio of dielectric constants and viscosities as a function of temperature at position z
s	ratio of r_c/a_c
t	time (sec)
T	temperature (^oK)
U_e	electrophoretic mobility (μm cm/volt sec)
U_{os}	electroosmotic mobility (μm cm/volt sec)
U_{osr}	electroosmotic mobility of rear wall (μm cm/volt sec)
U_{osf}	electroosmotic mobility of front wall (μm cm/volt sec)
v	valency
v_o	maximum velocity of electrolyte in CPE channel (cm/sec)
V_A	attractive energy of interaction (ergs)
V_R	repulsive energy of interaction (ergs)
x	displacement distance (μm)
z	distance from midplane in CPE channel (cm)

β	complex function of τ and s
ϵ	dielectric constant
μ	viscosity (gm/cm sec)
σ	surface charge density ($\mu F/cm^2$)
π	pi
τ	product of κa_c
ψ	surface potential (mV)
θ	thickness of sample plug or band (cm)
κ	reciprocal double layer thickness (cm^{-1})

Abstract

Electrophoretic separation techniques such as static free-fluid electrophoresis and continuous particle electrophoresis offer the means whereby substantial quantities of collected fractions may be obtained. Previously, most electrophoresis techniques were used mainly for qualitative analysis and for categorizing various fractions. However, now that substantial quantities of the fractions are available, more detailed analyses may be carried out on the fractions; and the possibilities exist for production on a small scale of very expensive, hard-to-obtain chemicals such as certain biological enzymes or antibodies.

The most recent free-fluid electrophoresis experiments carried out by NASA consisted of separations of fixed red blood cells, viable kidney cells, and B and T lymphocytes. An analysis of the photographic record of the separations demonstrated that free-fluid electrophoresis can successfully fractionate a sample according to mobility without the distorting effect of electroosmosis.

Continuous particle electrophoresis, although being a difficult machine to operate at times, can be a rather quick means of obtaining a lot of information about a sample. In addition to the collected fractions, a properly equipped CPE can provide information on absolute particle mobilities, particle-particle interactions, and surfactant addition. This type of information can be extracted from recorded traces of the band shape and positions.

Computer modeling of these two systems with the present theory

and a few modifications to include temperature effects, has been very important in defining how the many parameters interact to produce a desired separation. Through the use of these models, the optimum conditions may be chosen to maximize resolution and throughput. Accurate comparisons and predictions may also be made between theory and experimental results.

Chapter I

Introduction

Electrophoresis may generally be considered as the movement of charged species in an electric field. This concept has found many applications as an analytical tool in determining surface charge, zeta potential, and for identifying the various components in a mixture of species. The many variations include gel electrophoresis, paper electrophoresis, microelectrophoresis, continuous electrophoresis, isotacho electrophoresis, free-fluid electrophoresis, as well as other techniques. While these forms of electrophoresis have mainly been used in the past as analytical and preparative tools, their preparative capabilities have been limited in terms of resolution and sample size. More recent interest has been directed towards expanding these separation techniques especially continuous, free-fluid, and isotacho electrophoresis techniques, for processing larger quantities of sample.

Space, with its microgravity environment, has provided the means whereby larger amounts of sample and better resolution may be obtained. Because of the microgravity environment, higher voltages may be applied without the resulting convective mixing which results from the Joule heating and density gradients within the fluid. This results in a much more stable and predictable flow profile in the various electrophoresis techniques and much better resolution with higher sample throughput. For these reasons NASA has been active in electrophoretic separation techniques in space, with the hope that these techniques

may form the basis for budding industries in space which can accomplish separations that earth-based industries cannot achieve.

Much of the effort in this program has been directed towards improved separation capability both in free-fluid (static) electrophoresis "FFE" and continuous particle electrophoresis "CPE". Free-fluid electrophoresis development has entailed four areas, namely (1) coating development, (2) development of the generalized theory, (3) computer modeling and (4) analysis of the Apollo-Soyuz Test Project (ASTP) photographic record. Both the coating and theoretical developments have been covered in previous work[1]. The coating work has led to a methylcellulose coating on a glass surface bound by an epoxy-silane intermediate, and the theoretical modeling has shown the migration distance to be a strong function of electrophoretic and electroosmotic mobility, radial position, and temperature. The computer modeling and final analysis, which will be presented as part of this work, will show that the coating and particles behaved as predicted.

Continuous particle electrophoresis development has been in three principle areas, namely (1) computer modeling, (2) absolute mobility measurement, and (3) particle-particle interactions. The computer modeling has taken Strickler's equations[2], applying them to species with a specified mobility distribution, and, through the power of the computer, has taken into account the effect of the many parameters. This has allowed accurate theoretical comparisons to be made to experimental results and analysis of specific parameter effects. Absolute mobility measurement is possible by injecting a marker

species of known mobility which allows separation distances to be converted into mobility values. This can be a powerful technique for particles which do not lend themselves readily to micro-electrophoresis techniques due to particle size or concentration. Lastly, particle-particle interactions, which are critical for predicting colloid stability, are difficult to measure experimentally. It is felt that the CPE can be sensitive enough to show the interaction due to double layer and ionic concentration effects as one band of particles moves through a second band. The double layer theory of Deryaguin, Landau, Verwey, and Overbeek (DLVO)[3,4,5] has been used to analyze and predict these interactions. As an offshoot of this area, particle concentration and surfactant adsorption have also been investigated to some degree.

Polystyrene latexes, being hard round spheres, lend themselves well as an ideal colloid in this type of work. Using ionic strengths in the range from 10^{-2} to 10^{-4} allows the polystyrene latexes to fall in a favorable κa range[6,7] where mobility is a strong function of size. Therefore, a fractionation can be realized for these latexes as a function of size. Since these latexes are available in monodisperse form with quite narrow size distributions at a large number of sizes, they are ideal for this type of study. Also the surface of the particles may be altered with respect to surface charge densities or surface groups so that polystyrene latexes as a whole offer a wide range of possibilities for study and separation. Finally, due to the large surface area of these latexes, they can be a good indicator of

the stability of a coating since any adsorption onto the latex particle will alter the mobility.

Chapter II

Background and Previous Work

Electrophoresis in space is not new. Experiments have been going on since the days of the Apollo missions. The first experiment, consisting of a free-fluid separation of a red and blue dye, was carried out on the Apollo 14 flight[8]. The separation gave satisfactory results, demonstrating that the boundary dividing the two dyes was sharper than possible on earth. The hardware was simply a lexan channel with an electrolyte circulation system at each end separated from the channel by a semi-permeable membrane. Electrolysis products could be easily removed in this manner.

The next experiment in space was on Apollo 16, where two monodisperse polystyrene latexes were the species of interest[9,10]. For this experiment, there were three electrophoresis columns similar to the Apollo 14 experiment with a removable non-permeable membrane which maintained the latex at one end until the start of the experiment. The two latexes were a 0.8 and 0.2 micron monodisperse latex with the 0.8 micron latex having the higher mobility. The three channels contained a mixture of the two and each latex separately. Data was recorded photographically by a camera which took pictures at twenty second intervals for about five minutes. The pictures indicated well developed parabolic cones showing no detectable separations apparent until an analysis was done with color contour densitometry. Actually some separation did occur but the resolution was poor due to

the overlapping cones. The elongated parabolic cones can be predicted by theory from the high value of electroosmosis for uncoated Lexan channels. Similar experiments were performed on earth resulting in no separation due to convective mixing of the fluid. Reducing the electric field strength allows some comparison over a longer time span, but under these conditions, Brownian diffusion makes the bands less sharp. Therefore, a definite advantage may be realized by performing this type of experiment in space. Also, it was apparent that the electroosmosis must be reduced or counteracted to improve the resolution.

These two experiments then set the stage for the ASTP experiment in the summer of 1975, which included an electrophoretic separation experiment of biological cells (MA-011).[11,12] The nature of these experiments was to determine if biological separations could be carried out in space under microgravity conditions and with better resolution than obtainable on earth. The experiments consisted of a series of static and isotacho electrophoresis experiments in which mixtures of aldehyde-fixed red blood cells, B and T lymphocytes, and urokinase-producing kidney cells were separated. The separation results of the aldehyde-fixed rabbit, human and horse red blood cells, which were taken in the form of photographs at three minute intervals in columns one and five, and from sample collection by slicing techniques, demonstrated the success of the experiments.

Lehigh University first became involved in this project through the analysis of the Apollo 16 results, then later through the develop-

ment of low electroosmotic mobility coatings under NASA contract NAS8-28654. The development of a low electroosmotic mobility coating greatly improved the resolution of the electrophoretic separations. A complete description of the coating development and theory may be found in previous work[1,11,13] so only a brief discussion will follow. The coating for glass channels consisted of a precoat of Dow Corning Z-6040, γ-glycidoxypropyltrimethoxysilane, which bound the methylcellulose to the glass surface. The surface was then repeatedly washed or rinsed to remove unbound methylcellulose. Such a coating generally reduced the value of electroosmosis from values of -4.00 to -0.20 μm cm/volt sec. This reduction in electroosmosis results in sample migration by bands rather than elongated cones which cannot be resolved. Therefore, this coating played a significant role in improving the results and resolution for the ASTP electrophoresis experiments.

Also under the coating development work, other substrates such as Plexiglas and Lexan were investigated. Coatings for both reduction of electroosmosis and water permeability were developed. Low water permeability was achieved with Saran copolymer coatings.

Another type of electrophoresis carried out on the ASTP mission was a continuous electrophoresis experiment which was provided by a group of West Germans headed by Hannig[14]. Continuous particle electrophoresis, sometimes referred to as continuous flow electrophoresis, has been developed over the past fifteen years primarily by two independent investigators, Hannig[15-18] and Strickler[2,19-22]. Strickler has been instrumental in developing the basic theory and a commercial

instrument while at Beckman Instruments. However, these instruments are no longer in production. During this time, the CPE has been used primarily as a preparative method for the separation of biological materials[15,16,19]. The Beckman CPE has also been investigated as a method for the separation of latex particles according to size[21] by Vanderhoff and McCann at Dow. Most recently, NASA has been looking at continuous particle electrophoresis as a possible space manufacturing project which might be scaled up for production in space.

Chapter III

Free-Fluid Electrophoresis on the ASTP Flight

The Apollo-Soyuz Test Project (ASTP) flight occurred in July of 1975 and carried on board a series of electrophoresis experiments designed to demonstrate the feasibility and advantages of electrophoresis in space. Of particular interest, is the free-fluid electrophoresis separation of a mixture of fixed red blood cells. In addition to the pre-flight development of suitable low-electroosmotic mobility coatings, a post-flight analysis of the actual flight photographs was contracted at the request of Dr. John Vanderhoff and Dr. Fortunato Micale. The analysis consists of a computer model of theoretical equations and parameters which is compared to the data from the photographs taken at three minute intervals. This type of analysis demonstrates the success of the low-electroosmotic mobility coating as well as the effect of the important parameters and how to best improve resolution and sample quantity. Also, it shows that the theory does correlate well with the experimental results.

A. Experimental

Low-electroosmotic mobility coating development has led to a two-stage coating of Dow Corning Z-6040, γ-glycidoxypropyltrimethoxysilane followed by a methylcellulose coating of molecular weight 110,000. The exact details of the coating procedure are documented in earlier work[1,13]. This was followed with a three-day rinse cycle with distilled water to remove unbound methylcellulose. All measurements of

electrophoretic and electroosmotic mobilities were performed in an A-1 buffer which was also used in the ASTP flight experiment. The A-1 buffer composition is listed in Table 3.1.

Table 3.1

A-1 Buffer Composition

d-glucose (anhyd.)	40 gm/l.
Na_2HPO_4	0.25 gm/l.
KH_2PO_4	0.05 gm/l.
NaCl	0.375 gm/l.
$Na_2EDTA \cdot 2H_2O$	0.125 gm/l.
glycerol	38 ml/l.

Many species of fixed red blood cells were considered as candidates for the space experiment. Among these were chicken, dog, horse, human, turkey, cow, pig and rabbit red blood cells fixed with both formaldehyde and glutaraldehyde solutions. The species finally chosen to give the broadest range of electrophoretic mobilities and the best chance of separating were horse, human, and rabbit fixed red blood cells. Mobility distributions were determined by microcapillary electrophoresis techniques and are shown for the three candidate species in Figure 3.1. Measurements were done by both Dr. Robert Knox of the University of Oregon [12] and ourselves and are displayed on the graphs in two forms. The data of Dr. Knox is represented in bar graph form and shows one hundred measurements per cell species with the area under each curve proportional to the relative concentrations of the space samples. Our data is presented in a smoothed form and shows one hundred fifty measurements per cell species. The measurements were performed in the A-1 buffer formulated for these experiments and agree well with respect to average mobility and range for each cell type.

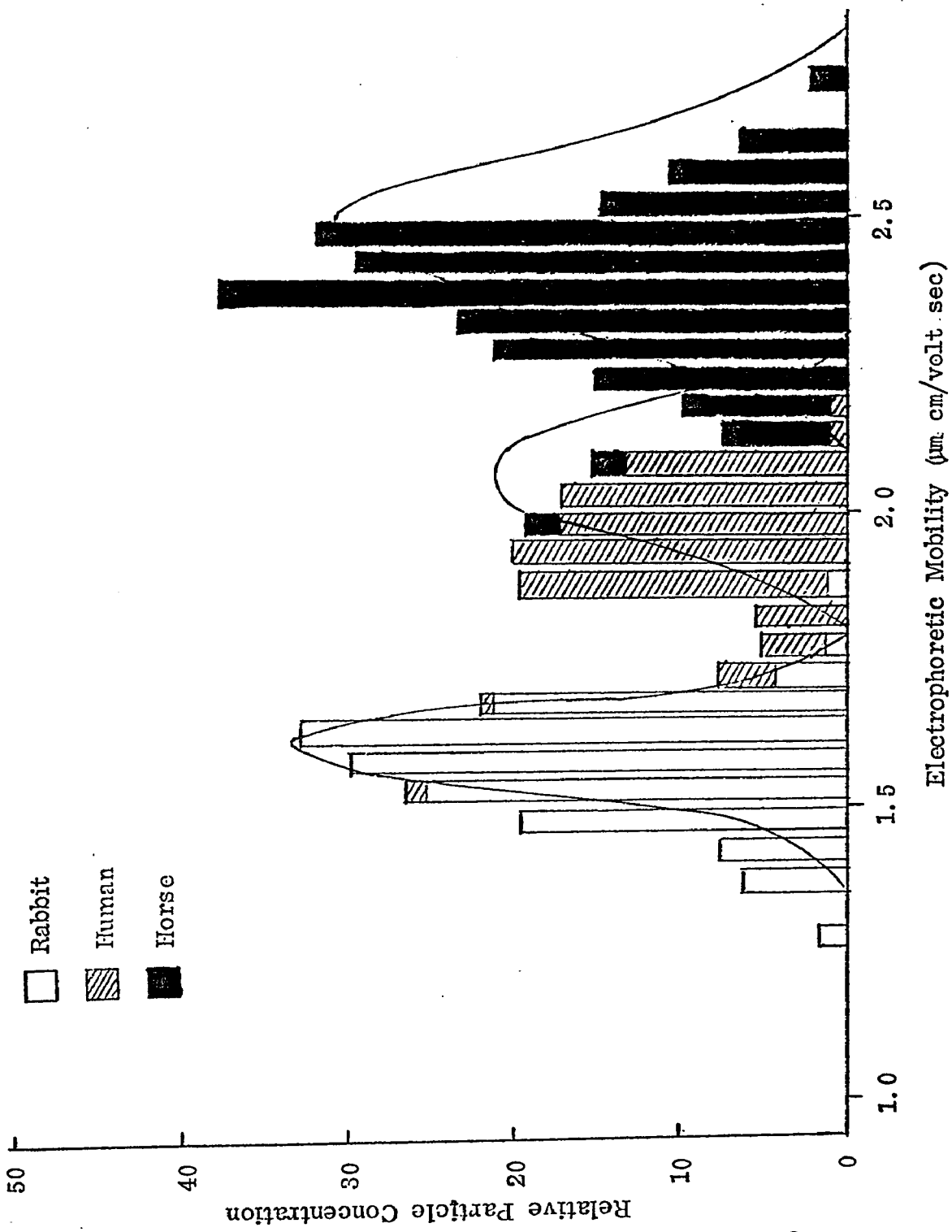

Figure 3.1. Electrophoretic Mobility Distributions of Rabbit, Human, and Horse Fixed Red Blood Cells.

The basic procedure for the electrophoresis experiments entailed the preparation of the columns and sample slides on earth. Each column was thoroughly cleaned then coated with the Z-6040+MC coating and rinsed for three days, after which they were separately sealed in plastic bags and stored for travel into space. The red blood cells were aldehyde-fixed and dispersed in A-1 buffer. A mixture of 32.8% rabbit, 21.6% human, and 45.6% horse cells, with a total concentration of 2.52×10^7 red blood cells per slide, was prepared by freezing the cells in a small disc shape, 0.478 centimeters in diameter by 0.312 centimeters thick. These sample discs were then placed in a freezer for storage until time for the experiment. All electrophoresis experiments were done in duplicate on two separate days. Columns preloaded with A-1 buffer were first placed in the apparatus. A sample disc was then removed and inserted into one end of the column and allowed to thaw after which the current was turned on. The samples were allowed to electrophorese for sixty minutes with photographs taken every three minutes to record data. After sixty minutes the current was turned off and the freezing cycle initiated. The frozen columns were then removed and placed in storage for return to earth for further analysis. Postflight analysis consisted of removing the frozen core from each column and slicing it into five millimeter sections which were analyzed for red blood cell count and mobility.

Two problems arose which marred the experiment and the collection of important data. First, column #5 probably developed an air bubble which migrated to the far electrode causing the voltage to sat-

urate. For this reason the voltage was turned off temporarily and restarted, but migration did not proceed down the entire column and some swirling was observed. The second problem occurred in the post-flight slicing of column #1. Upon removal of the core, it broke and only very large slices were able to be prepared, which reduced the amount of information obtainable. As luck would have it, this was the column that performed well in space and should have provided the best information. Therefore, only a fraction of the data was obtained from which conclusions could be drawn as to success. Further information and analysis was extracted from the photographs which will be covered in detail later in this chapter.

B. Theoretical Computer Modeling

A large amount of effort was expended in developing a theoretical computer model of a static electrophoresis column[1,11]. With such a model many parameters can be varied very easily to determine the specific effect of each one; this information can then lead to a better design or choice of operating conditions by which the resolution can be maximized. Also, before an experiment is performed the model can be used to predict separations, or afterwards, to compare results to theory. Therefore, the development of such a model is very useful as an analytical tool in studying static electrophoresis.

The model which has been used is rather simple in that it only accounts for effects on a macroscopic scale, ignoring particle interactions, diffusion, relaxation effects, and electric field distortion effects on individual particles. Of prime interest is the displace-

ment and distortion of each particle band and the relative particle concentration along the column axis. This information is best expressed with the equation:

$$x = \left[U_e E \left(\frac{\epsilon_2 \eta_{298}}{\eta_2 \epsilon_{298}} \right) - U_{os} E \left(\frac{\epsilon_1 \eta_{298}}{\eta_1 \epsilon_{298}} \right) \left(\frac{2r^2}{a^2} - 1 \right) \right] t \qquad (3.1)$$

where: x = displacement distance (μm)
U_e = electrophoretic mobility (μm cm/volt sec)
U_{os} = electroosmotic mobility (μm cm/volt sec)
r = radial distance from column center (cm)
a = channel radius (cm)
E = applied potential gradient (volts/cm)
t = time (seconds)
ϵ = dielectric constant of suspending fluid - f(T)
η = viscosity of suspending fluid - f(T)

and:

$$T_2 = T_3 - (T_3 - T_1)\, r^2/a^2 \qquad (3.2)$$

The subscripts 1, 2, and 3 refer to temperatures at the wall, at a distance $\underline{r}$, and at the center respectively, while 298 refers to the reference temperature in degrees K at which the electrophoretic and electroosmotic mobilities were measured. Equation 3.1 describes the displacement of a discrete element as a function of radial position in the channel. It also shows that the radial dependence can be reduced but not eliminated if the electroosmotic mobility is reduced to zero since the second term then becomes zero and the first term is a function of $\underline{r}$ through ϵ_2 and η_2. This implies that the band would migrate as if it were a plug with planar boundaries.

Equation 3.1 may be used to define the band shape and particle concentration for each species as a function of time. First, a least squares algorithm is used to fit a smoothed curve of up to a fifth order polynomial through a set of points from the bar graph mobility

distribution of each particle species. These computed mobility distributions are shown in Figure 3.2 where the area under the curves is proportional to the actual concentrations of cells. Next, the initial sample disc is divided into a series of small finite radial elements, and Equation 3.1 is applied to each element as a function of radial position. Each element is assumed to have the same mobility distribution which is used to determine the spread and concentration profile for each element. Then the contribution from each element is summed up to determine the total concentration profile for each species and the band as a whole. With a computer, this summing process can be done very quickly and accurately for a large number of elements so as to allow a very high degree of confidence in the results. This is essentially how the computerized model was constructed so as to allow determination of band displacement, shape, and concentration for species exhibiting a broad mobility distribution. It could also be used to determine where each mobility fraction from a bar graph should be found. A listing of the actual program may be found in Appendix A.

With the help of this program, it was possible to compare the theoretical resolution for a number of experimental conditions using the mobility distribution and relative concentration of the fixed red blood cells used for the space experiment where the location of the cells, from left to right, are always rabbit, human, and horse. Figures 3.3 through 3.6 show the predicted separations and the effects of four important parameters on the resolution. In each figure, one parameter is compared at three values maintaining all other conditions

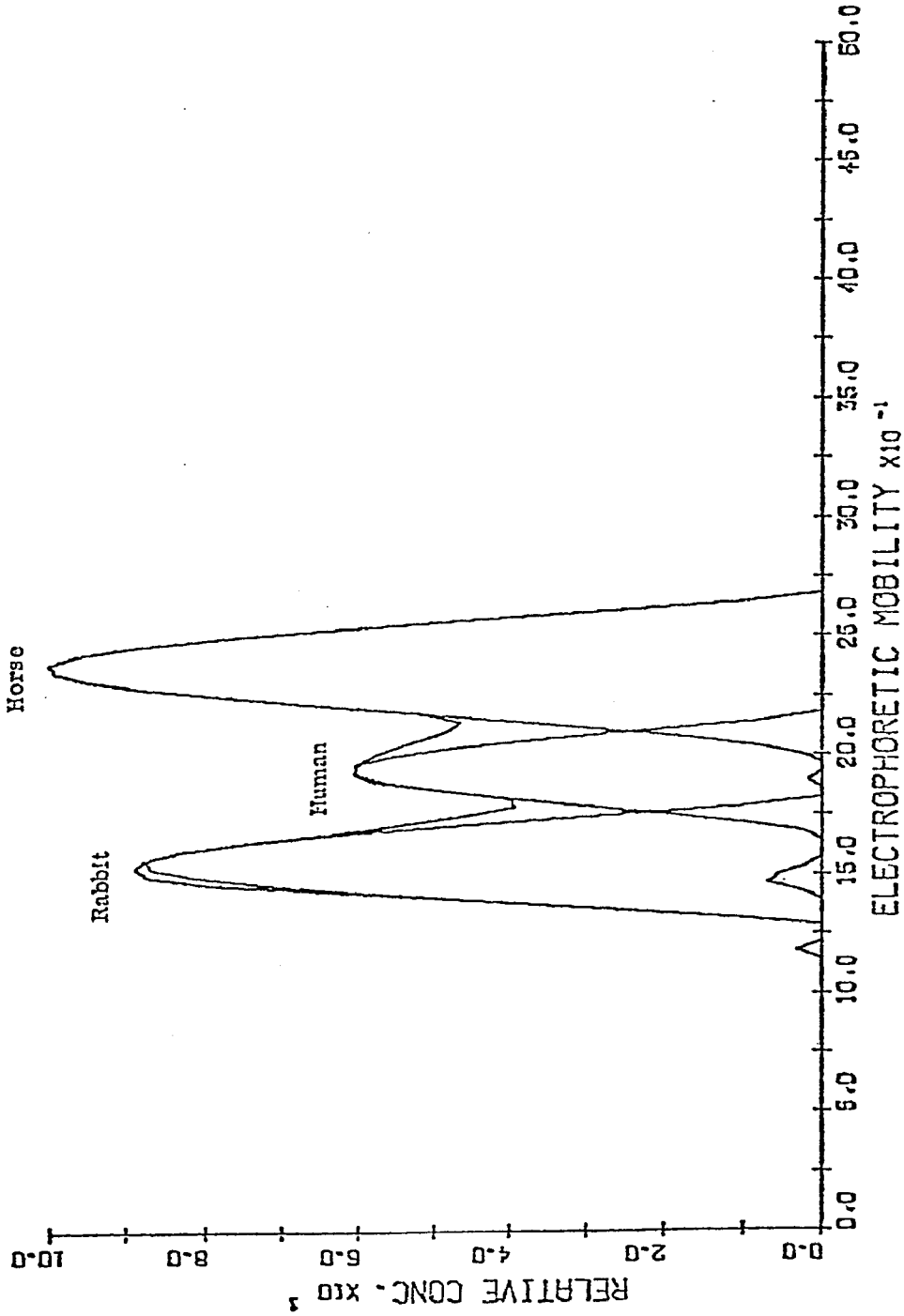

Figure 3.2. Computer Fitted and Smoothed Electrophoretic Mobility Distributions of Fixed Red Blood Cells.

constant, and the separation time is sixty minutes. The central figure in each case corresponds most closely to the actual experimental conditions used on ASTP and is, therefore, the same in the four figures. Figure 3.3 shows the effect of electroosmosis, U_{os}, on resolution for values of -0.40, -0.20, and 0.00 μm cm/volt second. It is readily apparent that this parameter can have a profound effect on the resolution, with best results expected for electroosmotic mobility values as close to zero as possible. It should be noted that even for a value of 0.00 μm cm/volt second there is still some curvature to the band boundaries and this results from the 2° C temperature gradient predicted from Joule heating in the channel. Temperature is important because both dielectric constant and viscosity are strong functions of temperature and vital in determining electrophoretic and electroosmotic mobility. Figure 3.4 shows the effect when this temperature gradient, ΔT, is the variable. The three cases correspond to gradients of 10°C, 2°C, and -6°C from channel center to channel wall. Obviously if it were possible to maintain the center at a cooler temperature than the walls, conditions would be improved. Such a condition is physically impossible for this system where Joule heating predominates. Figure 3.5 shows the effect of decreasing the sample plug radius in relation to the channel radius, $\underline{R}$, for values of 1.00, 0.75, and 0.50. Smaller values of this ratio can improve the resolution especially if U_{os} is high, but at the cost of less sample volume which might be more important. Another factor affecting the volume is the initial sample plug thickness, $\underline{\theta}$, and this result is shown in Figure 3.6. This

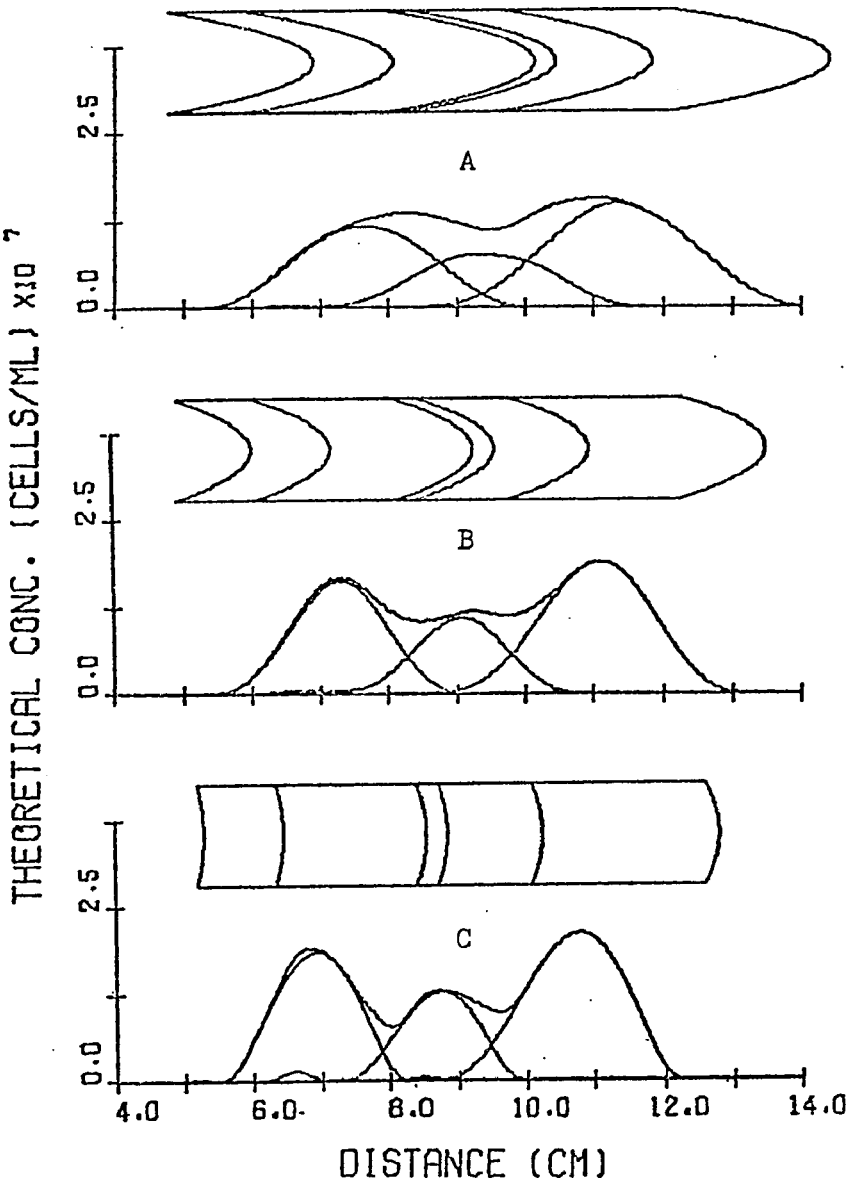

Figure 3.3. Computed Cell Displacement Showing the Effect of Electroosmosis on Cell Separation with $\Delta T = 2^{o}C$, R = 0.75 and θ = 0.3 cm.; A. U_{os} = -0.4 μm cm/volt sec., B. U_{os} = -0.2 μm cm/volt sec., and C. U_{os} = 0.0 μm cm/volt sec.

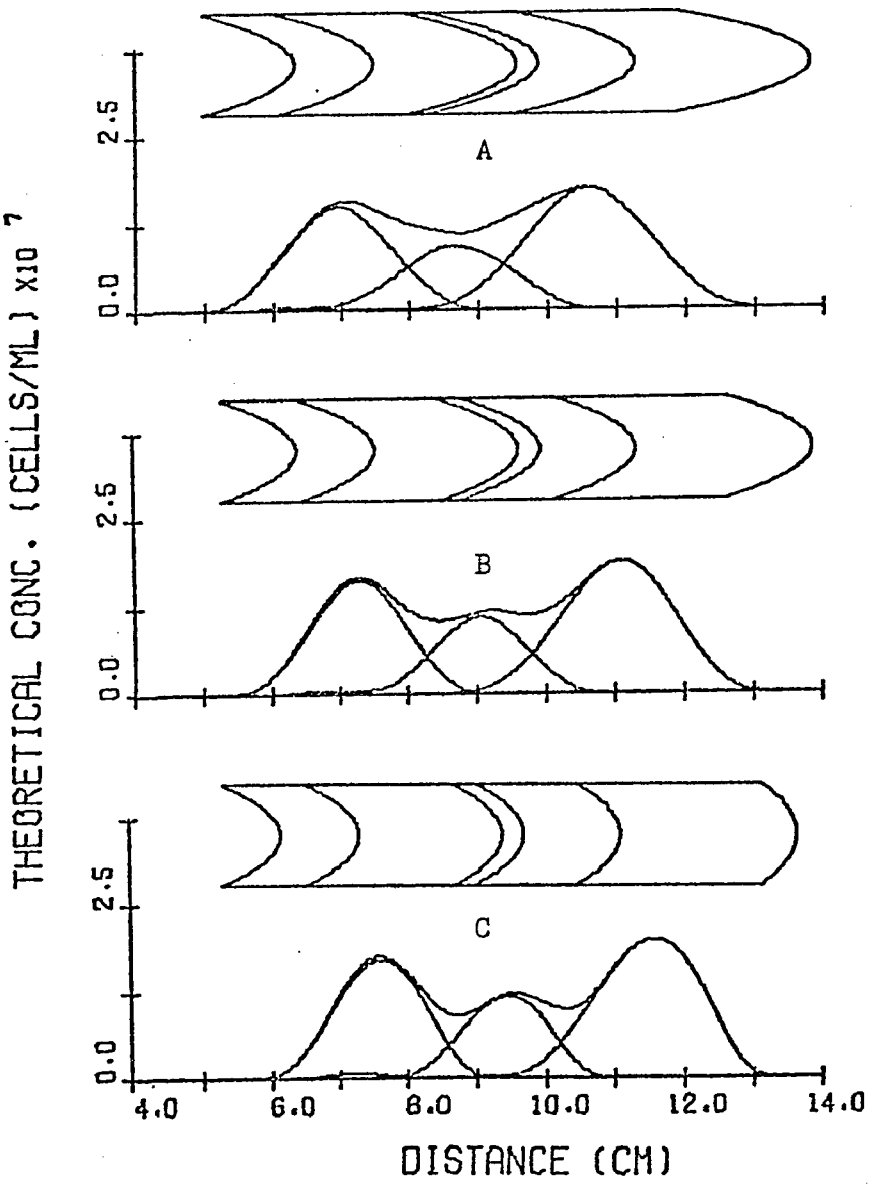

Figure 3.4. Computed Cell Displacement Showing the Effect of a Temperature Gradient, ΔT, on Cell Separation with U_{os} = -0.20 μm cm/volt sec., R = 0.75 and θ = 0.3 cm.; A. $\Delta T = 10^{\circ}C$, B. $\Delta T = 2^{\circ}C$, and C. $\Delta T = -6^{\circ}C$.

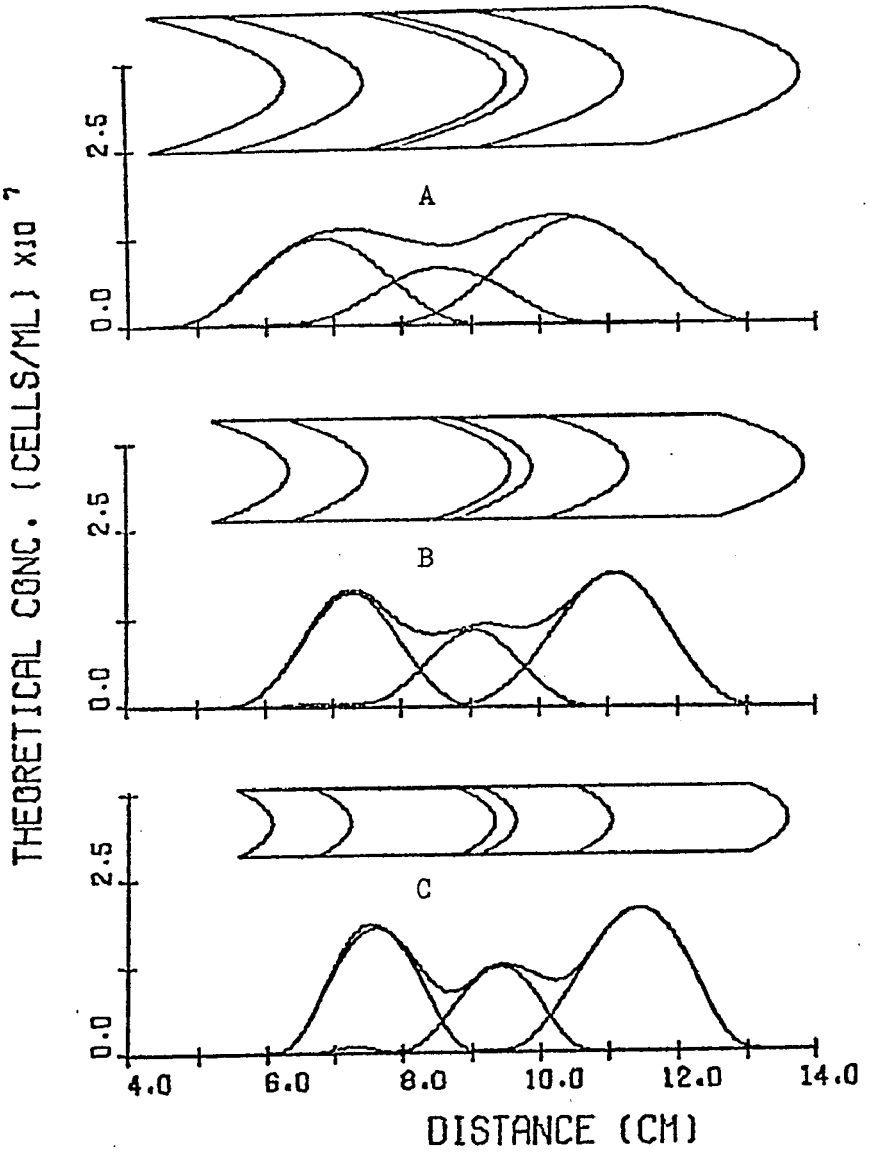

Figure 3.5. Computed Cell Displacement Showing the Effect of Ratio of Sample Plug Radius to Channel Radius, R, on Cell Separation with U_{os} = -0.2 μm cm/volt sec., $\Delta T = 2^{o}C$, and θ = 0.3 cm.; A. R = 1.0, B. R = 0.75, and C. R = 0.50.

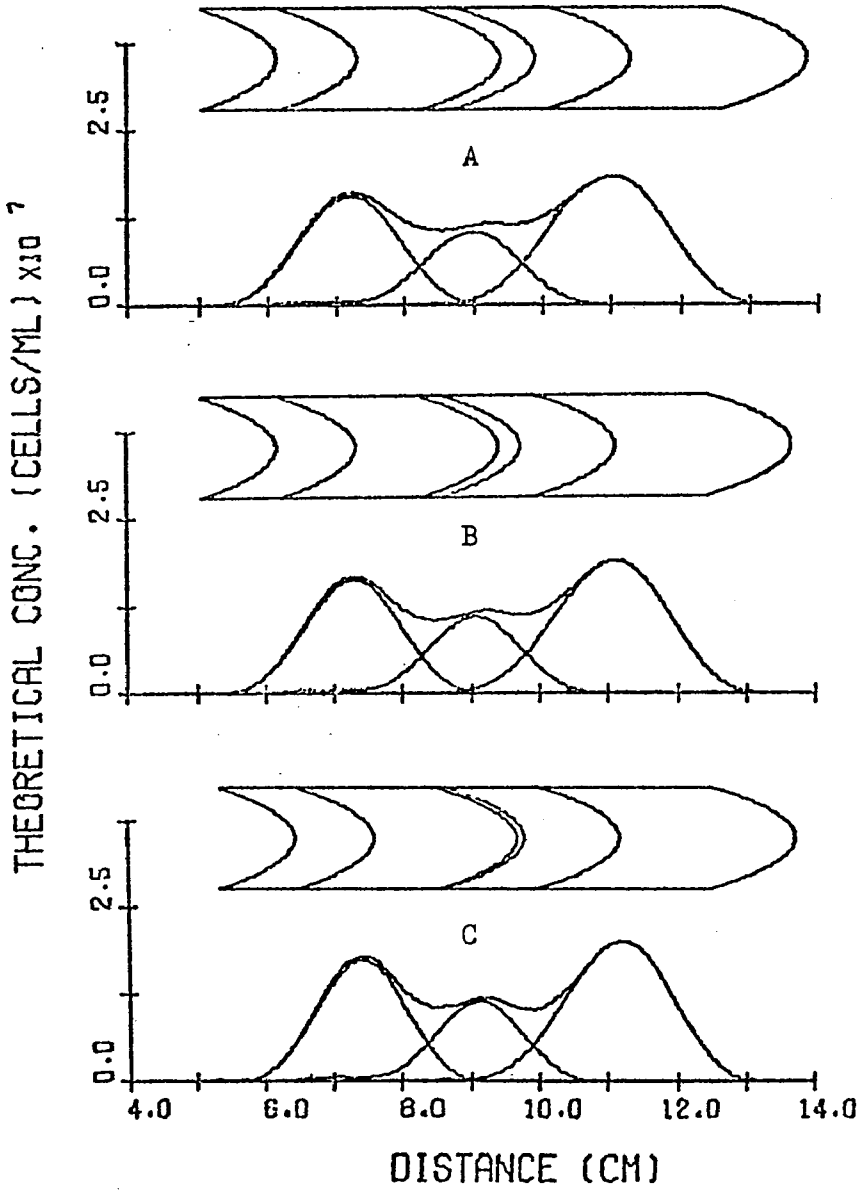

Figure 3.6. Computed Cell Displacement Showing the Effect of Sample Plug Thickness, θ, on Cell Separation with U_{os} = -0.2 μm cm/volt sec., $\Delta T = 2^{\circ}C$, and R = 0.75; A. θ = 0.5 cm., B. θ = 0.3 cm., and C. θ = 0.1 cm.

parameter, for values of 0.5, 0.3, and 0.1 centimeters, is found to have only a small effect on the resolution, but this is because the migration distance is large in relation to θ, making it negligible. For cases with a large migration distance, R could be reduced and θ increased to maintain the desired volume but with improved resolution. After all, volume is not important if the desired separation cannot be collected in resolved fractions. It should be noted that even under optimum conditions these particles could not be completely resolved into separate fractions because the mobility distributions overlap; however, they could be resolved according to their average mobilities.

C. Photographic Analysis

As mentioned before, photographs were taken at three-minute intervals, providing a pictorial account of the progress of the experiments. These photographs were able to provide valuable information as to the success of the low-electroosmotic coating, validity of the theory, and the results of the separation.

Initially only the second generation film was available for observation; therefore only information on the apparent band boundaries could be extracted by visual examination. Figures 3.7 and 3.8 show the discernible boundaries and displacements versus time for the two columns containing fixed red blood cells. Of course, the exactness of these measurements depends entirely on the photographic quality and the judgement of the observer, but they are representative of the separation that took place. Figure 3.7 shows the results from Col-

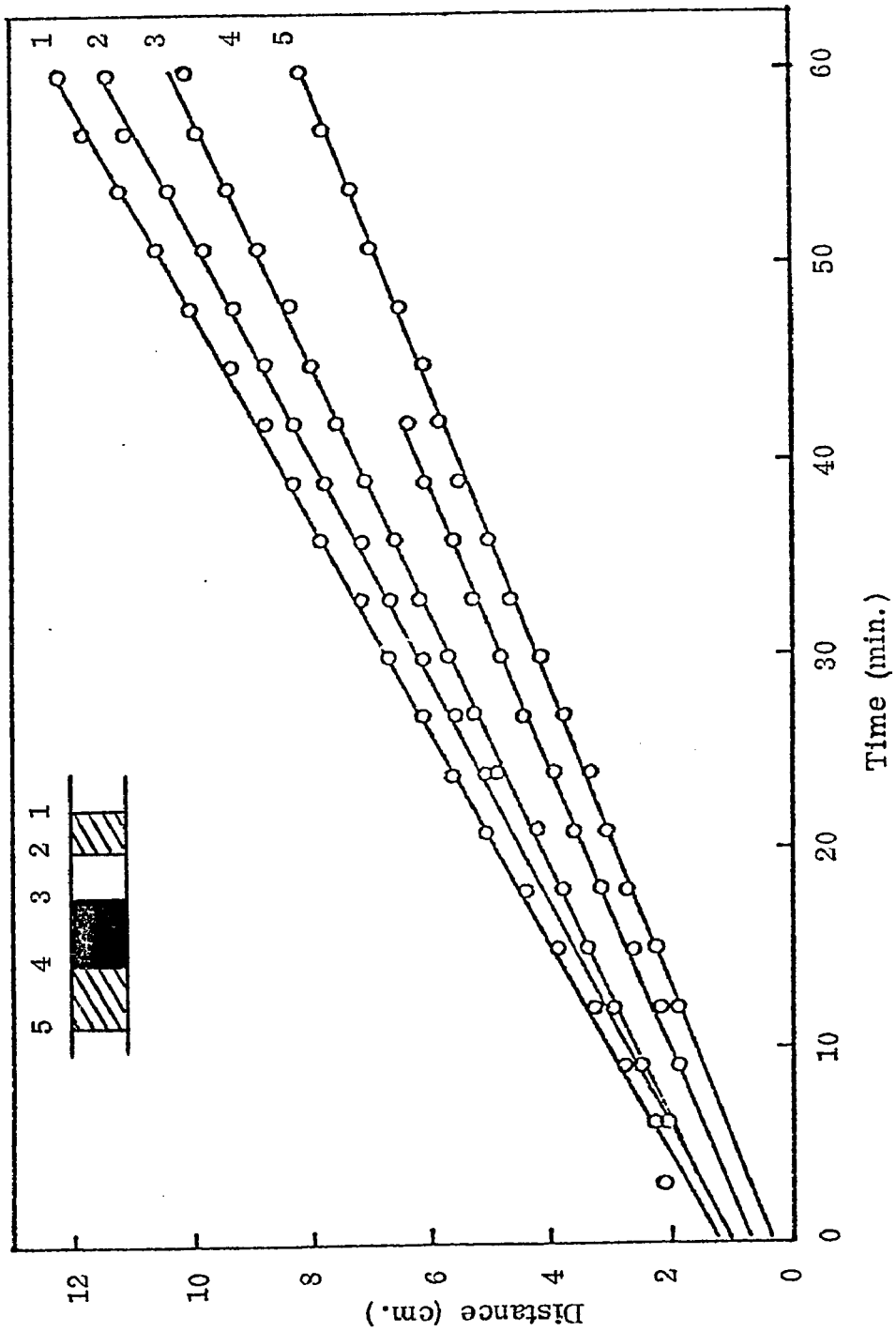

Figure 3.7. Band Displacement as a Function of Time in Column #1.

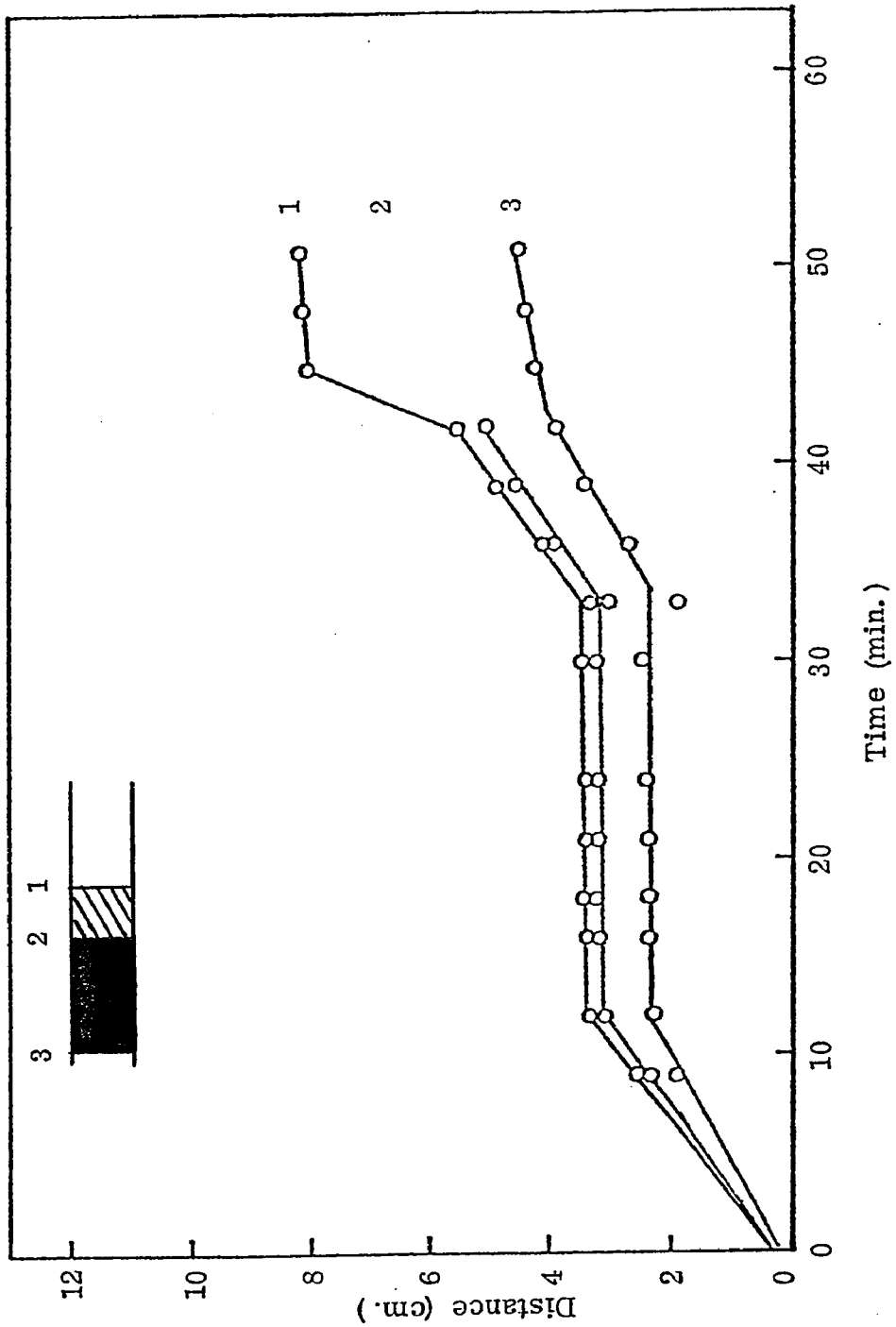

Figure 3.8. Band Displacement as a Function of Time in Column #5.

umn #1 in which two bands were clearly discernible as the experiment progressed. At first, only one band of a lighter and darker region followed by another lighter region was visible. Then, approximately twenty-five minutes into the experiment, the leading lighter region appeared to separate from the main portion as a separate band with apparently few fixed red blood cells in between. At about forty-two minutes, the darker and lighter regions of the second band were no longer discernible. This data shows that the migration of the band boundaries with respect to time proceeded at a linear rate which is as expected, and the rate corresponds to the mobility values that were determined for the fixed red blood cells and the electroosmosis with an applied gradient of 10.6 volts/centimeter. Also, the sharp planar boundaries attest to the low value of electroosmosis due to the methylcellulose coating. However, it seemed distressing that very few red blood cells could be detected in the region between the two bands when the mobility distributions of the three species clearly overlapped. It could be possible that the concentration was low enough that it would not appear on the second generation film.

Figure 3.8 shows the results from Column #5 which incurred technical problems when an air bubble resulting from a leak migrated to the far electrode and probably caused the voltage to saturate. Some information may still be obtained from the two regions in which the migration proceeded normally. As in Column #1, there was a lighter and darker region as the bands emerged from the Column end. Also the migration rate of the bands seemed to be very close to that in Column

#1 confirming those results.

In an effort to compare these photographic results to the theoretical concentration, the computer was supplied with the best known values for all the parameters and allowed to compute the expected concentration profile which was divided into four concentration regions. These results are shown in Figure 3.9 along with the experimental band appearances for Column #1. The experimental and theoretical concentrations are shown every six minutes versus migration distance. This shows that fixed red blood cells should have been observed over a much larger portion of the column and in between the two bands. However, the agreement is acceptable, assuming the concentration of cells was not sufficient to show up on the second generation film. There does seem to be some disagreement between experimental and theoretical results in the displacement of the second band. This could be explained if there was some clumping of the cells due to the freezing and thawing process on such a high concentration of fixed red blood cells.

More recently, micro-densitometer scans of the first generation film, showing much more detail, have been provided on request by NASA. The scans were taken by measuring the optical density of the separation column while traversing from one end of the column to the other end with a small orifice in the direction of the traverse. Figure 3.10 shows two graphs obtained by this technique. Figure 3.10A shows a reproduction of scans obtained from frame one and frame two; frame one is used as a base line with no cells yet present in the column. It

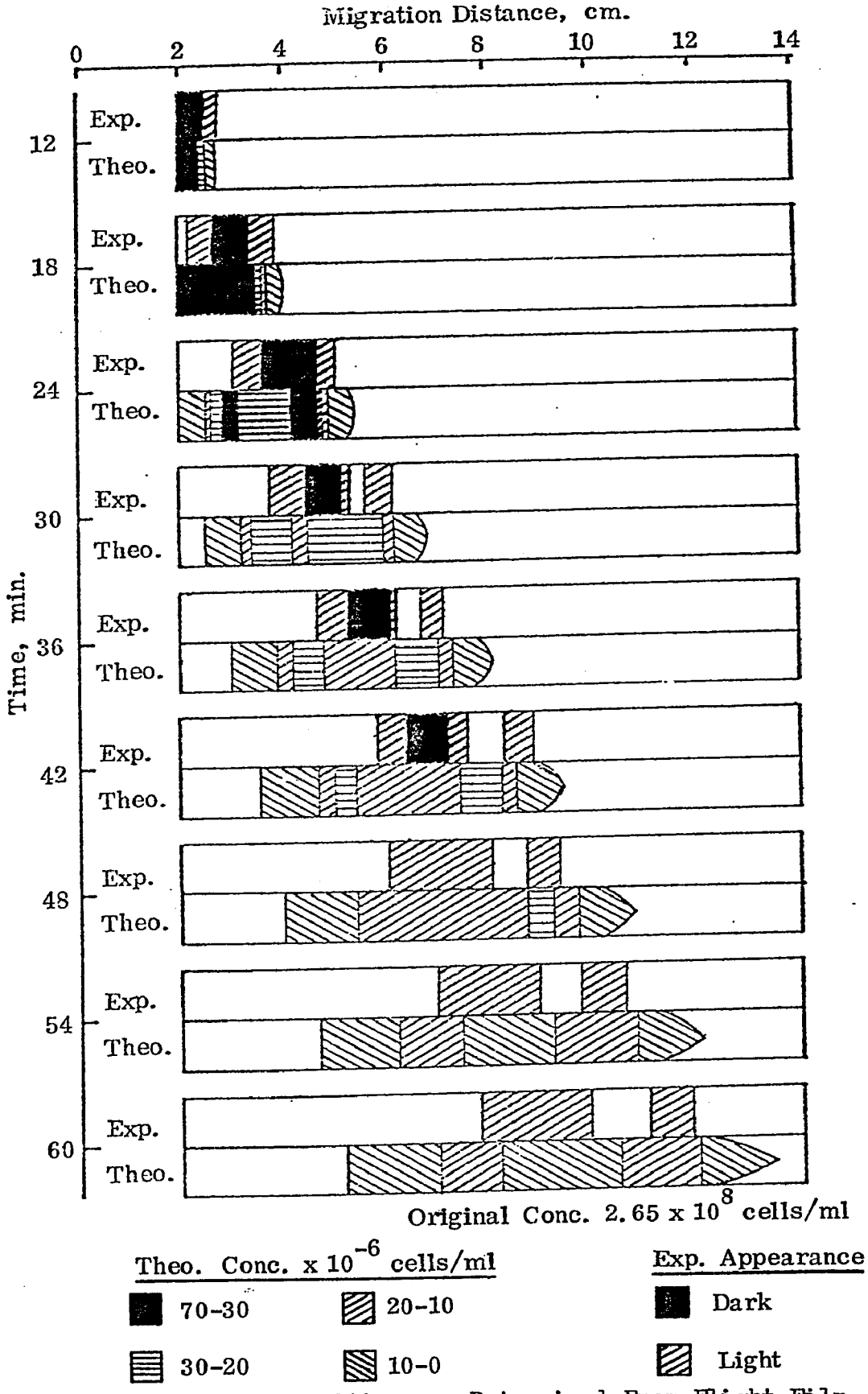

Figure 3.9. Band Positions as Determined From Flight Film and Theory.

should be noted that the two traces agree quite closely with only a small deviation in the background at a distance of two centimeters. This is because the cells were only beginning to emerge in frame two. The large deflection at about 7.5 centimeters is from the thermocouple present in the column at that position for monitoring temperature. Figure 3.10B shows two curves, one of the subtracted difference between the micro-densitometer scans corresponding to the left hand axis and the second of the computed cell concentration as evaluated from the theoretical model corresponding to the right hand axis. The theoretical model for these computations assumes an applied potential gradient of 10.6 volt/second and U_{os} of -0.2 μm cm/volt second. Both the micro-densitometer and theoretical curves are generated by the computer and the areas under each curve equated for comparison. Since the cells have not totally emerged from the left side, this has resulted in an amplification of the background noise.

Figures 3.11 through 3.15 show the results at six minute intervals or every second frame from four through twenty-two. The theoretical results indicate the presence of two peaks as early as twelve minutes into the separation whereas the micro-densitometer results show the initiation of two peaks in frame eight or twenty-four minutes into the separation. The breaking up of the band into two bands by visual observation of the flight film, Figure 3.9, occurs after thirty minutes of separation, frame ten. The micro-densitometer results, however, show that although the advancing peak increases in definition, it does not split off from the main band, Figures 3.12

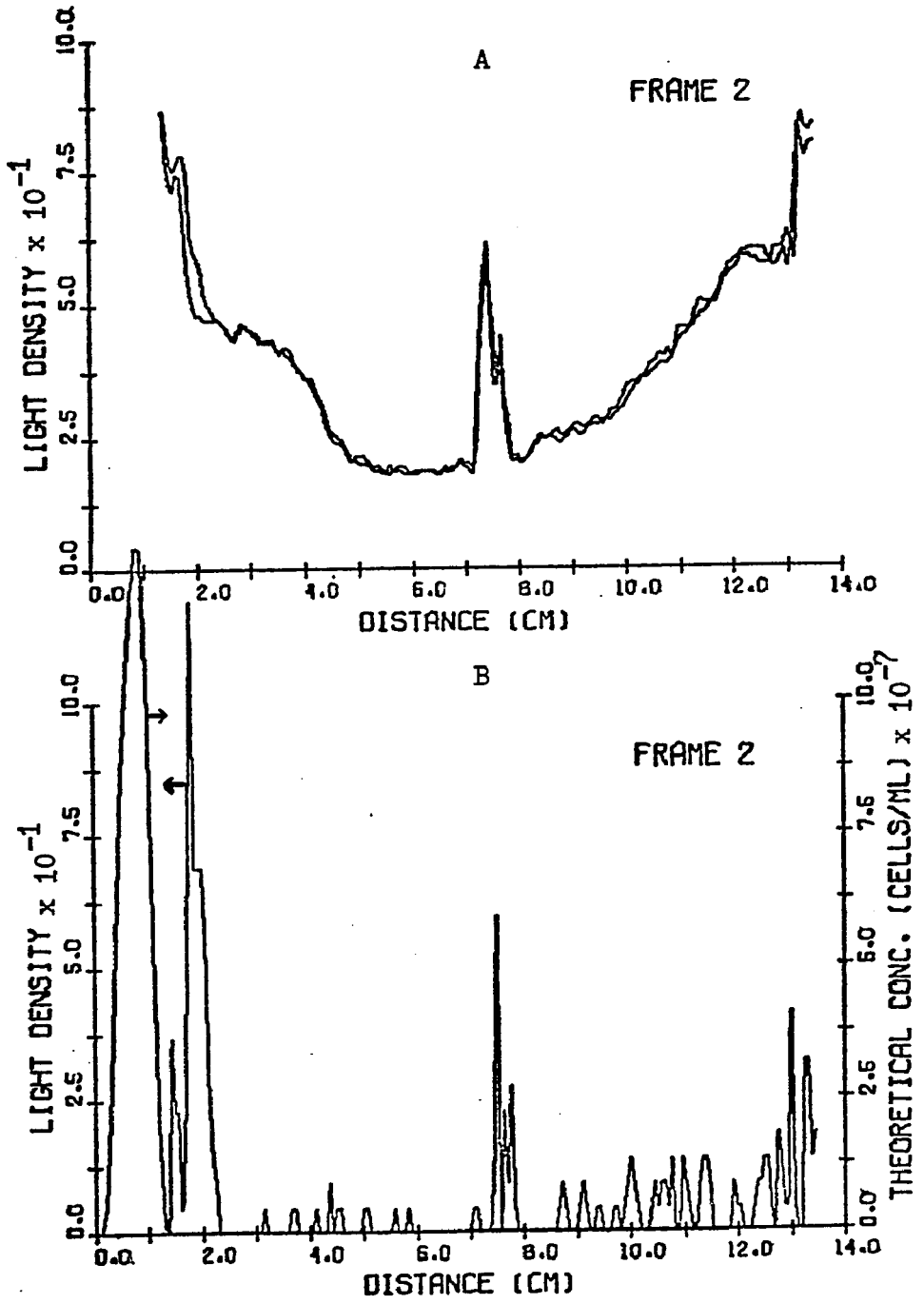

Figure 3.10. A. Raw Data Micro-densitometer Scan for Frames 1 and 2. B. Net Micro-densitometer Scan and Computed Displacement.

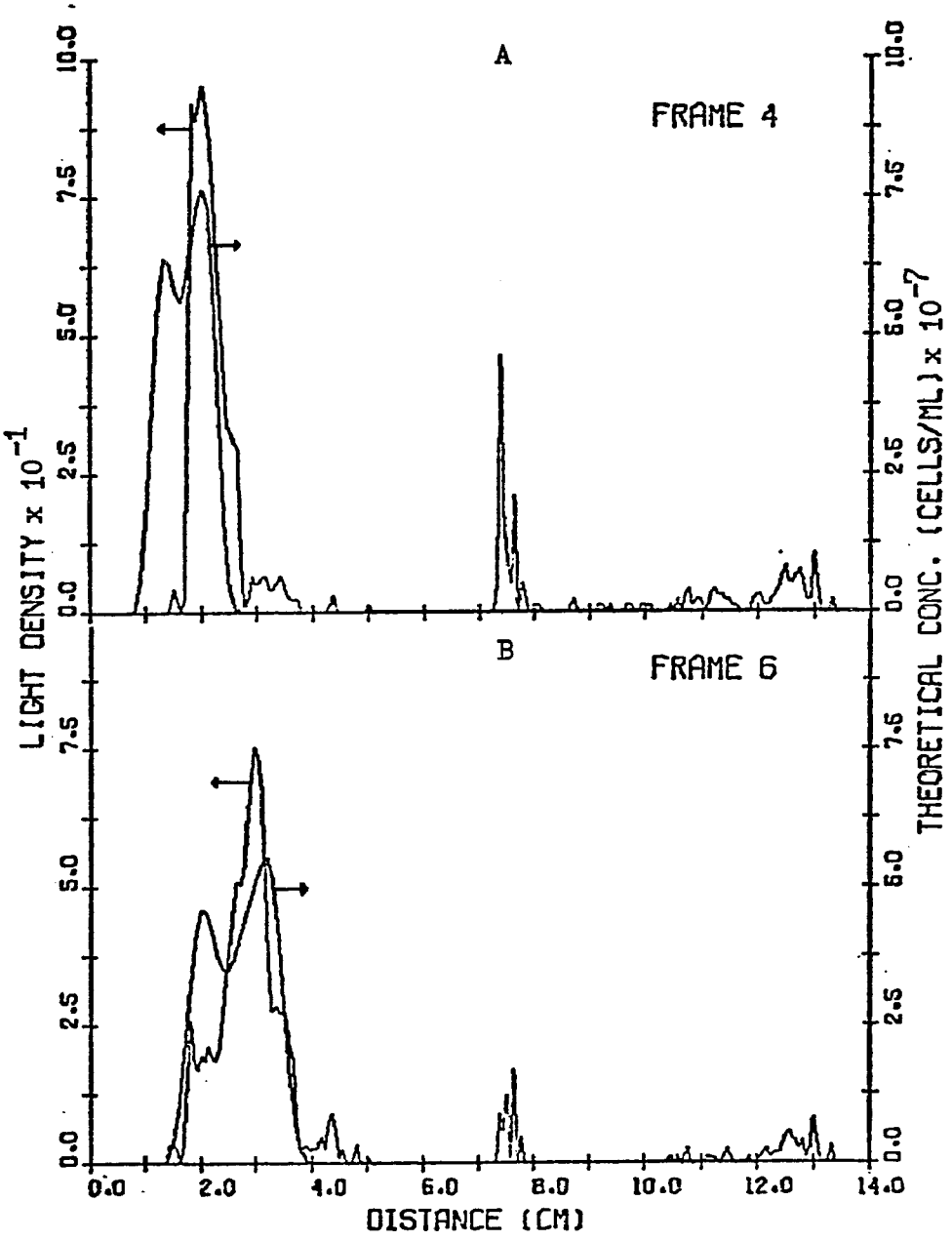

Figure 3.11. A. Frame 4, 12 Minutes Separation; B. Frame 6, 18 Minutes Separation.

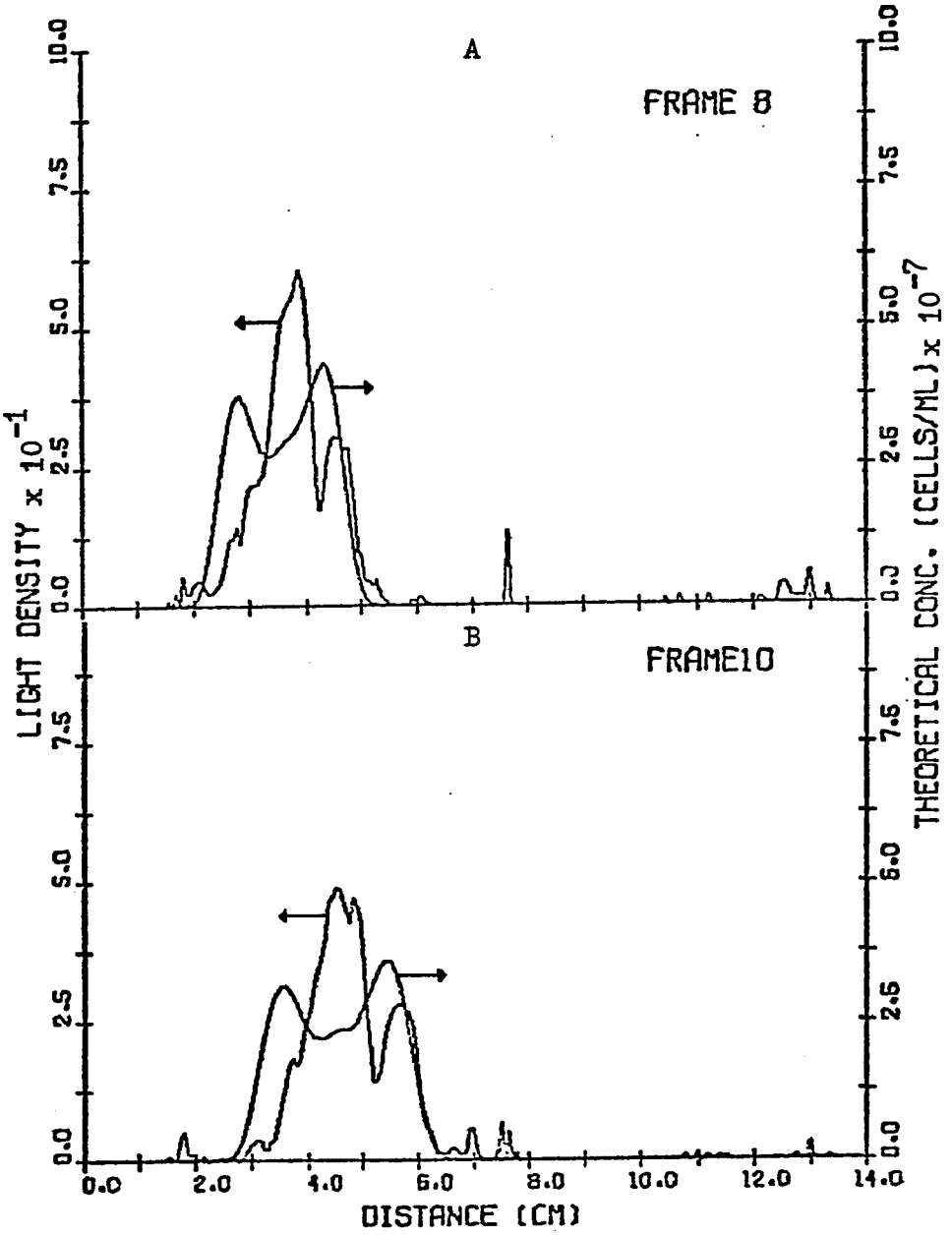

Figure 3.12. A. Frame 8, 24 Minutes Separation; B. Frame 10, 30 Minutes Separation.

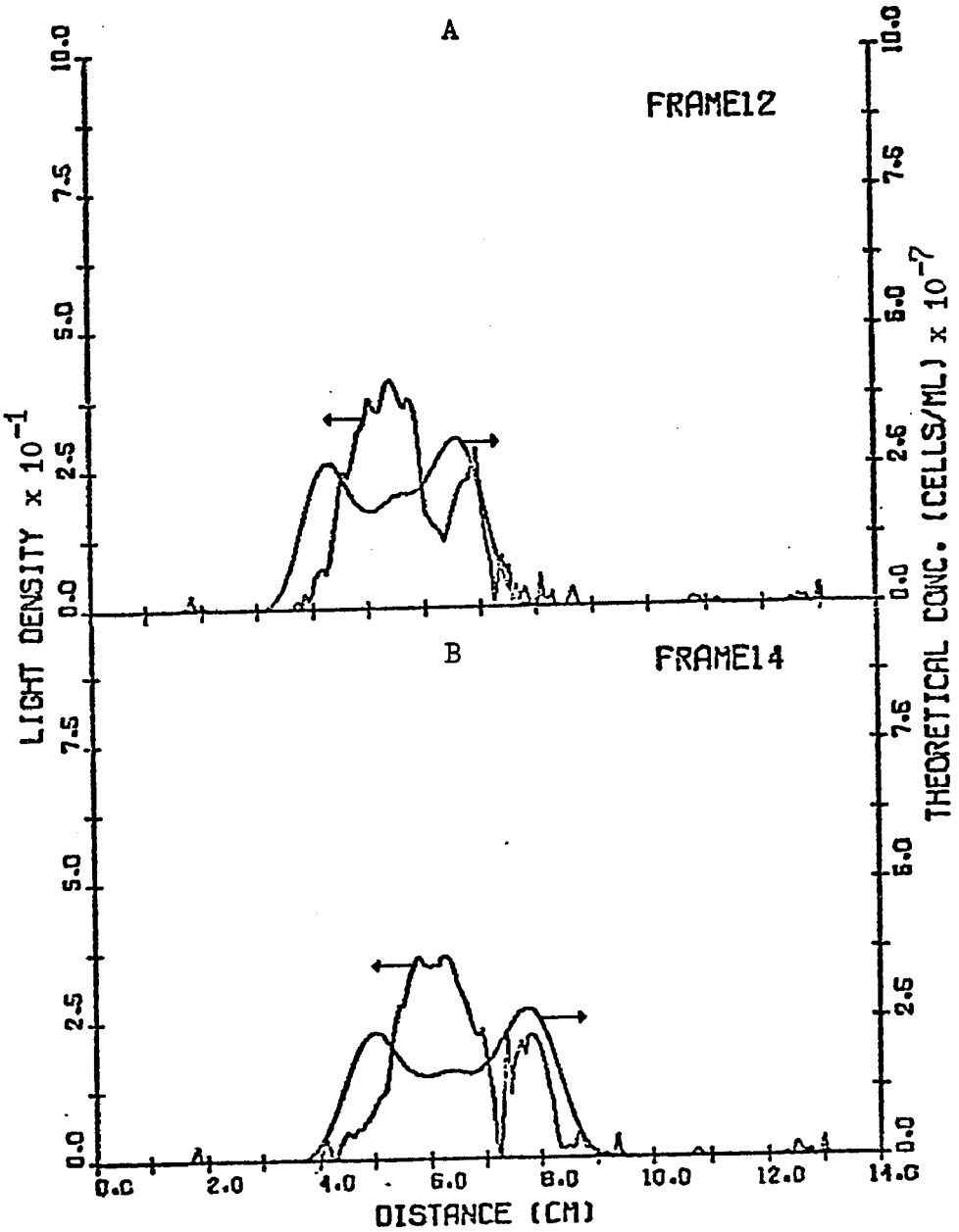

Figure 3.13. A. Frame 12, 36 Minutes Separation; B. Frame 14, 42 Minutes Separation.

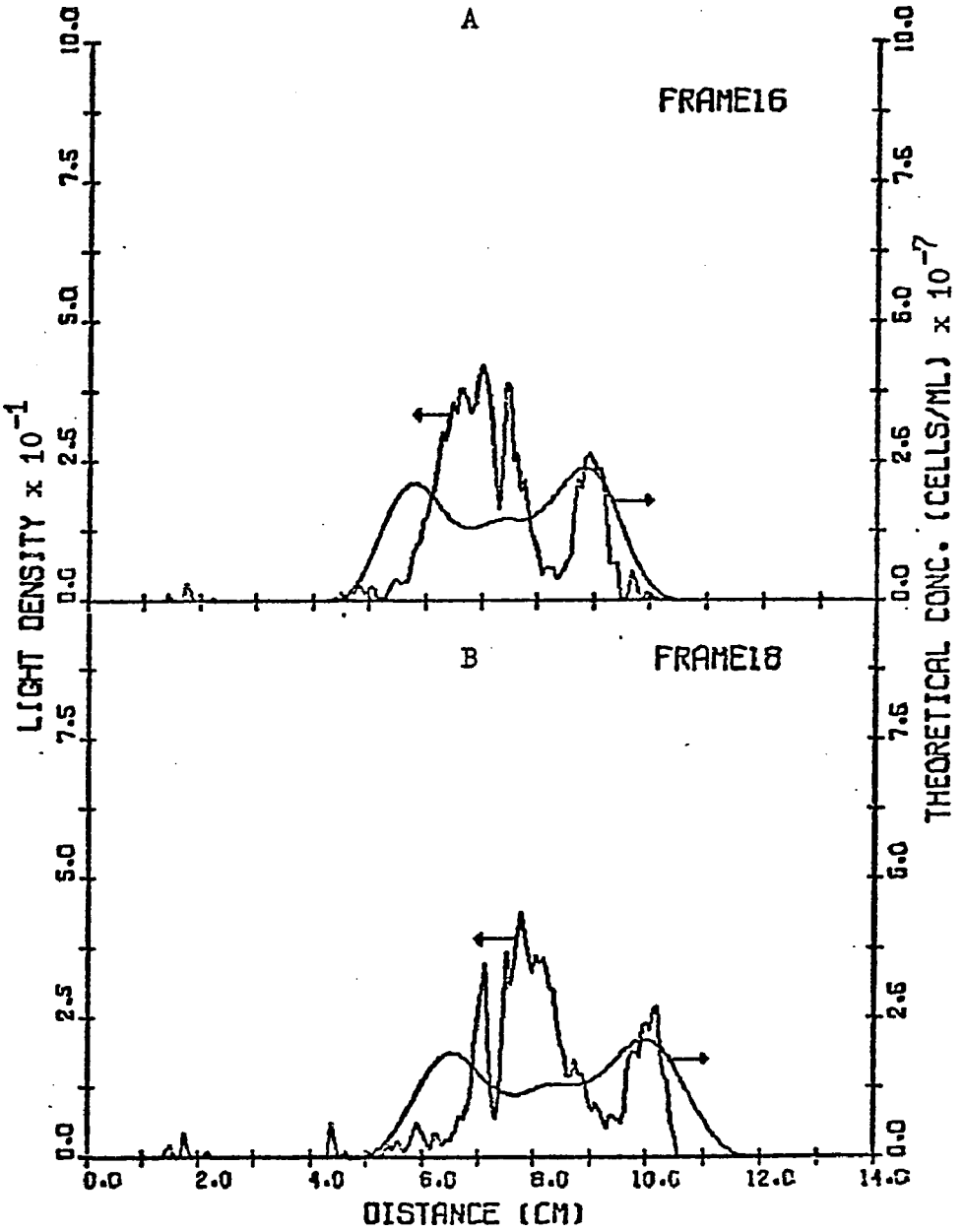

Figure 3.14. A. Frame 16, 48 Minutes Separation; B. Frame 18, 56 Minutes Separation.

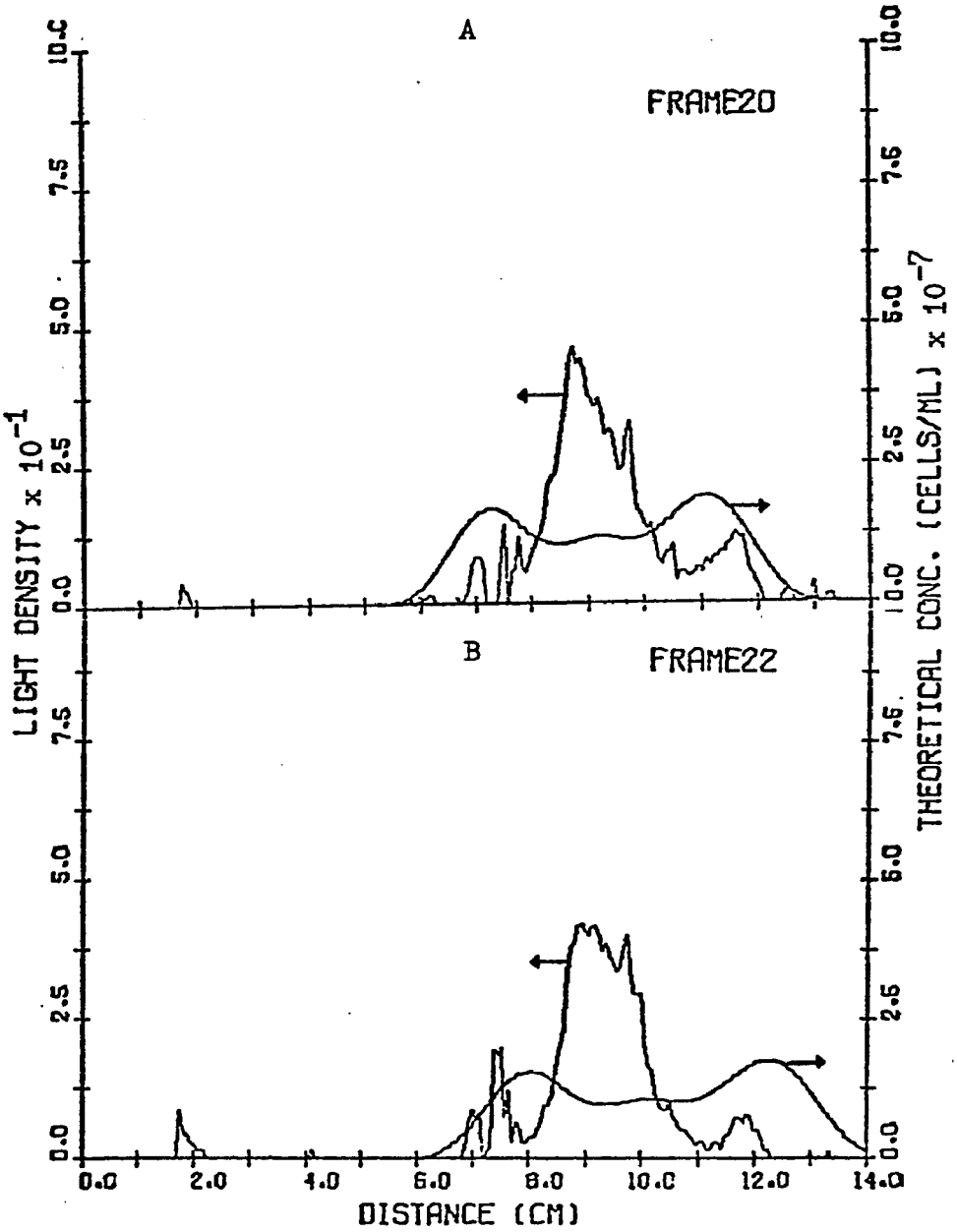

Figure 3.15. A. Frame 20, 60 Minutes Separation; B. Frame 22, 66 Minutes Separation.

through 3.15. Furthermore, while the position of the band as it proceeds through the separation agrees extremely well with the theoretical prediction, the magnitude and position of the second peak does not agree with theory. This discrepancy in band shape can be attributed to a number of reasons, including photographic quality, the complex function between light density and cell concentration and type, and a possibility of clumping by the cells. Although the specific effect of these considerations cannot be determined, the agreement between micro-densitometer results and the theoretical predictions seems quite reasonable and would support both the theoretical model and the assigned experimental parameters.

D. Conclusions

The electrophoretic separation of a mixture of three species of fixed red blood cells in space was successful in that fractionation according to mobility did occur and was found in the sliced samples although technical problems occurred in the operation of one column and the slicing of the second. Photographic evidence indicates that the low-electroosmotic methylcellulose coating was successful in reducing the electroosmosis to a near zero value. Also the flight film shows that the bands migrated down the column as theory would predict, producing two bands of high cell concentration separated and surrounded by regions of lower cell concentration. However, most likely some clumping of the cells occurred to cause the trailing band to be larger and darker than expected from theory.

The theoretical computer model gave good agreement with the ex-

perimental results and was used in defining the effect of the various experimental parameters. The best resolution can be obtained by reducing U_{os} to near zero with as small a temperature gradient between channel center and wall as possible. The effect of U_{os} can be minimized by reducing the ratio of the sample plug radius to the channel radius but at the expense of sample volume. This may be compensated for with little loss in resolution by increasing the sample plug thickness as long as this is negligible in relation to the total separation distance.

Overall, the experiment was a success in demonstrating a static electrophoresis separation under microgravity conditions with a resolution not possible on earth.

Chapter IV

Electrophoretic Mobility Measurements and Separations

Continuous particle electrophoresis, as opposed to static electrophoresis, offers the possibility of continuously collecting separated fractions rather than batch or semi-batch collections. Theoretically, therefore, more sample can be separated and collected with supposedly more uniform results due to the continuity of the process. Although the basic principle of electrophoresis is the same, the flow fields are different and this necessitates a different approach to the theory and the maximization of parameters for good resolution.

A. Apparatus Description

Figure 4.1 shows a schematic representation of the Beckman CPE instrument. The 0.15 x 4.5 x 50 centimeter electrophoresis channel is positioned vertically with the 30.5 centimeter long electrodes on opposite sides. Electrolyte solution is pumped into the top of the channel to form the electrolyte curtain. This curtain flows downward through the channel and empties at the bottom through forty-eight one millimeter O.D. stainless steel tubes set edge-to-edge, hence it is separated into forty-eight fractions. The electrodes are separated from the electrophoresis channel by semi-permeable membranes while a separate pumping system circulates another supply of the same electrolyte solution through the electrode compartments to remove any products of electrolysis. The sample to be separated is pumped into the center of the electrolyte curtain near the side of the cell. This

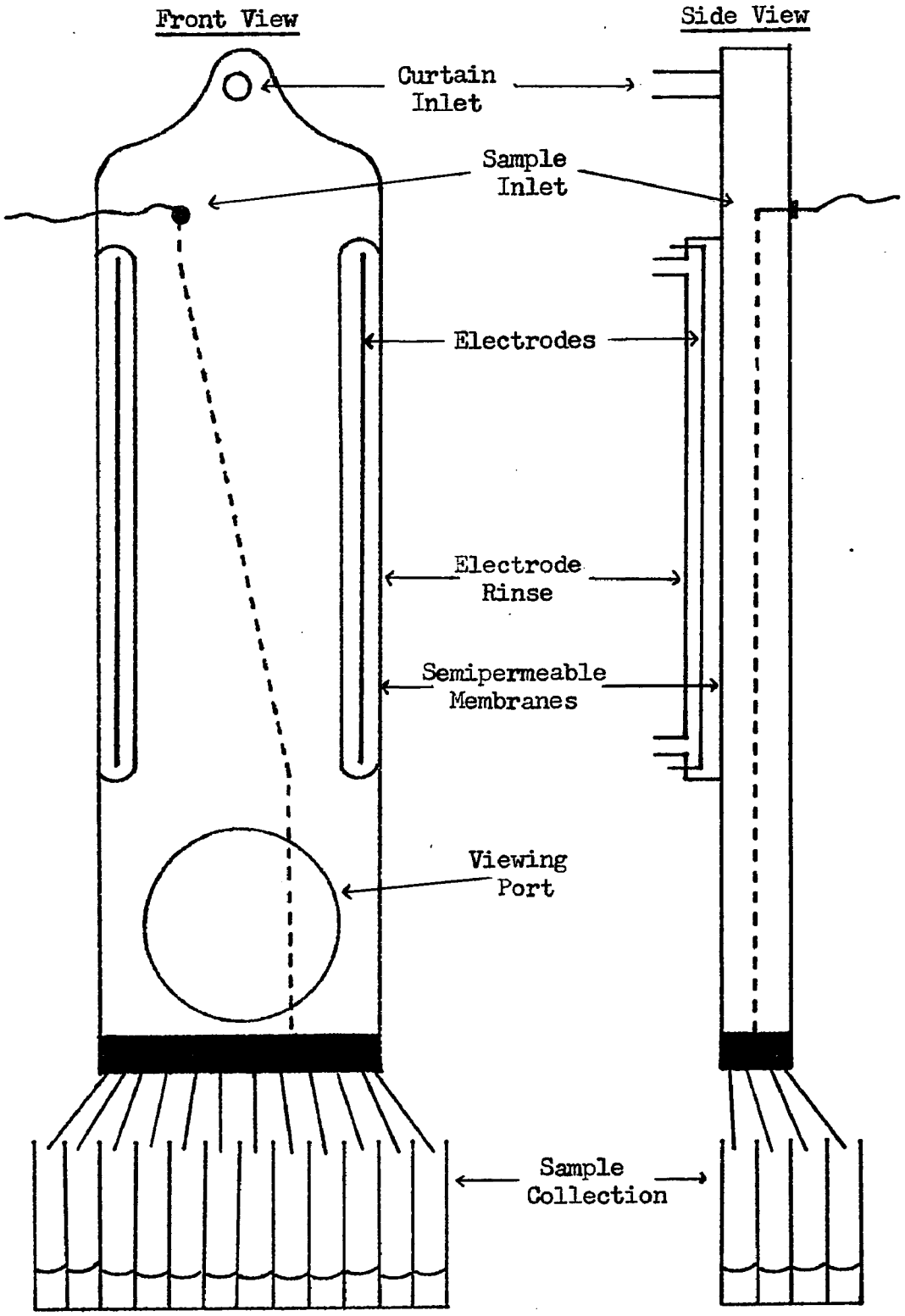

Figure 4.1. Schematic Representation of the Beckman CPE.

sample stream descends vertically in the absence of a voltage gradient. However when the voltage gradient is applied, it is displaced to the right according to the electrophoretic mobility of the particles. When the sample stream passes beyond the electrodes, it again descends vertically but now is displaced to the right. A viewing port with a millimeter scale allows the measurement of the migration distance, i.e., the lateral displacement of the particle stream. The electrolyte curtain and electrode rinse pumping systems use peristaltic pumps or gravity feed. The sample pumping system uses gas generated by the electrolysis of water; this in turn is governed by a rheostat. This instrument was used to separate monodisperse polystyrene latexes according to their electrophoretic mobilities(and hence particle sizes); mixtures of as many as ten different-sized latexes were separated successfully[23].

The Beckman CPE Instrument was modified in two ways. The sample delivery system, which was originally controlled by an electrochemically induced pressure head, was replaced by a micrometer syringe attached to a variable speed motor. This modification resulted in a more reproducible sample delivery rate, which could be controlled over a wider range of flow rates and results in a more accurate definition of the sample stream diameter. The second modification concerns the determination of the lateral displacement of the particle stream due to electrophoresis. The Plexiglas viewing port at the bottom of the separation cell, which is used for visual observation of the sample stream by means of reflected light, was replaced by a quartz window

which is transparent to ultraviolet light. A small optical bench with an ultraviolet light source and slit for control of beam dimensions was placed in front of the window. The optical bench was attached to a motor, moving it horizontally across the middle third of the window to scan the particle stream after the separation, and a resistance box, establishing the precise position of the ultraviolet light beam electronically. A UV-sensitive phototube was located in a fixed position on the other side of the window. A Houston Instruments Model 2000 X-Y recorder was used to record the intensity of ultraviolet radiation on the Y-axis and the horizontal position of the optical bench on the X-axis. The horizontal position of the recorder is magnified by a factor of 18.2 X.

B. Buffers

Two buffer systems were primarily used in the CPE. The first was a barbital-sodium barbital buffer which has a pH of 8.6 and was purchased from Harleco Lot Number 3208C. This buffer system was chosen because of its frequent use for paper electrophoresis. Generally, the ionic strength was held at 1×10^{-3} for most experiments, but it was also varied from 1×10^{-2} to 1×10^{-4} in order to investigate the effects of ionic concentration.

The second buffer system was referred to as the R-1 buffer and was formulated by Dr. Geoffrey Seaman[25] specifically for the SPAR electrophoresis flights. The composition and physical characteristics of the R-1 buffer are listed in Table 4.1.

Table 4.1 R-1 Buffer Composition

Substance	Mol. Wt.	g/liter	millimolarity
$Na_2HPO_4 \cdot 7H_2O$	268.07	0.472	1.76
KH_2PO_4	136.09	0.050	0.367
$Na_2EDTA \cdot 2H_2O$	372.24	0.125	0.336
Ionic Strength		3.3×10^{-3} moles/liter	
pH		7.39 @ 23°C	
Conductivity		375 μmho/cm @ 20°C	
Viscosity		1.00 @ 20°C	
Density		0.9982 @ 20°C	

This buffer system was used as is, with no variation in ionic strength for the curtain fluid. A 10X concentrate was used, however, in the electrode rinse system for some experiments.

C. Latexes

The latexes used as ideal model colloids in this work were Dow monodisperse polystyrene latexes, ranging in size from 2.02 μm to 0.088 μm in size. In some experiments the latexes were used "as is" but in others they were subjected to serum replacement to bring them to the same electrolyte level as the curtain fluid and to remove excess surfactant or other unknown species. This replacement was accomplished using a Nucleopore forty-three millimeter Ultrafiltration Cell[26], which keeps the latex suspended while slowly permitting the original serum to filter out of the system and be replaced by the new serum. This process generally had a small effect on the elec-

phoretic mobility of the latexes and was found to cause some spreading of each band if some surfactant was not also added. This is probably due to ionic effects and will be discussed later. Some of the same polystyrene latexes, which had been dyed red or blue, were also used. The coloring process has been described in earlier work[1], and generally has no effect on particle size or electrophoretic mobility.

D. Theoretical Aspects

The principles of flow in the CPE system have been described by Strickler[2] and Hannig[17]. A schematic representation of the electroosmosis and induced flow in the curtain is presented in Figure 4.2. The parabolic flow profile, due to electroosmosis, is in the X-Z plane and is either positive or negative in the X direction. However the induced parabolic flow profile is in the Y-Z plane and is always positive in the Y direction. The sample is injected into the center of the stream in a cylindrical configuration and moves with a constant electrophoretic velocity in the X direction in the presence of an applied potential. The migration of the particles is affected by two factors, both being a function of their position in the Z direction: the electroosmosis of the electrolyte medium which affects the net particle velocity in the X direction, and the induced parabolic flow profile which affects the velocity of the particle in the Y direction and hence the time of exposure of the particle to the electric field. Both factors ultimately affect the migration distance of the particles and the configuration of the sample stream. Both the electroosmotic and induced parabolic flow profiles of the electrolyte medium have compensating effects, i.e., as the particle

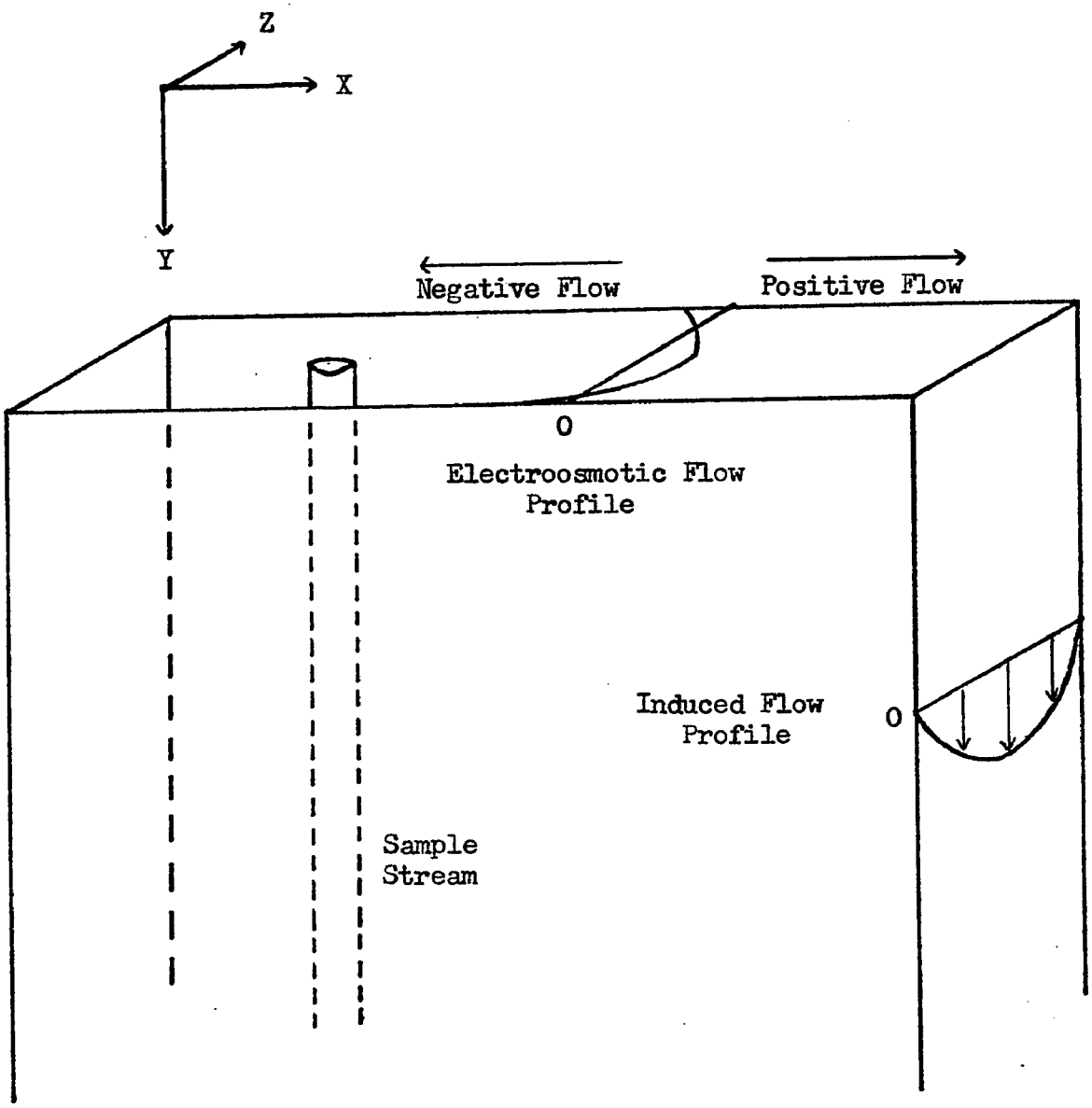

Figure 4.2. Schematic Representation of Flow Profiles Present in the Electrolyte Curtain of the CPE.

position moves away from the center of the channel, the net fluid velocity decreases in both the Y and X direction. This means that the slower-moving particles will be subjected to electrophoretic migration for a longer period of time than the faster-moving particles in the center of the curtain flow. In principle, therefore, it is possible to match the electroosmotic flow to the induced flow so that the sample streams will remain undistorted after separation. Under these conditions, the displacement of the sample stream will be controlled by the particles in the center of the curtain where the velocity of buffer in the Y direction and the positive velocity of buffer in the X direction are both at a maximum.

There is also an induced parabolic flow in the X-Y plane which is always positive in the Y direction. The effect of this flow profile will be minimal due to the much larger X dimension as compared to the Z dimension (about thirty times), and the fact that particles are usually kept in the middle third of the curtain where the variation in velocity is relatively flat.

The migration distance x of the particles as a function of position relative to the center of the channel in the Z direction and the electroosmotic and induced parabolic flow profiles has been given by Strickler[2] as follows:

$$x = (HE/v_o)\left[(U_{os} + U_e)/\left(1 - (z^2/d^2)\right) - (3U_{os}/2)\right] \qquad (4.1)$$

where H is the length of the electrodes, E is the potential gradient, v_o is the induced solvent flow velocity in the center of the channel, i.e., at $z = 0$, and d is one-half the channel thickness. If the sam-

ple stream is injected in the center of the channel and the radius of the sample stream is small relative to d, i.e., less than twenty per cent, then for all practical purposes the value of z in Equation 4.1 may be set equal to zero, to yield

$$x = (HE/v_o)\left[U_e - (U_{os}/2)\right] \tag{4.2}$$

Equation 4.2 is valid only if there is no distortion of the sample stream due to the electroosmotic and induced parabolic flow profiles.

The physical dimensions of the electrolyte curtain are such that $v_o = 2.25\ F/A$, where F is the curtain flow rate and A is the cross-sectional area of the curtain. Substitution of v_o into Equation 4.2 yields:

$$x = (A\ H\ E/\ 2.25\ F)\left[U_e - (U_{os}/2)\right] \tag{4.3}$$

Substitution of the physical dimensions of the Beckman CPE Instrument, i.e., $A = 0.675\ cm^2$ and $H = 30.5$ cm, into Equation 4.3 yields:

$$x = (0.0549\ E/F)\left[U_e - (U_{os}/2)\right] \tag{4.4}$$

Equation 4.4 predicts the migration distance of the particles as a function of the instrument parameters E and F and as a function of the electrophoretic mobility of the particles U_e and the electroosmotic flow at the channel-wall interface U_{os}. Equation 4.4 may be rearranged to yield:

$$U_e = (x\ F/0.0549\ E) + (U_{os}/2) \tag{4.5}$$

where U_{os} must be evaluated in order to calculate U_e from an experimental measurement of x. In practice, the 1.10 μm diameter monodisperse polystyrene latex was used as a standard to determine U_{os} from microcapillary measurements of U_e.

Another method, used to determine the electrophoretic mobility of an unknown dispersion when standard latex particles were mixed with the dispersion, measures the difference in migration distance, Δx, between the unknown and standard particles. Thus, $\Delta x = x_1 - x_2$ where x_1 and x_2 are the migration distances of the standard and unknown particles, respectively. Equation 4.4 may be used in this definition of x to yield:

$$U_{e2} = U_{e1} - (\Delta x \, F/0.0549 \, E) \qquad (4.6)$$

where U_{e1} and U_{e2} are the electrophoretic mobilities of the standard and unknown particles, respectively. Thus Equation 4.5 may be used to calculate the absolute electrophoretic mobility from the migration distance of the particles $\underline{x}$ and from a knowledge of U_{os} determined using the standard particles. Equation 4.6 may be used to calculate the absolute electrophoretic mobility from the difference in migration distances, Δx, between the unknown and standard particles.

Other assumptions in this development are: (1) there is little or no temperature gradient to change mobility values or flow profiles, (2) there are no particle-particle interactions and little or no Brownian diffusion, (3) there are no end effects, either entering or leaving the electric field or at the channel edges near the electrodes themselves, and (4) the curtain pH and conductivity are constant across the channel. In most cases these effects are minor in relation to the electrophoretic migration and can be ignored.

E. Experimental Results

Figure 4.3 shows a typical recorder scan of a mixture of three

Particles - 0.234, 0.46, 1.10 μm Polystyrene Latexes
Buffer - Barbital-Sodium Barbital (1 x 10^{-3} Ionic Strength)
Curtain Flow Rate - 12.5 cc/minute

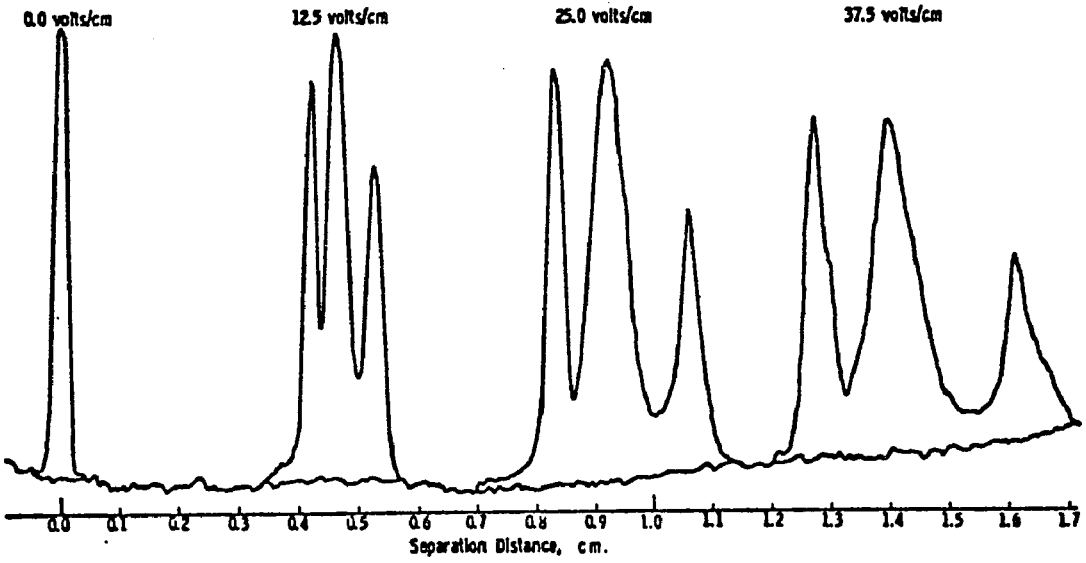

Figure 4.3. Recorder Scan of Separation of Monodisperse Polystyrene Latexes in Beckman Continuous Particle Electrophoresis Instrument.

monodisperse latexes (diameters of 0.234, 0.46, and 1.10 μm) separated in the Beckman CPE. The electrolyte was 1 x 10^{-3} M sodium barbital while the curtain flow rate was 12.5 cc/minute. The four different runs presented in Figure 4.3 were at applied potentials of 0.0, 12.5, 25.0, and 37.5 volt/centimeter. The microcapillary electrophoretic mobilities of these latexes in this medium were 3.74, 4.65, and 5.64 μm centimeters/volt second for the 0.234, 0.46, and 1.10 μm diameter particles, respectively.

A necessary condition to establish that the Beckman CPE is operating properly is that the migration distance must be a linear function of the applied potential which extrapolates back to zero at zero potential. There may be some curvature due to the very extended parabolic flow profile in the direction of migration, but it should only be very slight. Figure 4.4 shows the variation of migration distance with $\underline{E}$ for a mixture of three latexes for curtain flow rates of 12.5 and 25.0 cc/minute. The plots are linear and are compatible with Equation 4.4 when the 1.10 μm diameter latex is used as a standard to calculate U_{os}.

These results demonstrate that the Beckman CPE is operating properly according to theory. The feasibility of using this instrument to measure the absolute electrophoretic mobility of particles was determined by the following procedure. The sodium barbital buffer was prepared at five different ionic concentrations in the range of 1 x 10^{-4} to 1 x 10^{-2} M. The electrophoretic mobilities of seven different monodisperse latexes were measured in the sodium barbital buffers

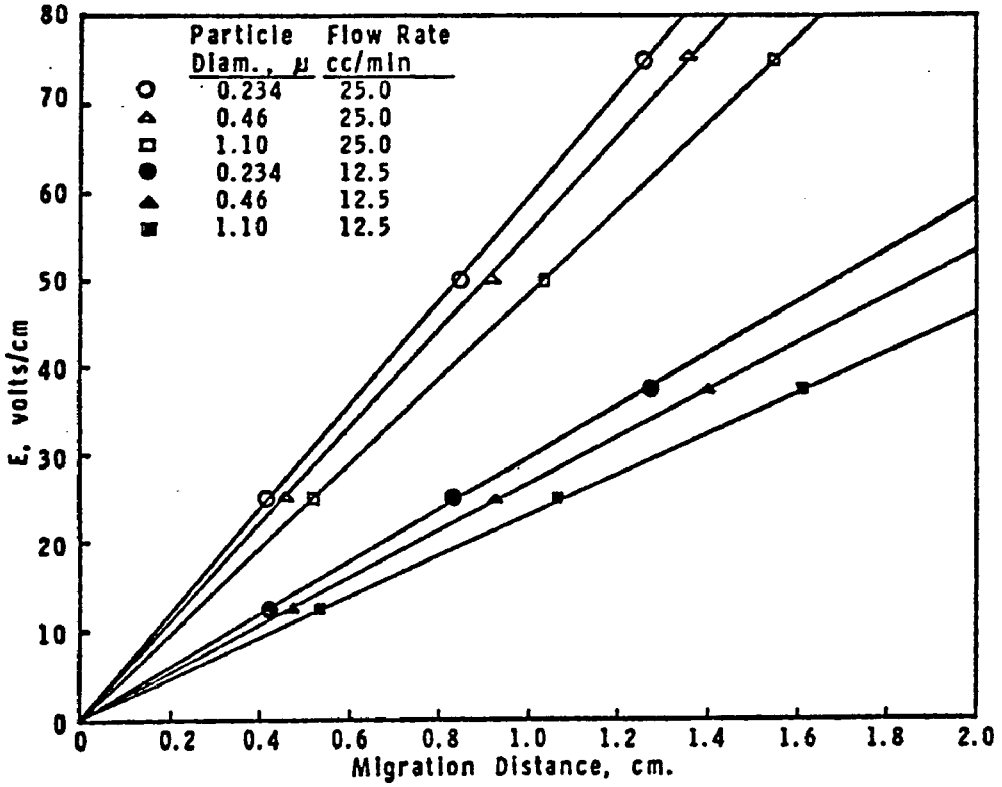

Figure 4.4. Variation of Migration Distance of Polystyrene Latex Particles with Voltage Gradient in Continuous Particle Electrophoresis.

by microcapillary electrophoresis. The 1.10 μm diameter latex was used as the standard to calculate the electrophoretic mobility of all the other latexes at the different sodium barbital buffer concentrations, according to either Equation 4.5 or Equation 4.6. The results are summarized in Table 4.2 where column 1 identifies the latex, column 2 the buffer concentration, and columns 3, 4, and 5 the electrophoretic mobility results obtained from Equation 4.6, Equation 4.5, and microcapillary electrophoresis, respectively. Column 6 gives the difference between the results obtained from microcapillary electrophoresis and Equation 4.6. Column 7 gives the electroosmotic mobility at the channel wall calculated from Equation 4.4 using the 1.10 μm diameter latex as the standard. The agreement between microcapillary electrophoresis and the CPE (column 6) is generally good and demonstrates that the CPE method is a valid approach for measuring the electrophoretic mobilities of particles.

One important caution is that Equations 4.5 and 4.6 assume that the particle stream is not distorted by the electroosmotic and induced parabolic flow profiles of the electrolyte curtain and therefore are not applicable where such distortion is observed. If the band is properly centered in the curtain, this will not distort the results since the peak and main portion of the band will still be in the right place; but if the band is not centered properly, the electroosmotic distortions will lead to false values. This fact can usually be established by selecting two standard latexes which have electrophoretic mobilities near the upper and lower limits of the range of interest.

Table 4.2

Comparison of Electrophoretic Mobilities by Microcapillary and Continuous Particle Electrophoresis

PS Latex sizes μm	Barbital Na-Barbital Conc.	Electrophoretic Mobility, μm cm/volt sec				
		CPE		MCE	MCE-CPE	U_{os}
		Δx	x			
0.109	0	3.24		3.28	+0.04	-39.0
0.357	0	3.32		3.28	-0.04	
0.109	1×10^{-4}	3.87		4.11	+0.24	- 8.76
0.357	1×10^{-4}	4.01		4.03	+0.02	
0.045	1×10^{-3}	3.22	3.32			- 7.73
0.088	1×10^{-3}	2.99	2.92			
0.109	1×10^{-3}	2.99		2.64	-0.35	
0.234	1×10^{-3}	3.76	3.68	3.74	-0.02	
0.357	1×10^{-3}	3.93		3.90	-0.03	
0.460	1×10^{-3}	4.47	4.41	4.65	+0.18	
0.109	2×10^{-3}	3.06		3.28	+0.22	-10.89
0.234	2×10^{-3}	3.98	4.05	4.20	+0.22	
0.357	2×10^{-3}	4.17		4.30	+0.13	
0.460	2×10^{-3}	5.00	5.03	4.93	-0.07	
0.80	2×10^{-3}	5.11		5.18	+0.07	
2.02	2×10^{-3}	6.94		6.45	-0.49	
0.234	5×10^{-3}	3.80		4.10	+0.30	-11.82
0.357	5×10^{-3}	4.02		4.54	+0.52	
0.46	5×10^{-3}	5.27		5.47	-0.14	
0.109	1×10^{-2}	3.10		3.68	+0.58	-12.13
0.357	1×10^{-2}	4.30		4.54	+0.24	

It is also possible to distinguish such distortion by visual observation[20].

There is very little difference between the results obtained from Equations 4.5 and 4.6. From practical considerations it is easier experimentally, and thus possibly more accurate, to use Equation 4.6 because the zero point does not have to be measured. The equilibrium positions between bands, due to electrophoretic mobility differences, is set up rather quickly (about fifteen to thirty seconds), whereas the equilibrium total displacement distance from the zero point,also a function of the electroosmotic mobility, takes much longer to develop (usually five or more minutes). There is also an unexplained phenomenon that affects the use of Equation 4.5: the large calculated values of U_{os} given in column 7 of Table 4.2. The zeta potentials calculated from these values range from 150 to 300 mV in the sodium barbital buffer and have a value of about 1000 mV in deionized water, i.e., without sodium barbital buffer. Since these values seem unreasonably large, it must be assumed that there is a flow in the same direction of the separation which is not entirely due to electroosmosis along the channel wall. This flow has been referred to by Strickler as endoosmotic flow[2]. For all practical purposes however, Equation 4.5 is not concerned with the source of the flow, only that this flow be proportional to the applied potential. Since this proportionality has been established experimentally, it may be assumed that the additional flow is electroosmotic in origin and probably occurs in the semi-permeable membranes which separate the electrodes

from the channel.

Figure 4.5 shows the separation of a mixture of seven monodisperse polystyrene latexes measured at applied potentials of 30 and 60 volts/centimeter. Seven peaks can be identified and it is possible to estimate the resolution of the CPE method from these results. The differences in the calculated electrophoretic mobilities of latexes 1 and 2, and latexes 3 and 4 are 0.16 and 0.37 μm centimeters/volt second, respectively. The microcapillary electrophoresis results for latexes 3 and 4 show a difference of 0.10 μm centimeters/volt second; latex 1 could not be measured by this method because the size of its particles is too small for detection in dark field illumination. Although microcapillary electrophoresis is considered to be more accurate for determining absolute mobilities, the CPE method gives directly the different mobilities of a mixture of two samples.

F. Collection of Separated Fractions

Although the UV scanner can detect bands with a difference in mobility of as little as approximately 0.15 mobility unit, the collection efficiency is limited to about forty-eight one millimeter slices of the curtain. For this reason, many of the resolved bands may emerge through the same collection tube unless one is fortunate enough to have the boundary between two tubes occur between the two bands. However, it is interesting to see how clean the various fractions are for a well separated mixture of monodisperse latexes.

A separation was made on a mixture of three monodisperse polystyrene latexes, 1.1 μm, 0.357 μm, and 0.109 μm, with electrophor-

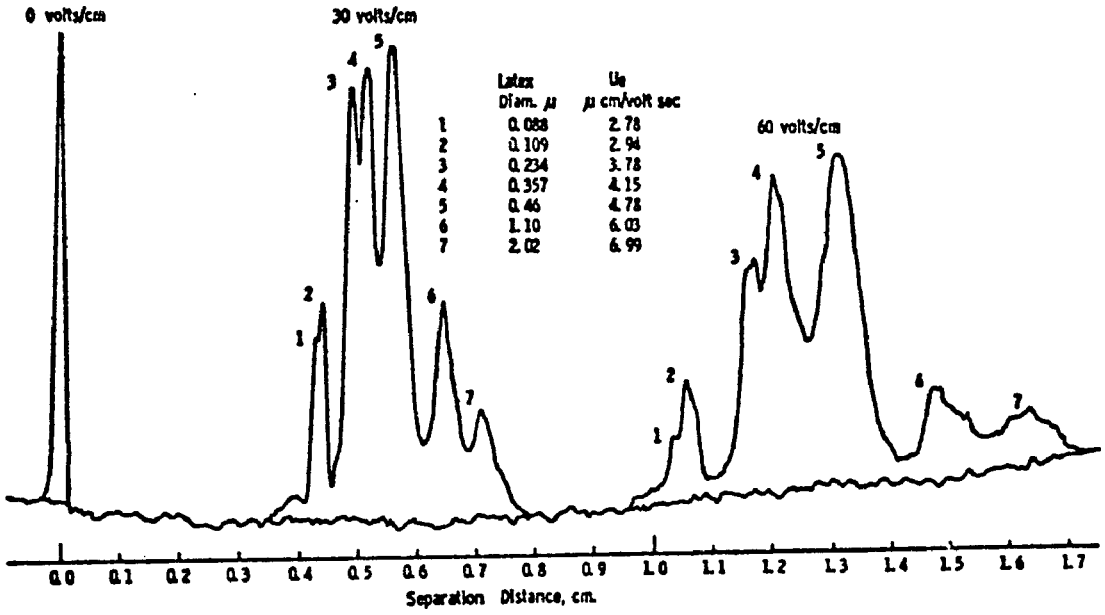

Figure 4.5. Separation of Seven Polystyrene Latexes in Beckman Continuous Particle Electrophoresis Instrument.

etic mobilities of 6.68, 4.56, and 3.50 μm centimeters/volt second respectively. With such large mobility differences, these three species should separate into different tubes. To assure a good separation, the Beckman CPE was run at conditions which were on the verge of instability as far as maintaining good laminar flow. The conditions were at a flow rate of 16 cm^3/minute which gives a mean residence time of thirty-three seconds and an applied voltage of 30 volts/centimeter in the R-1 buffer with a 10 X concentration in the electrode rinse system. These conditions cause a significant heating of the curtain fluid but not enough to disrupt the flow profiles. The total concentration of the mixed latexes was fifteen percent by weight with each species being of equal weight percents. Upon applying the voltage gradient, the electroosmotic flow was allowed to come to equilibrium for five minutes before collection was begun. Samples were colected for nine to ten minutes; this gave about three cubic centimeters of collected sample in each tube. Figure 4.6 shows the recorded scans of the separation. During the collection, the bands were found to still be moving slightly to the right possibly due to the conditions which were near instability. However, the movement was not enough to significantly affect the collected samples. The latex was found in tubes twenty-five through twenty-nine which spans about 5 millimeters and is 8.5 to 13 millimeters displaced from the reference position, tube seventeen, at no applied voltage.

These five collected samples plus the initial mixture and each latex separately were then prepared for the transmission electron mi-

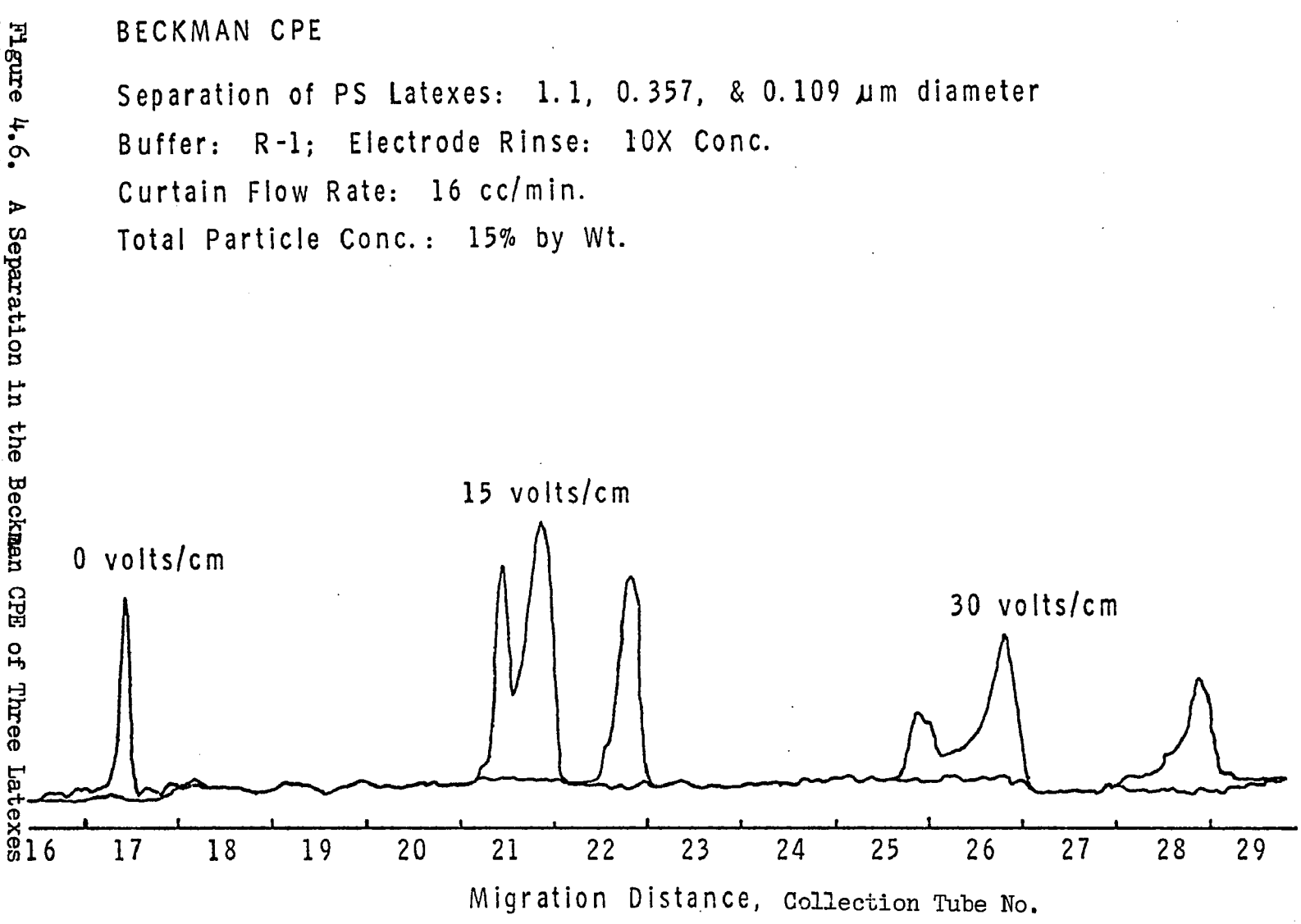

Figure 4.6. A Separation in the Beckman CPE of Three Latexes Which Were Collected and Viewed with the Electron Microscope.

croscope, a Phillips Model J300. Figure 4.7 shows a collection of the pictures for each species separately and the mixture at a magnification of 21,700X. As expected, the diameter ratio of the larger 1.1 μm particles to the smaller 0.357 μm and the 0.109 μm particles appears to be about 3 and 10 respectively. The 1.1 μm and the 0.109 μm latexes appear to be quite clean and uniform in size while the 0.357 μm latex appears to have been, possibly, contaminated with some 0.109 μm latex. The contamination, as observed in other parts of the grid, was not great. The pictures of the mixture were not sharp because of an inability to clearly focus on all sizes of particles and a sparsity of particles on the grid. Figure 4.8 shows the pictures of the collected fractions at the same magnification. Figures 4.8A and 4.8B show the sample from tube twenty-five which represents the shortest migration distance. The majority of the particles are the 0.109 μm with a few of the 0.357 μm and no 1.10 μm particles. Figures 4.8C through 4.8E show the sample from tube twenty-six. Here the majority of the particles are the 0.357 μm with a good number of the 0.109 μm also, and one 1.1 μm particle was found. No pictures are shown for tube twenty-seven where the particle concentration was seen to be very low. The prepared grid had only a few particles present which appeared to be the 0.357 μm and the 1.1 μm latexes. Figure 4.8F shows a picture of the collected sample from tube twenty-eight which showed almost entirely the 1.1 μm particles, but only sparsely populated. Lastly, tube twenty-nine is shown in Figure 4.8G and 4.8H. Here the particles appeared to be entirely the 1.1 μm particles and

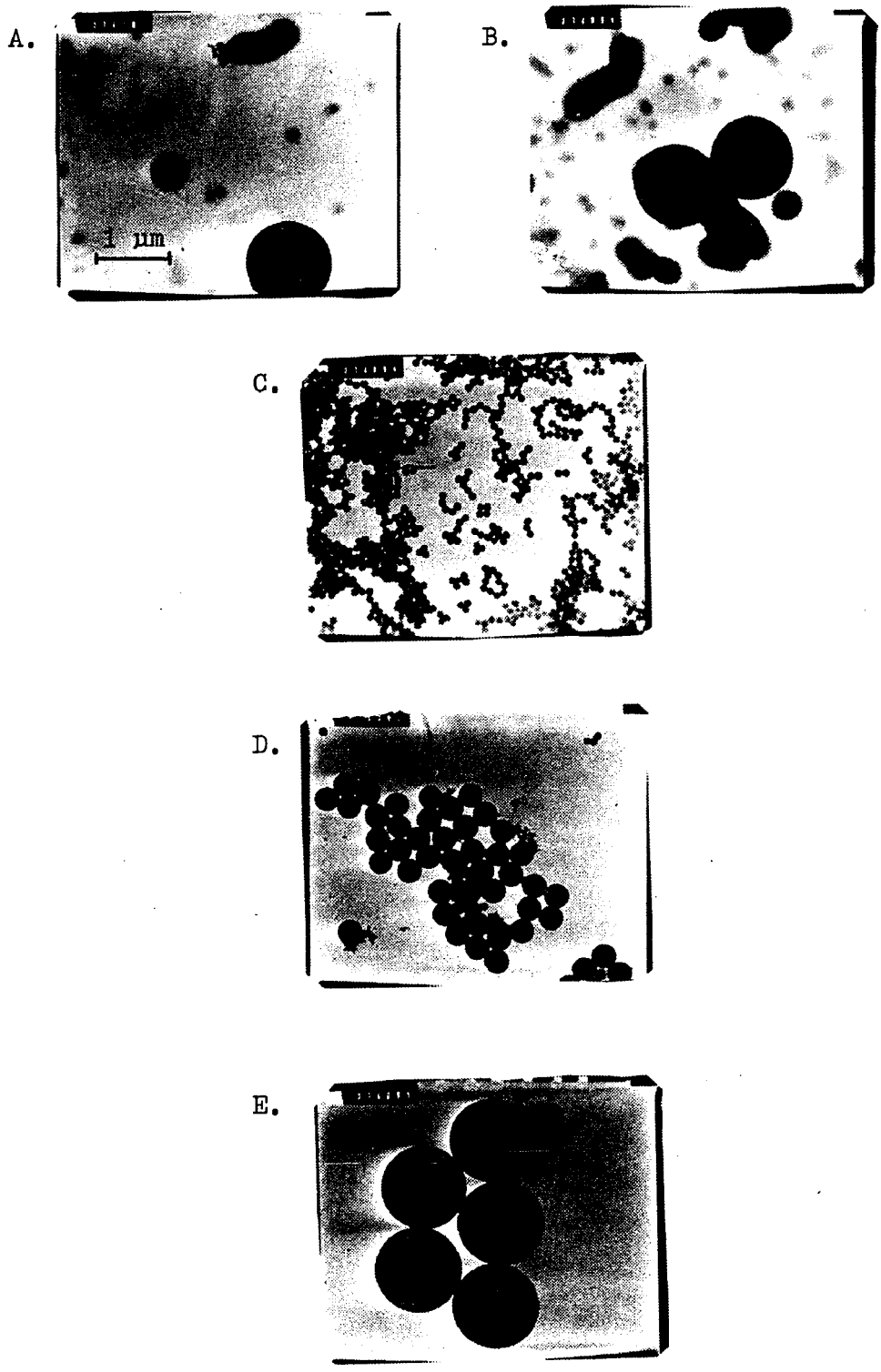

Figure 4.7. Electron Micrographs of Three Species of Polystyrene Latexes; A. and B. Mixture of the Three, C. 0.109 µm. Latex, D. 0.357 µm. Latex, and E. 1.10 µm. Latex.

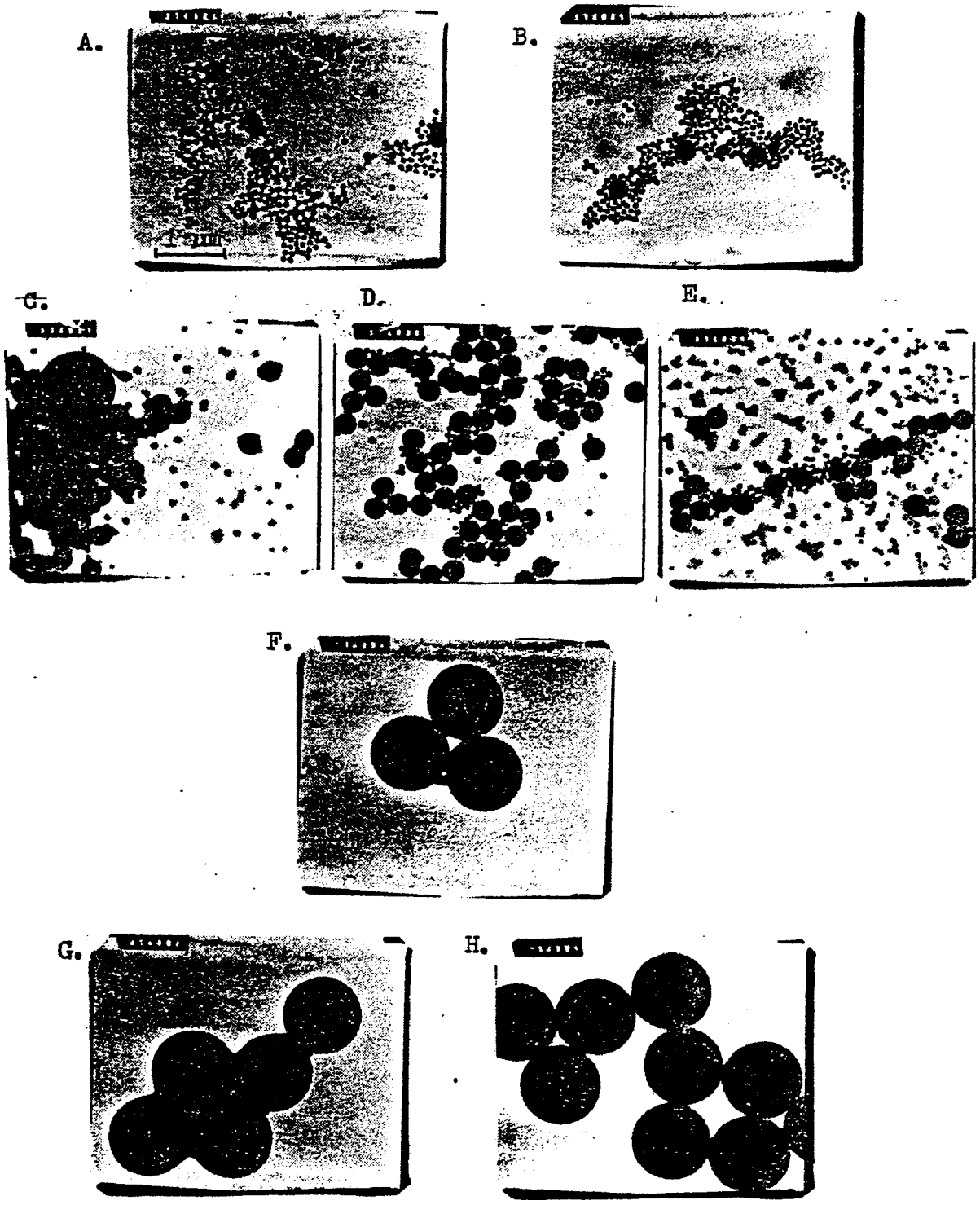

Figure 4.8. Electron Micrographs of the Collected Fractions After Separation in the CPE; A. and B. Tube #25, 8 mm. Displaced, C. D. and E. Tube #26, 9 mm. Displaced, F. Tube # 28, 11 mm. Displaced, and G. and H. Tube #29, 12 mm. Displaced.

in a much greater concentration than was detected in tube twenty-eight.

The electron micrographs show that the particles are indeed fractionated according to size, however the collection resolution is limited by the large geometry of the slicing. It is also interesting to note that a small number of the 1.10 μm particles are found in tubes twenty-six, twenty-seven, twenty-eight, and mostly in tube twenty-nine, and that the 0.357 μm particles were found in tube twenty-five, twenty-seven, and mostly in tube twenty-six while the 0.109 μm particles are not seen beyond tubes twenty-five and twenty-six. There seems to be a rather sharp delineation of the particles to the right of where they are expected, while there is some tailing off to the left of where they are expected. This shows, to a small degree, the effect of the electroosmosis which is very high (about -12.0 μm centimeters/volt second) as compared to the particle mobilities. This effect has been minimized by the small band diameter. There may also be some effect due to the long collection time and the slight drift of the bands to the right.

Chapter V

Computer Modeling of CPE

A. Theoretical Computer Modeling of Various CPE Parameters

In order to fully understand the effect of the many variables which can affect the resolution in any form of continuous particle electrophoresis, a rather complex computer program was developed to simulate the separation of particle bands under a wide variety of conditions which can be explained by the present theory. The program is capable of predicting the cross-sectional appearance of the separated bands at any stage of separation and also the particle concentration as a function of the separation distance as would be detected by a scanning device mounted in front of the cell to monitor the separation. Then this type of information is very useful in determining exactly what effect each parameter has on the resolution. In this way, a large number of experimental parameters can be simulated to predict performance or to compare theoretical computations to actual experimental performance.

The principle equation which describes the displacement of a particle in the flow fields has been derived by Strickler[2], and has been presented in Chapter IV as Equation 4.1:

$$x = \frac{HE}{v_o}\left(\frac{U_{os} + U_e}{1-z^2/d^2} - \frac{3}{2}U_{os}\right) \qquad (5.1)$$

where: x is the horizontal displacement distance (μm)

H is the electric field length through which the particle travels vertically (cm)

E is the applied potential (volt/cm)

v_o is the maximum fluid velocity at the midplane (cm/sec)

U_{os} is the electroosmotic mobility of the walls (μm cm/volt sec)

U_e is the electrophoretic mobility of the particles (μm cm/volt sec)

d is the curtain half-thickness (cm)

z is the particle depth from the curtain midplane (cm)

This equation describes the displacement of a particle as a function of the electrode length, applied voltage, curtain flow rate, electroosmotic and electrophoretic mobilities, and the particle depth to curtain half-thickness ratio. An important fact can be readily realized from this equation. The migration distance is directly proportional to the electric field length and applied voltage, and inversely proportional to the curtain flow rate. Changing any of these three parameters will directly affect the particle migration and therefore the attainable separation. All, however, can affect the Joule heating of the curtain fluid therefore creating an upper limit to this ratio of parameters above which mixing from convection will occur and result in unpredictable flow.

Equation 5.1 assumes that the electroosmosis of both walls is the same, which may not always be the case if two different materials are used. Equation 5.2, also developed by Strickler[2], takes this effect into account:

$$x = \frac{HE}{v_o}\left[\frac{1}{2}\left(\frac{U_{osr}}{1-z/d} + \frac{U_{osf}}{1+z/d}\right) - \frac{3}{4}(U_{osr} + U_{osf}) + \frac{U_e}{1-z^2/d^2}\right] \qquad (5.2)$$

where U_{osr} and U_{osf} are the electroosmotic mobilities of the rear and front walls respectively. Equation 5.2 reduces to Equation 5.1 if U_{osr} is equal to U_{osf}. This is then the starting equation that was used to simulate the performance of the CPE.

An important consideration in the CPE, as in any form of electrophoresis, is the effect of temperature on the mobility values. Due to the high potentials applied, a temperature rise and accompanying gradient develops. This temperature gradient will be small in a narrow channel CPE, but in a thicker channel the effect can be rather severe. Both the viscosity and dielectric constant of the fluid medium are temperature-dependent and affect the mobility values. Therefore, if a mobility is measured at a standard temperature of 25 ^{o}C and a CPE separation carried out at a different temperature or with cooling in the face plate, then a correction should be made to take into account the effect of temperature. This may be easily done by modifying Equation 5.2 to:

$$x = \frac{HE}{v_o}\left[\frac{1}{2}R_w\left(\frac{U_{osr}}{1-z/d} + \frac{U_{osf}}{1+z/d}\right) - \frac{3}{4}R_w(U_{osr} + U_{osf}) + \frac{U_e R_z}{1-z^2/d^2}\right] \qquad (5.3)$$

where,

$$R_w = \frac{\epsilon_w \eta_{298}}{\eta_w \epsilon_{298}} \quad , \qquad R_z = \frac{\epsilon_z \eta_{298}}{\eta_z \epsilon_{298}} \qquad (5.4)$$

where ϵ and η are the dielectric constant and viscosity respectively at the wall position, w, and at the particle position, z. These ratios then correct the electroosmosis values to the temperature at the walls where the driving force is located, and the electrophor-

etic values to the particle position temperature. By doing this the effect of a temperature gradient may be superimposed on the particle migration. This treatment only accounts for changes in mobility, not for changes in the flow profiles due to the temperature dependent fluid viscosity. This second effect, however, is felt to be small for the Beckman CPE where the temperature increase is relatively small. Also, the temperature gradient is not constant as the particles pass through the electric field, but gradually develops to a maximum as the particles leave the electric field. This effect may be easily accounted for in a computer simulation.

Another area which the theory does not cover is the laminar flow profile in the direction of migration, X, as shown in Figure 5.1. Although this dimension, as discussed in Chapter IV, is large in comparison to curtain thickness(about thirty times larger in our CPE, 4.5 cm. versus 0.15 cm.) and the sample stream is maintained in the middle third of the column(1.5 cm. from both sides), there is still some velocity variation which can effect the exact separation distance of each band. This effect has been accounted for in the simulation by a trial and error procedure to determine an average vertical velocity as a function of the migration distance.

These equations and modifications fairly well describe the movement of a particle anywhere within the CPE curtain, however in actuality we are dealing with bands of particles that may have a distribution of mobilities. To model this overall effect it has been necessary to divide the initial band cross-section into a number of

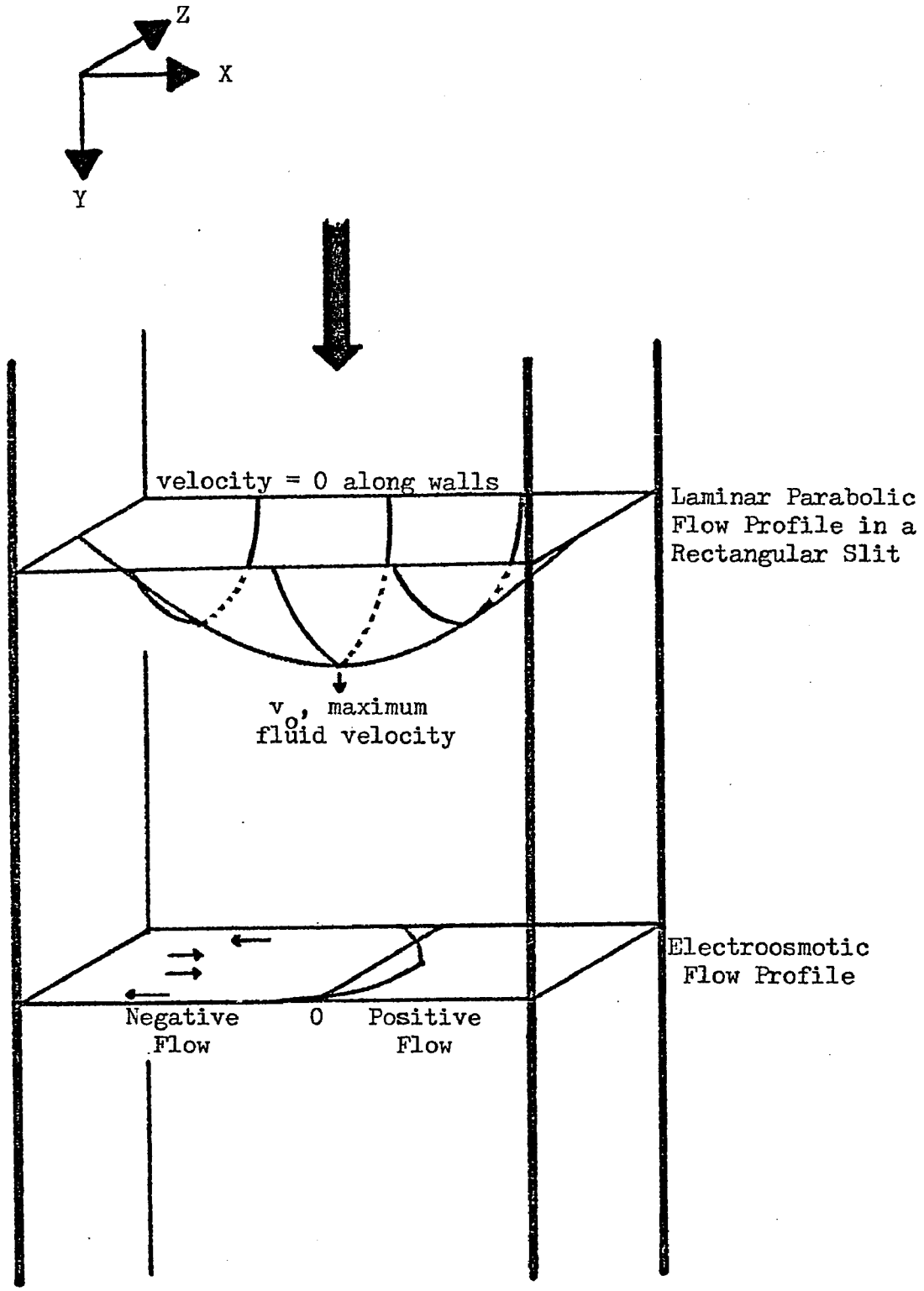

Figure 5.1. Schematic Representation of Flow Profiles Present in Electrolyte Curtain of CPE.

points. Then by calculating the displacement as a function of position, the total cross-sectional image and particle distribution may finally be obtained by adding the contribution from each segment. First, however, since most samples exhibit a range of electrophoretic mobilities, it is necessary to characterize this mobility distribution in order to determine the breadth of the sample band , and how to add the contribution from each segment to gain the overall concentration profile. The computer program provides four standard mobility distribution shapes, classified as Gaussian, triangular, rectangular, and parabolic in shape, plus a provision for a computer fitted nth order polynomial to any random shape such as a bimodal distribution. Once a distribution shape can be mathematically defined, this can then be applied to each point into which the initial band cross-section has been divided. This summing process can be done very easily and quickly by the computer thereby allowing the band to be divided into many points for a high degree of accuracy. A listing of the program is included in Appendix B. In this manner a concentration profile can be calculated as a function of all the parameters that affect the migration distance.

B. Results

Now let us see in what ways many of the important parameters can effect a separation either resulting in good resolution with well defined bands or in poor resolution with a smear of overlapping bands. Figure 5.2 shows a hypothetical separation of four particle species of different electrophoretic mobility. Above the particle concentra-

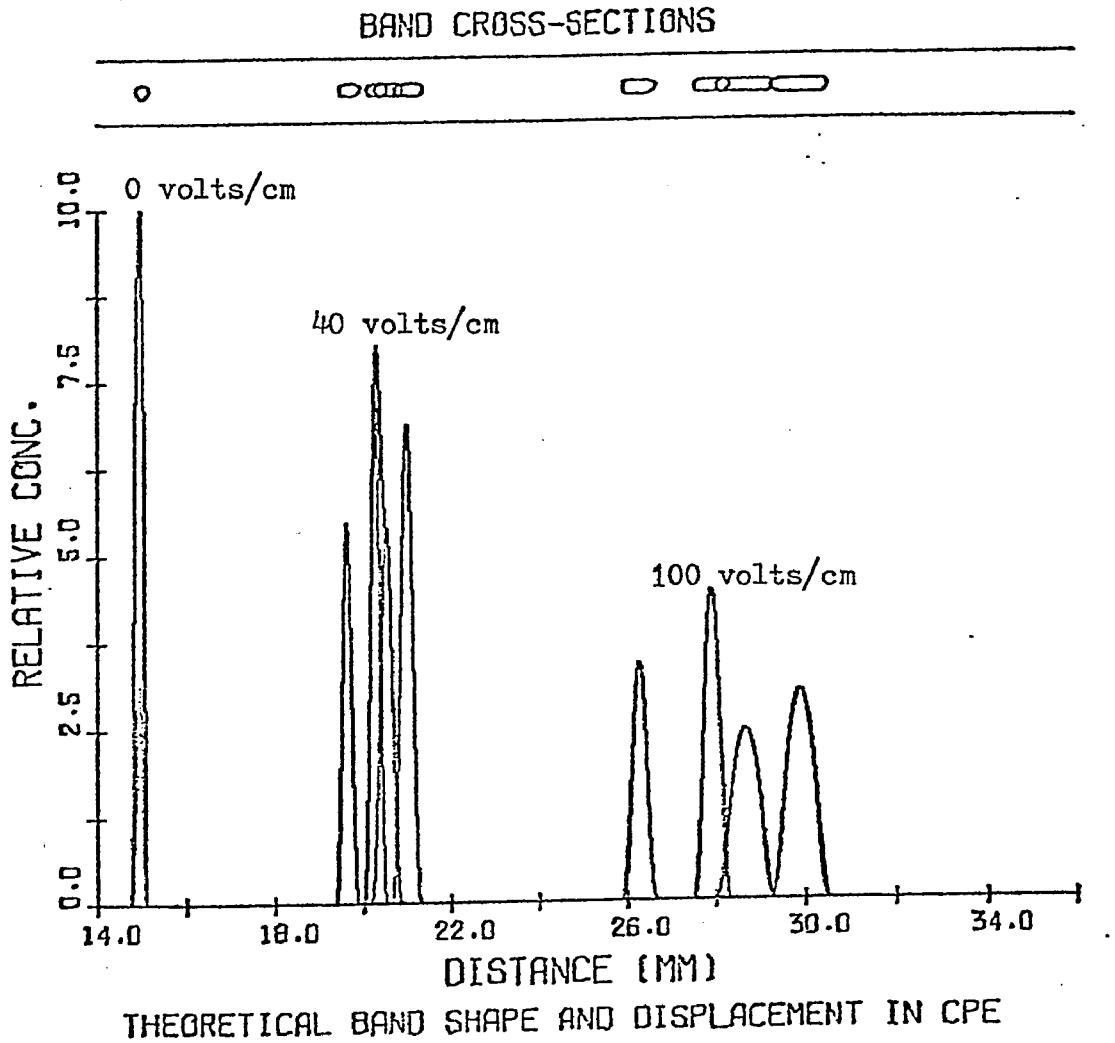

Figure 5.2. Hypothetical Separation at Two Stages of a Mixture of Four Species of Differing Mobility Distributions Under Ideal Conditions.

tion profile is shown the band cross-sections to further demonstrate how the bands appear and are separated.

All theoretical predictions that will be presented are for a CPE of the dimensions of the one originally manufactured by Beckman Instruments several years ago, namely 1.5 mm. thick by 4.5 cm. wide by 30 cm. long for the electrode region. This does not however mean that this theory and results are not applicable to other variations on these dimensions, because many of the effects are the result of R which is the ratio of the sample thickness to the curtain thickness.

The separation is shown at two stages, one corresponds to a potential of forty volts/cm. and the other to one hundred volts/cm. or to values of HE/v_o equal to 0.0864 and 0.216 volt sec/μm respectively where $\underline{H}$ is thirty cm. and the volumetric flow rate is twenty-five cm^3/minute. As Figure 5.2 shows, the migration distance is proportional to the value of HE/v_o. In this case the particles are shown injected in a cylindrical band with a diameter that is twenty percent of the channel thickness and is centered with respect to the thickness dimension. The migration distance scale runs from 14.0 to 36.0 mm. in absolute distance from the curtain edge which roughly covers the middle third of the column, with the sample being injected at 15.0 mm. Also, a 2^oC temperature gradient is assumed to develop as the particles progress through the electrode region. The particle mobility distribution and concentration data along with the wall electroosmotic mobility values are listed in Table 5.1 below, and the assumed electrophoretic mobility distributions are shown in Figure 5.3.

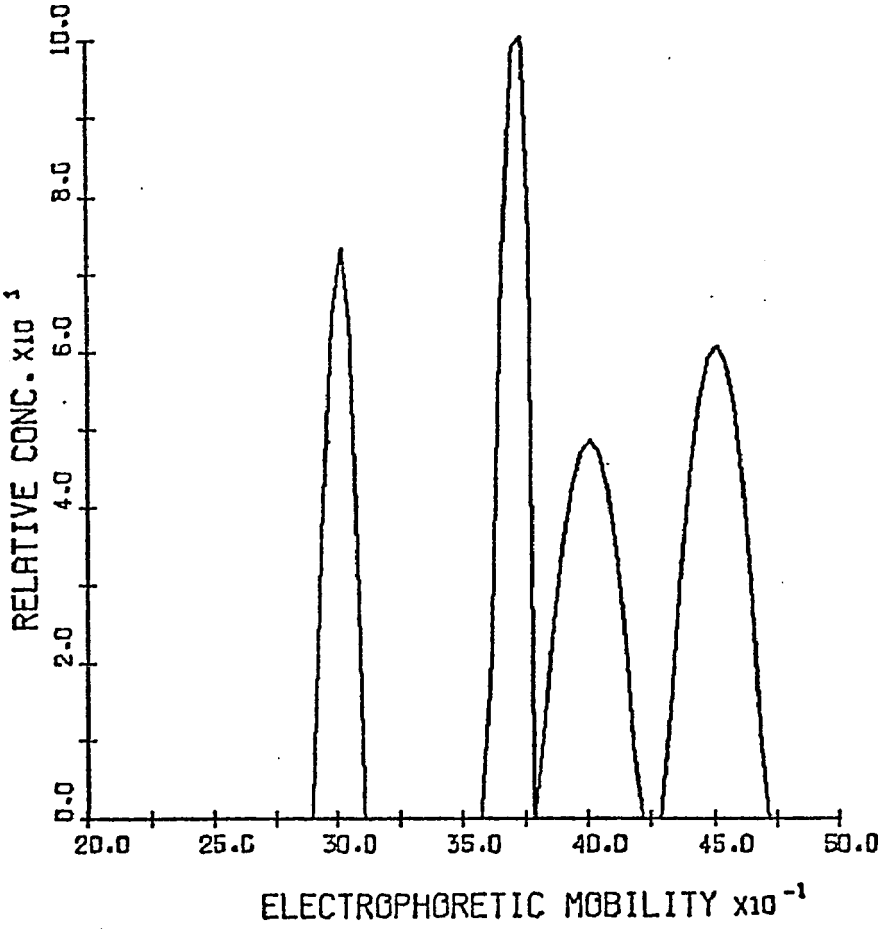

Figure 5.3. Mobility Distributions of Four Particles Which Were Used for Comparison of Various Parameters.

Table 5.1

Assumed Particle Mobility Distribution Data

Particle	Mean Mobility*	Range +	Range -	Relative Conc.	Distribution Shape
1	-3.0	0.1	0.1	60.0	Parabolic
2	-3.7	0.1	0.1	80.0	Parabolic
3	-4.0	0.2	0.2	80.0	Parabolic
4	-4.5	0.2	0.2	100.0	Parabolic

Electroosmotic Mobility Front and Rear Walls = -4.00 μm cm/volt sec

* - denotes negatively charged particles

The values presented above are not for any actual sample, but are values chosen to best exemplify the capabilities of the program and the effects of the various parameters. The first and second particle species have mobilities with absolute deviations of plus or minus 0.1 mobility units and are separable, while the third and fourth particle species have mobilities of plus or minus 0.2 mobility units and may be completely separable under optimum conditions. However, it should be noted that the mobility distributions of the second and third particle species touch but do not overlap. These two types of particles will never be completely separable since the sample stream has a finite thickness which will always show up as an overlap of the two bands. Also, the relative concentrations of the four species are varied to show the concentration effect on the peak height. In this case, the electroosmosis has been matched to the mean particle mobility which gives the best resolution under

these conditions.

When the above electrophoretic mobilities of the particles are assumed as a standard model, it is possible to change the different experimental parameters to determine the specific effect of each parameter. Figure 5.4 shows the effect of injecting the particles off-center in the curtain stream. The further off-center the bands are injected the poorer the resolution. This poor resolution results because the difference between the electrophoretic mobility of the fast or slow particles and the electroosmotic mobility is large; this distorts the bands as they are positioned closer to the wall. The resolution would be decreased even further if the electroosmotic mobility was higher or lower.

Figure 5.5 shows another effect where the electroosmotic mobilities of the two walls are different. The greater the difference in electroosmosis between the two walls, the more distorted will be the sample bands. The migration distance has remained about the same in all cases because the average electroosmotic mobility for both walls has remained the same. If the average mobility had increased or decreased then the migration distance would have increased or decreased proportionately.

Figure 5.6 shows the effect of increasing the injected band radius. This is similar to the effect shown in Figure 5.4 and results from a mismatch of the electroosmotic mobility and the electrophoretic mobility of the leading and trailing bands. In many cases the amount of processed sample or throughput rate is important and Figure

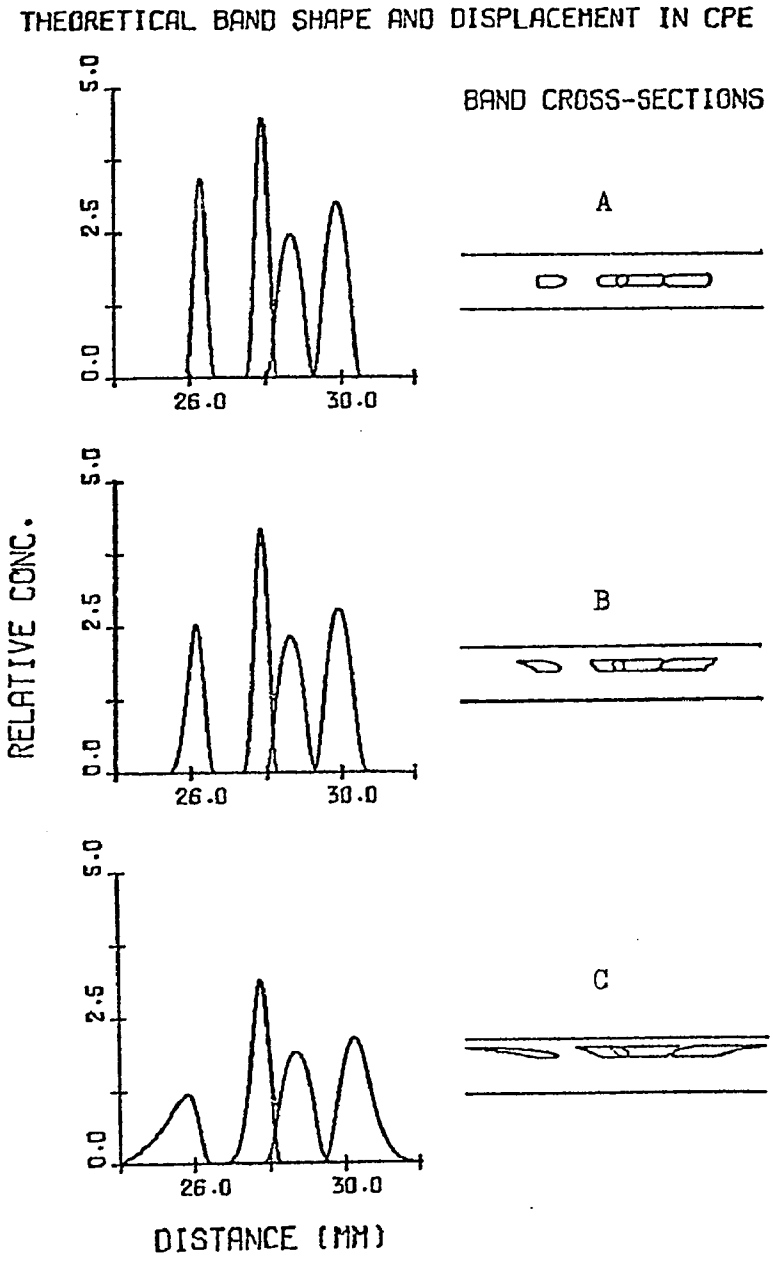

Figure 5.4. Computed Particle Displacement Showing the Effect of Off-center Injection on Band Separation with U_{os} = -4.00 μm cm/volt sec., and R = 0.2; A. Centered, B. 0.25 Off-center, and C. 0.5 Off-center.

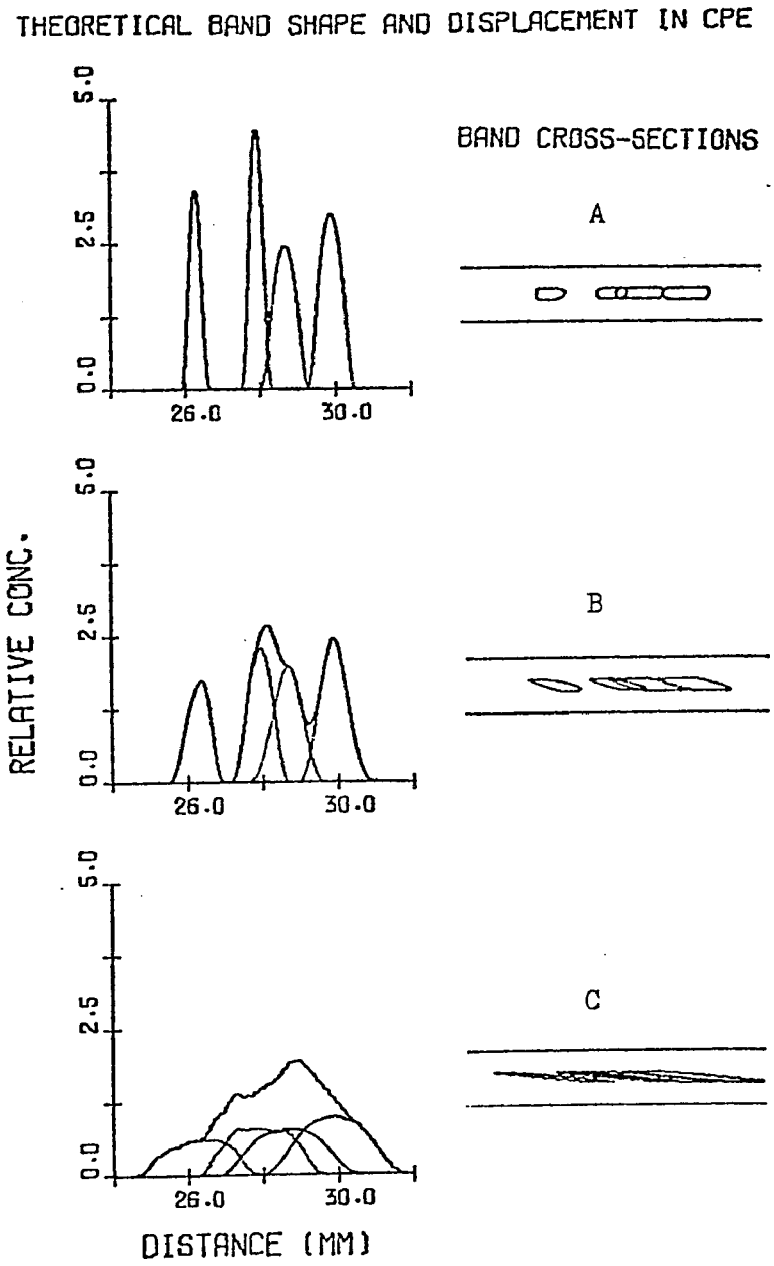

Figure 5.5. Computed Particle Displacement Showing the Effect of Different Values of U_{os} for the Front and Rear Walls with R = 0.2, and Average U_{os} = -4.00 μm cm/volt sec.; A. $U_{osf} = U_{osr}$ = -4.00 μm cm/volt sec., B. U_{osf} = -5.00 μm cm/volt sec, U_{osr} = -3.00 μm cm/volt sec., C. U_{osf} = -7.00 μm cm/volt sec, U_{osr} = -1.00 μm cm/volt sec.

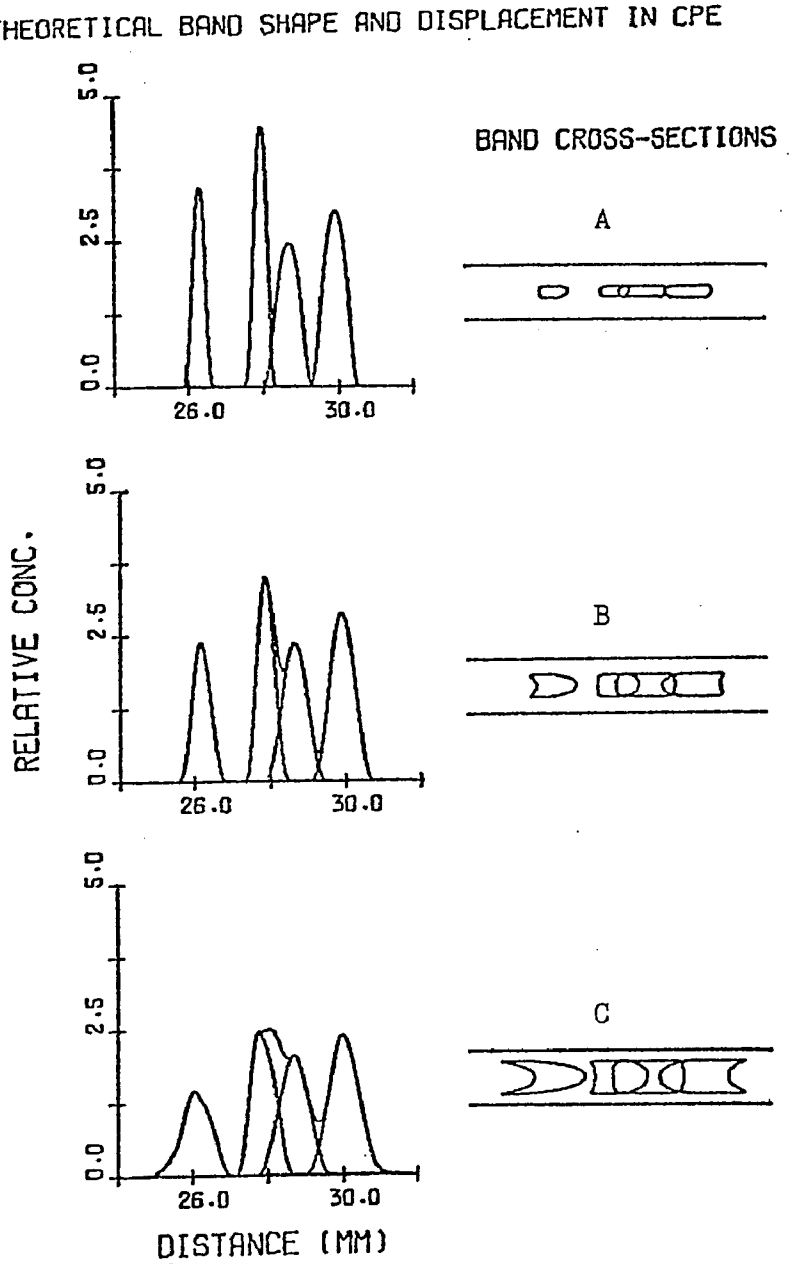

Figure 5.6. Computed Particle Displacement Showing the Effect of Increasing the Injection Radius with U_{os} = -4.00 μm cm/volt sec.; A. R = 0.2, B. R = 0.4, and C. R = 0.6.

5.6 demonstrates the trade off in resolution by going for higher band volume. Again, the resolution would appear much worse if the electroosmotic mobility was not matched to the mean particle mobility.

Continuing along the same lines of increasing the sample throughput volume, it would be interesting to find out which dimension, i.e., in the X or Z direction as defined in Figure 5.1, is the most detrimental to the resolution. Figure 5.7 shows this effect when the sample is injected in a rectangular shape rather than a circular shape. For simple circular geometry, if the radius is doubled the area and sample throughput increases by a factor of four. However, in rectangular geometry one dimension can be doubled or tripled resulting in a corresponding doubling or tripling of sample throughput to determine the optimum direction of sample increase. In the upper left hand corner of each diagram the original size of the sample stream, relative to the cell thickness, is shown. From these results one would conclude that it is better to increase the sample width, or increase the $\underline{R}$ value, rather than the thickness, $\underline{\theta}$, in the direction of migration. However, this might not necessarily always be the case, as shown in Figure 5.8 where the electroosmosis value has been changed to a lower value, not matching the mean particle mobility. Now, increasing the band width, $\underline{R}$ value, results in highly elongated cones while increasing the thickness only causes minor distortions. In this case it would be better to increase the stream thickness to gain more throughput. These results show that the relative effects of the sample width and thickness on resolution are a sensitive func-

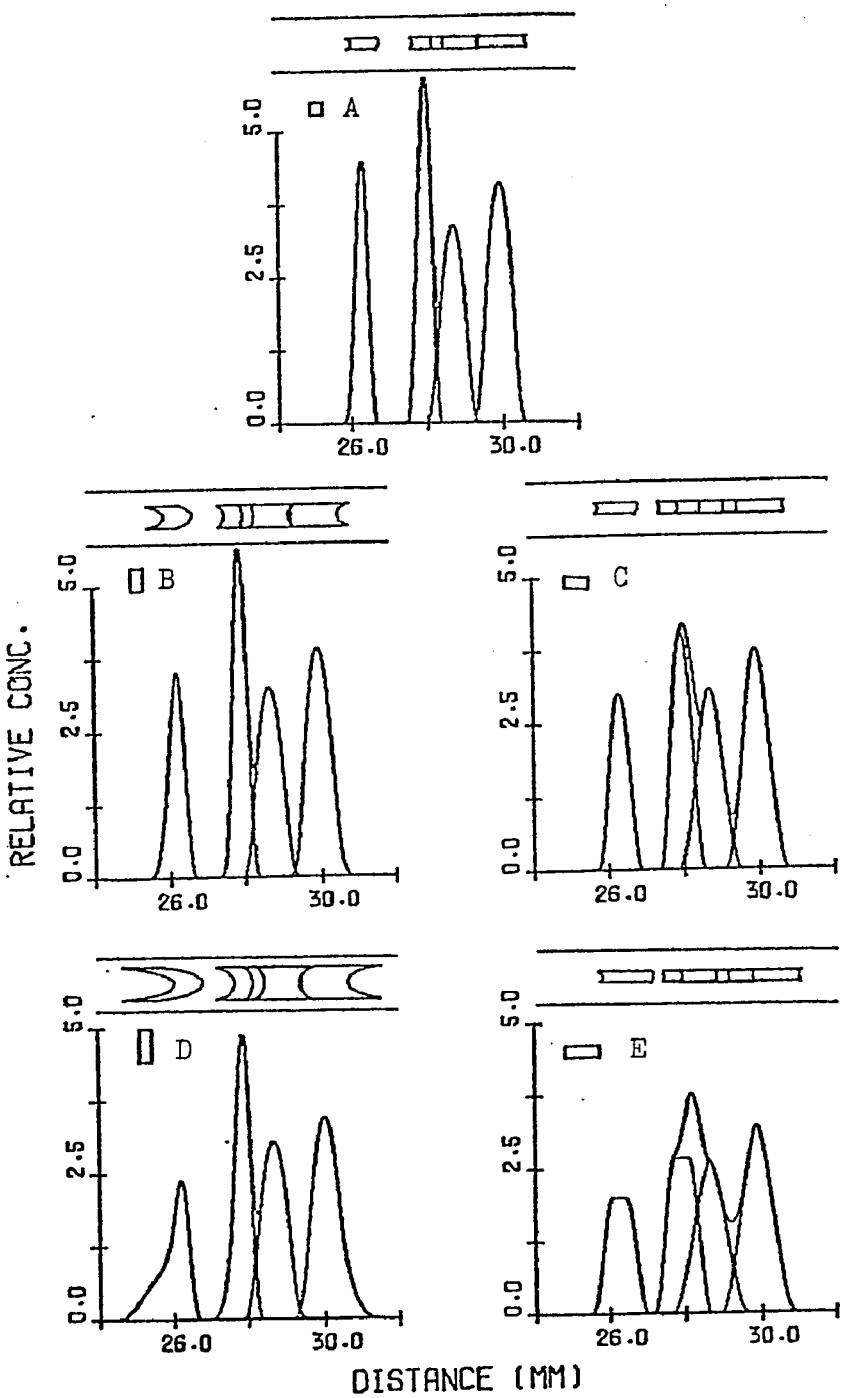

Figure 5.7. Computed Particle Displacement Showing the Effect of Increasing Band Volume in the R or θ Direction with U_{os} = -4.00 μm cm/volt sec.; A. R = 0.2, θ = 0.2, B. R = 0.4, θ = 0.2, C. R = 0.2, θ = 0.4, D. R = 0.6, θ = 0.2, and E. R = 0.2, θ = 0.6.

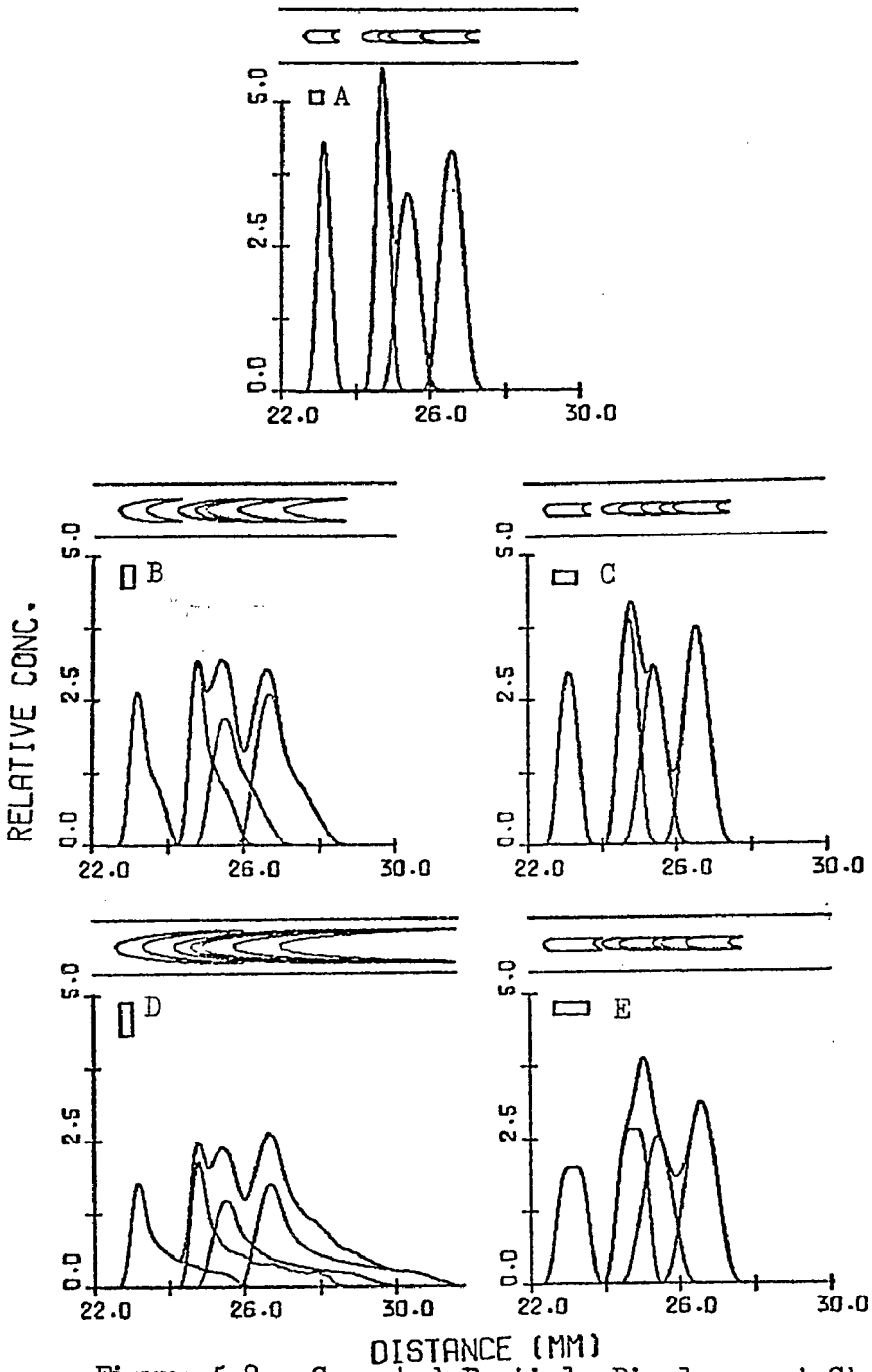

Figure 5.8. Computed Particle Displacement Showing the Effect of Increasing Band Volume in the R or θ Direction with U_{os} = -1.00 μm cm/volt sec.; A. R = 0.2, θ = 0.2, B. R = 0.4, θ = 0.2, C. R = 0.2, θ = 0.4, D. R = 0.6, θ = 0.2, and E. R = 0.2, θ = 0.6.

tion of the level of electroosmosis relative to the particle mobilities. In general, the value of electroosmosis relative to the particle mobilities is the most important consideration in obtaining high resolution and particle throughput.

Finally it is important to look at the effect of electroosmosis itself as presented in Figure 5.9. Electroosmosis is a horizontal motion of the fluid in the curtain, as shown before in Figure 5.1, which is additive to the particle velocity. Therefore, under the same applied potential but different electroosmotic values, the particle displacement distances will be different as seen in Figures 5.9A, 5.9B, and 5.9C where the electroosmosis is -4.00, -1.00, and -7.00 μm cm/volt second respectively. In Figures 5.9D and 5.9E the applied voltages were adjusted to the appropriate values to obtain the same migration distance as in 5.9A. When this is done the interpeak distances become quite different and therefore can affect the resolution.

Under the five conditions shown in Figure 5.9 the resolutions appear to be about equal, but when they are analyzed for the maximum amount of each species that may be obtained in pure form, it is possible to see which conditions yield the best resolution. Tables 5.2 and 5.3 based on the maximum attainable theoretical purity, show more clearly which conditions are best. In each table, the percentage of species which is in pure form is listed as a function of the value of electroosmosis and the applied potential, and these percentages are then totaled to give an indication of the resolution. Table 5.2 shows that it may be advantageous for short separation distances to have a

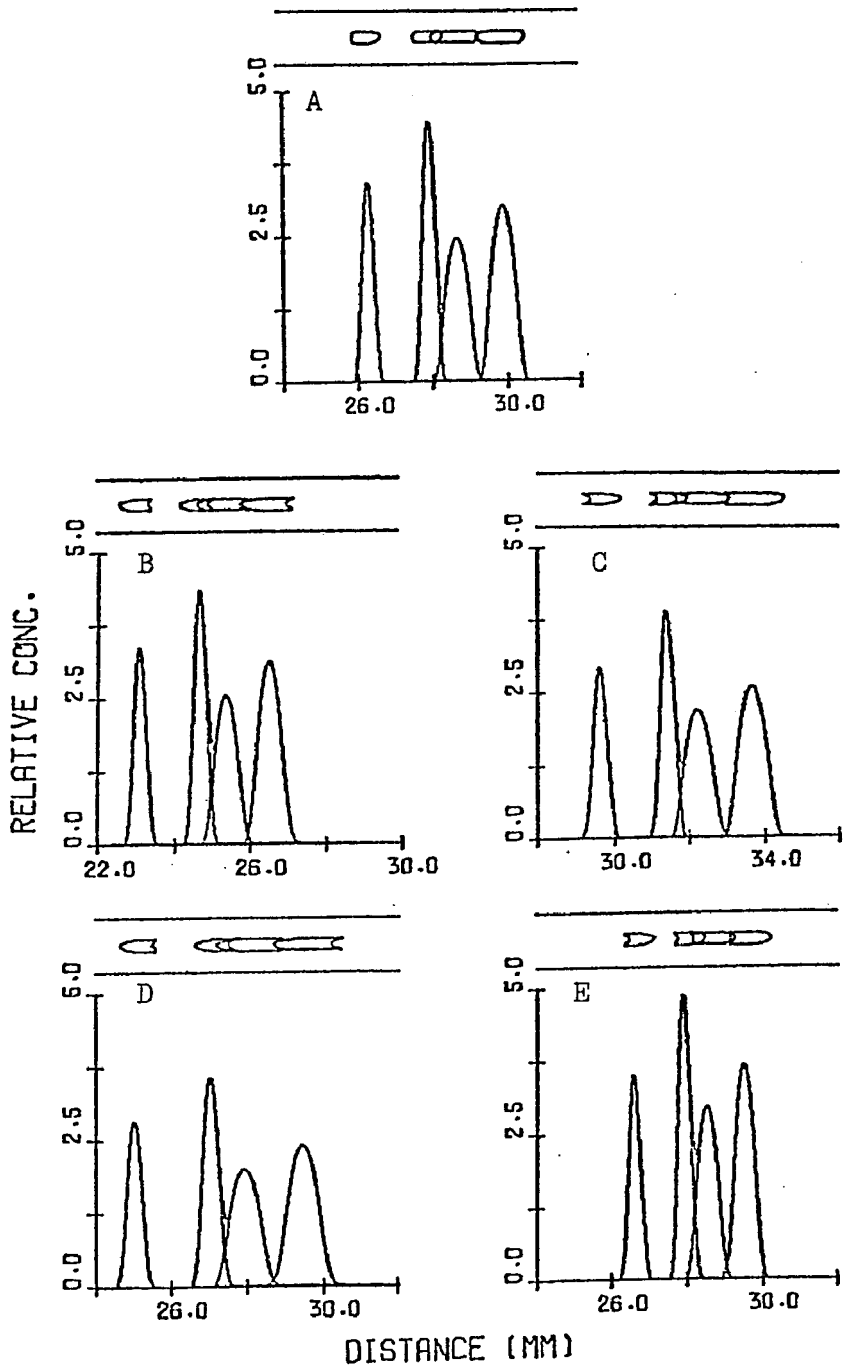

Figure 5.9. Computed Particle Displacement Showing the Effect of Electroosmosis and Adjusted Voltage Gradients with R = 0.2; A. U_{os} = -4.00 um cm/volt sec, 100.0 volts/cm, B. U_{os} = -7.00 um cm/volt sec, 100 volts/cm, C. U_{os} = -1.00 um cm/volt sec, 100.0 volts/cm, D. U_{os} = -7.00 um cm/volt sec, 80.0 volts/cm, and E. U_{os} = -1.00 um cm/volt sec, 130.0 volts/cm.

Table 5.2

Maximum Obtainable Purity for Resolution Comparison with R = 0.2

	U_{os} = -4.0	U_{os} = -1.0		U_{os} = -7.0	
Particle	Potential Gradient (volts/cm)				
	40	40	53	40	32
1	100.00	100.00	100.00	100.00	100.00
2	20.20	20.58	28.17	30.99	21.49
3	46.37	39.27	59.64	43.38	21.66
4	87.03	83.43	90.92	87.72	66.11
Total	253.60	243.28	278.73	262.09	209.26

Particle	Potential Gradient (volts/cm)				
	100	100	130	100	80
1	100.00	100.00	100.00	100.00	100.00
2	75.82	48.00	63.16	57.81	45.18
3	89.81	73.87	82.72	87.26	78.87
4	99.99	95.36	97.88	99.90	98.46
Total	365.62	317.23	343.76	344.97	322.51

Table 5.3

Maximum Obtainable Purity for Resolution Comparison with R = 0.4

Particle	U_{os} = -4.0	U_{os} = -1.0		U_{os} = -7.0	
	Potential Gradient (volts/cm)				
	40	40	53	40	32
1	95.38	82.74	94.74	62.04	57.55
2	8.06	0.00	0.00	0.00	0.00
3	0.00	0.00	0.00	0.00	0.00
4	46.59	18.86	16.51	31.38	25.87
Total	150.03	101.60	111.25	93.42	83.42

Particle	Potential Gradient (volts/cm)				
	100	100	130	100	80
1	100.00	99.89	100.00	85.54	75.58
2	42.38	14.08	19.15	1.95	0.00
3	65.81	0.00	0.00	0.00	0.00
4	95.43	17.93	22.21	80.17	63.68
Total	303.62	131.90	141.36	167.66	139.26

lower value of electroosmosis with a higher applied voltage gradient. This, in effect, uses more separation distance for electrophoretic migration and less for electroosmotic migration. Table 5.3 shows the same information, but at a higher sample throughput due to larger sample injection radius. This table readily shows how the resolution is affected by an increase in R, with many of the total percentages being less than half the magnitude in comparison to when R was equal to 0.2. For this case, matching the electroosmotic mobility and electrophoretic mobility again gives best resolution. The effect of a larger sample radius on the final band shape and appearance is shown in Figure 5.10, where matching electroosmosis to the mean particle mobility gives the best resolution.

The above considerations demonstrate that there is no simple method for choosing the optimum separation conditions. The resolution depends on many variables such as the mobility distributions of the species, the sample injection shape, thickness, and amount, the applied voltage, the value of electroosmosis in relation to the particle mobilities, and the channel dimensions. However, this theoretical analysis and prediction technique can be a valuable first step to obtaining the best separation conditions for a given set of restrictions. Even though we cannot define the absolute optimum conditions for every situation, these results do show the trends which should be considered in attempting to optimize the resolution.

Another useful feature of the computer model is that it allows one to predict where various fractions of a very broad mobility distribution might be found. For instance, if the data from a bar graph

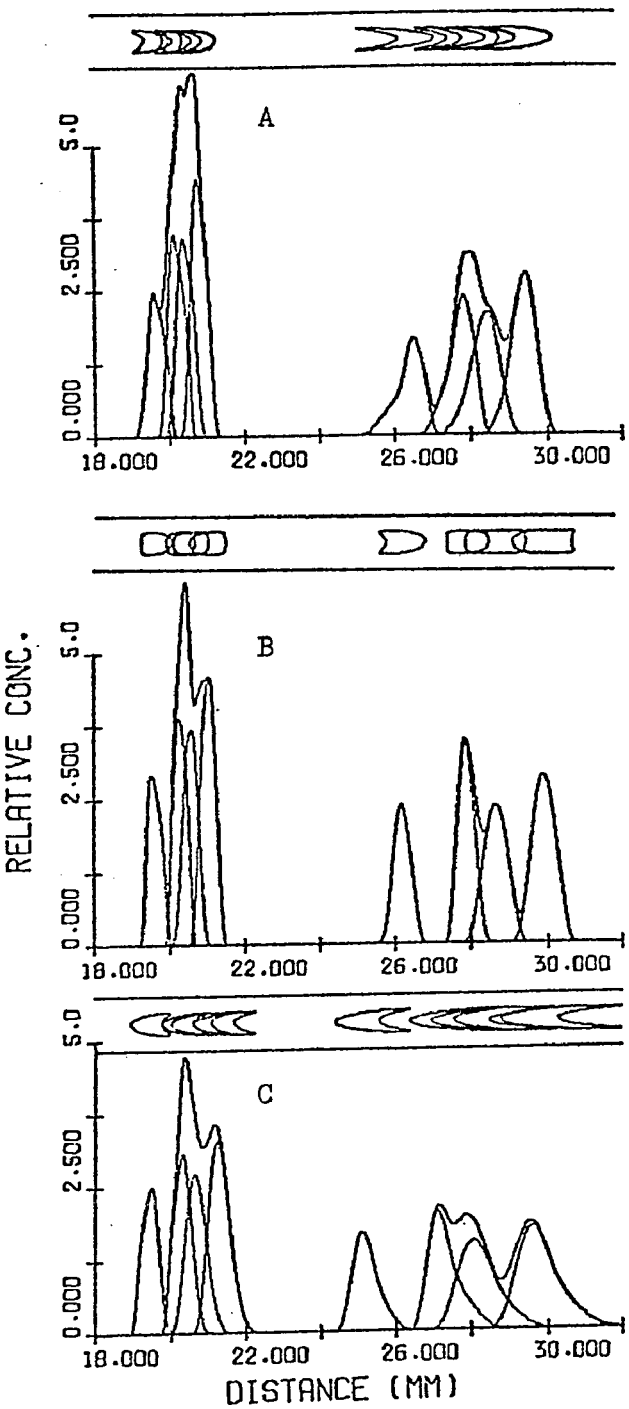

Figure 5.10. Computed Particle Displacement Showing the Effect of Electroosmosis with R = 0.4; A. U_{os} = -1.00 μm cm/volt sec., B. U_{os} = -4.00 μm cm/volt sec., and C. U_{os} = -7.00 μm cm/volt sec.

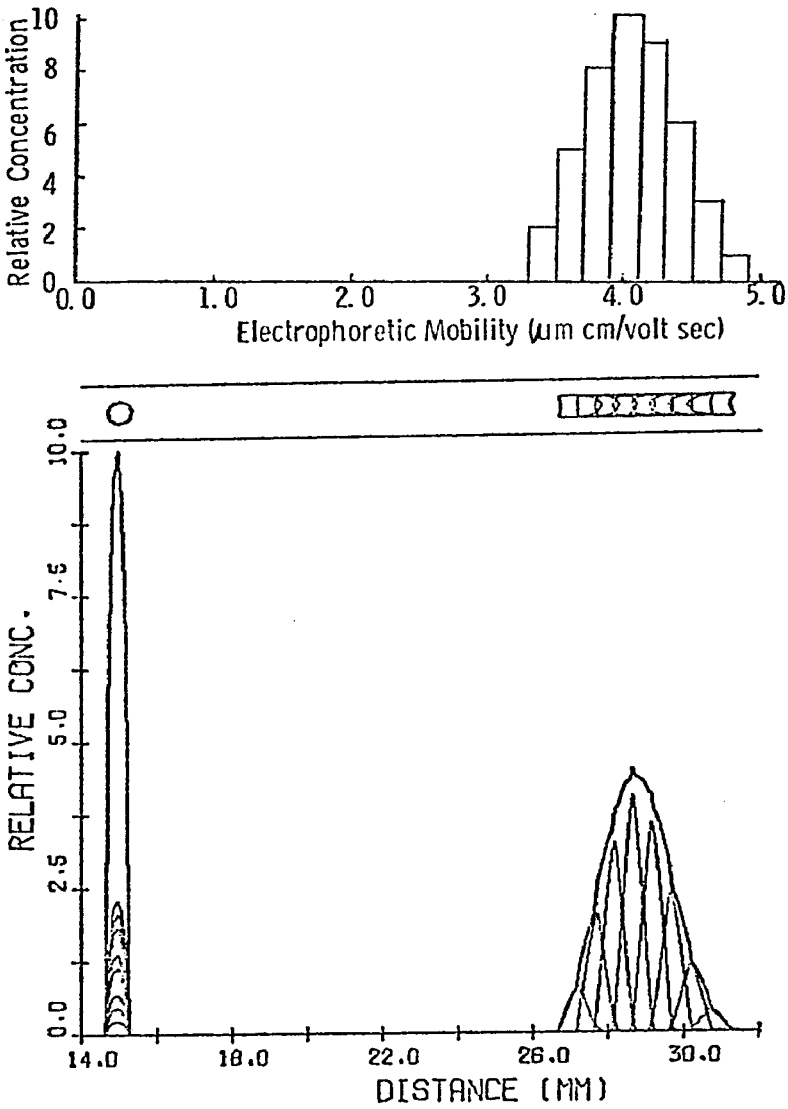

Figure 5.11 Computed Particle Displacement and Mobility Distribution Showing Usefulness for Predicting Where Various Fractions Will be Found for a Broad Mobility Species.

mobility distribution were fed in, it would show where each fraction, could be found and how it would be distributed. Figure 5.11, which demonstrates this approach, shows where the eight fractions of a bar graph, assuming a square distribution for each fraction, could be found. For this example the value of electroosmosis was chosen so as to be equal to the median electrophoretic mobility, and the injection radius is 0.4 of the cell thickness. Such an analysis can be very useful in determining what mobility fractions might be found in the collected samples of a CPE run for a practical biological system which are frequently singly peaked.

C. SPAR CPE Modeling

The computer program is also flexible enough to permit other configurations of a CPE to be modeled, provided the flows are laminar and stable and the theory and assumptions are still applicable. For instance, the SPAR(acronym for Space Processing Applications Rocket) CPE is a large slit width CPE which was designed for microgravity conditions, where the flow conditions would be laminar and unaffected by the high temperature gradients which develop in a wider slit. The dimensions of the SPAR CPE channel are 0.5 x 5.0 x 10.0 centimeters, so the thickness has been increased by a factor of 3.3 while the electrode length has been shortened by a factor of 3.0 from the conventional Beckman CPE design. The advantage of this thicker channel is that more sample can be injected by increasing the sample stream injection radius, while the effect of electroosmosis is not increased since the ratio of the injection radius to channel thickness may be

the same as in a narrow channel CPE or even less for improved resolution. The disadvantage of the cell dimensions is that a much larger temperature gradient from Joule heating will develop, which in a normal gravity environment would be disastrous to the laminar flow profile causing convection cells within the flow stream and a resulting loss of resolution. However, in a microgravity environment, which is the environment for which the SPAR CPE was designed, there will be minimal gravity-induced density differences to disrupt the laminar flow. A good deal of modeling has been done by D. A. Saville and S. Ostrach on these temperature induced flows[24], however this model is sufficient when one assumes that the system is in normal laminar flow as would be found in a microgravity space situation.

Figure 5.12 shows a predicted separation of three monodisperse latexes proposed for the SPAR mission, as would be seen in a Beckman narrow channel CPE at 15 and 30 volts/centimeter in an R-1 buffer under flow conditions which predict a residence time of twenty-two seconds. The value of 30 volts/centimeter is the maximum attainable voltage gradient in the Beckman due to the high conductivity of the R-1 buffer. Figure 5.13 shows the predictions for the same three particle species in the SPAR CPE at the proposed conditions of the experiment for two values of sample injection radius. In this case the potential gradient is 65 volts/centimeter and the residence time is thirty-three seconds. The much larger separation distance between peaks is quite evident from these models. Although the overall migration is about the same, the electroosmosis in both channels is different. In the SPAR CPE the electroosmosis is -3.00 μm cm/volt second

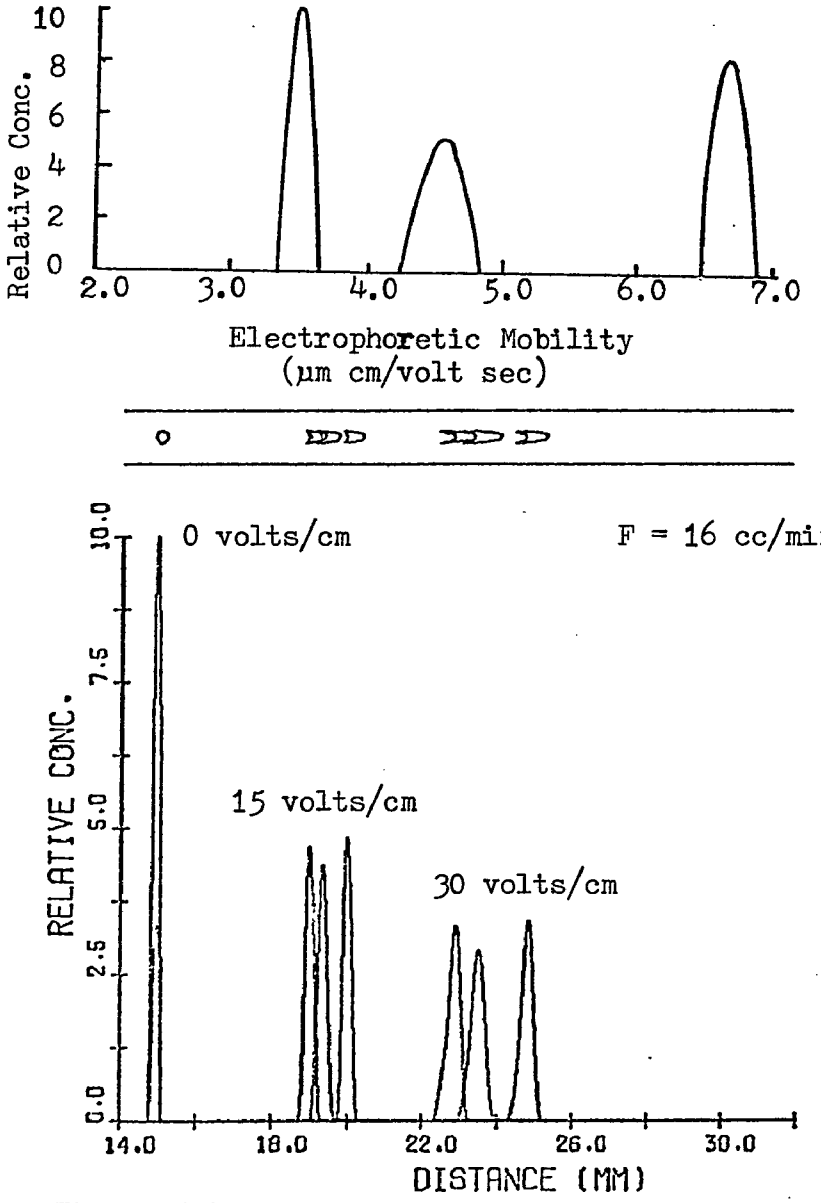

Figure 5.12. Computed Displacement and Electrophretic Mobility Distributions in the Beckman CPE of a Sample Proposed for the SPAR CPE.

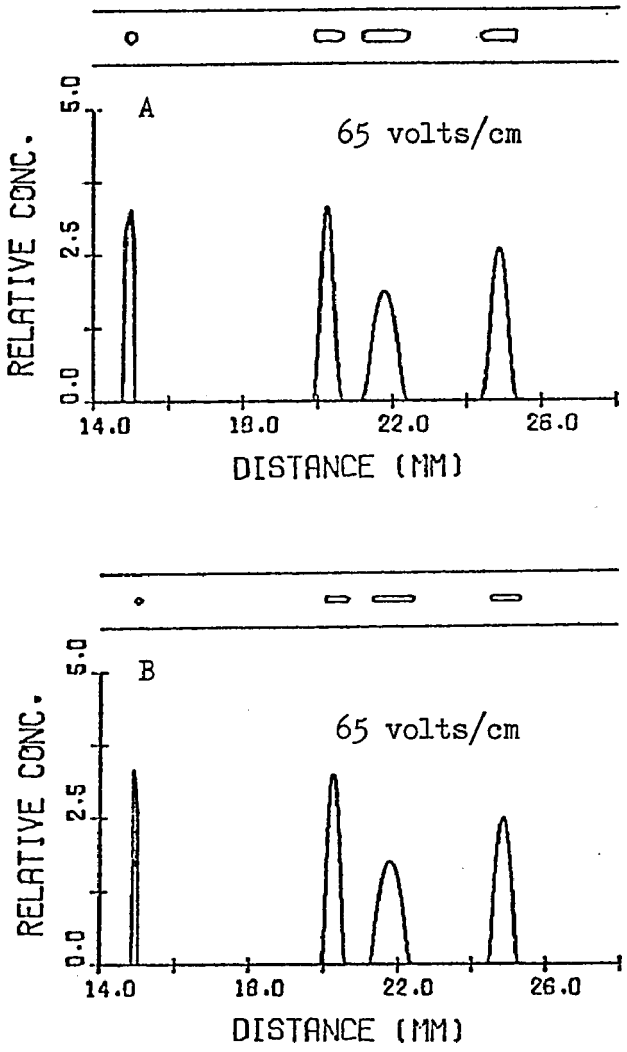

Figure 5.13. Computed Displacements in the SPAR CPE for Two Values of R; A. R = 0.2, and B. R = 0.1.

and the applied potential high while in the Beckman CPE the electroosmosis can greatly affect the overall migration distance but have a minimal effect on band distortion for small values of the ratio of sample thickness to cell thickness, R.

D. Comparison of Experiment to Theory

The computer model allows a direct comparison between theoretical and experimental separations. Figure 5.14 shows the separation of the three proposed latexes for the SPAR electrophoresis experiment as they were separated in a Beckman CPE. Figure 5.14A presents the theoretical separations, assuming equal weight percents of each particle and mobility distributions as shown in Figure 5.12. The heights of the peaks are related to the spread of each particle distribution since the area under each peak is the same. Figure 5.14B shows the experimental results obtained on the Beckman CPE. In this case, the peak heights are related to the narrowness of the bands also, but more importantly to the wavelength of the UV light source and the degree of absorbance and reflection of each particle species. Although the peak heights do not match, the actual displacement distances and the spreads of the peaks show very good agreement.

Figure 5.15 shows a separation of the seven latexes presented in Chapter IV. These latexes ranged in size from 2.02 μm to 0.088 μm, and were run in the Beckman CPE in the barbital-sodium barbital buffer at 2×10^{-3} ionic strength. Again the concentration by weight of each species was equal in both the theoretical and experimental curves and the experimental peaks show a strong dependence on particle size.

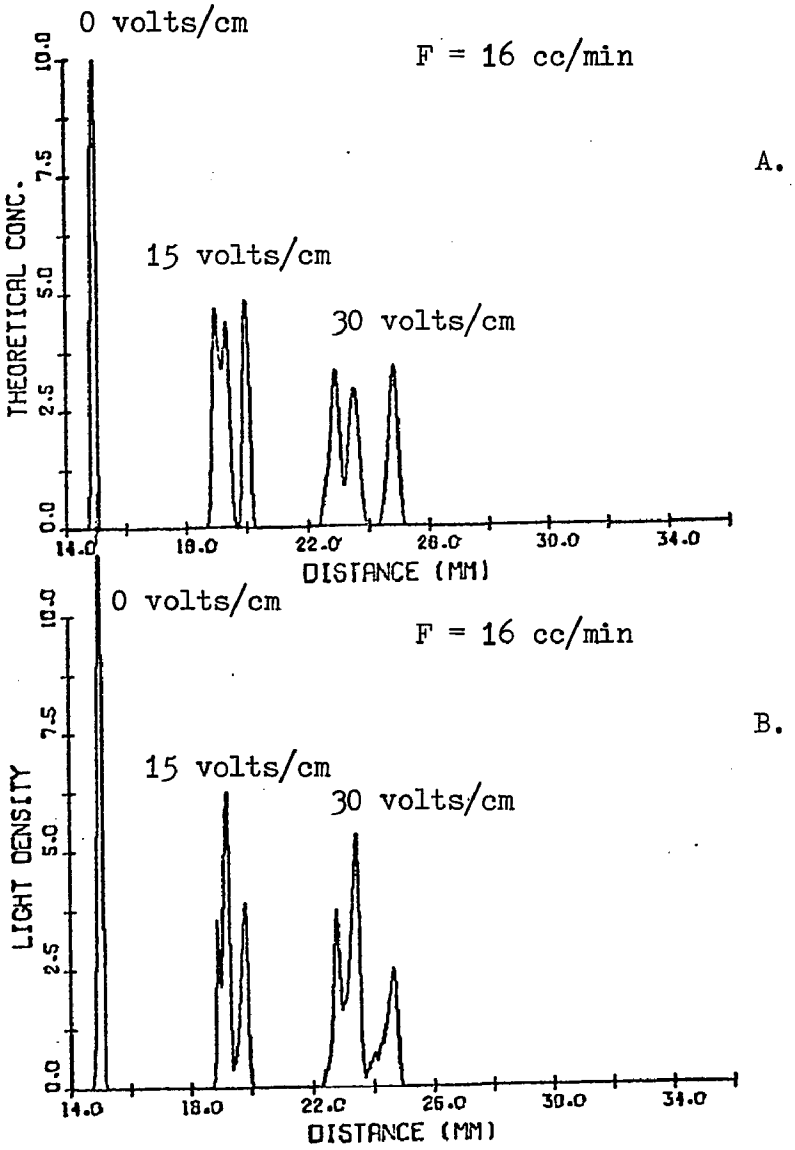

Figure 5.14. Comparison of the Theoretical and Experimental Separations of the Three Latexes Proposed for The SPAR CPE.

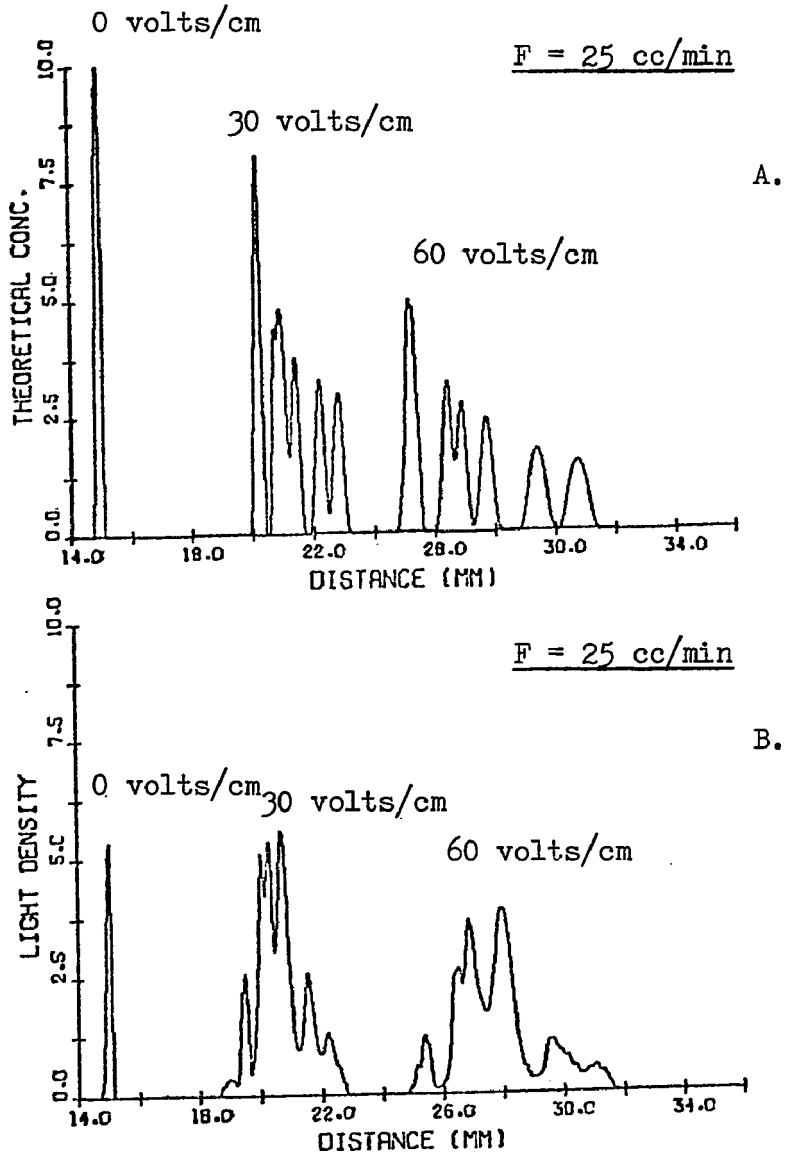

Figure 5.15. Comparison of the Theoretical and Experimental Separations of the Seven Latexes Ranging in Size From 2.02 μm to 0.088 μm.

The particle displacements compare well, but there is some difference at the lower voltage. This effect can result from not allowing the bands to reach the equilibrium position. It has been noticed that the peak-to-peak distance develops a rather quick equilibrium upon changing the voltage(on the order of fifteen to thirty seconds) while the absolute displacement from the zero voltage reference takes longer (often five minutes or more) to come to an equilibrium position. This is probably due to the slow development of the electroosmotic flow profile down the length of the cell. However, in both examples the agreement between theory and experimental is quite good.

No attempt has been made to relate the peak heights to the Mie[30] theory since the latex concentration is often very high(five to thirty percent by weight), and in this range there is usually no variation in the heights of the various peaks, or if there is, it is usually related to the sharpness of the peak rather than the particle size or concentration. At lower concentrations, however, it would be interesting to compare the Mie theory predictions to the band intensity.

Modeling of the CPE has allowed many possibilities, both in analyzing results and in predicting the theoretical optimum separations. By being very flexible and general, it allows many parameters to varied to determine the specific effect of each.

Chapter VI

Particle-Particle Interactions Affecting Mobility Measurements

The nature of the electrical double layer around a particle, and how it affects the behavior of that particle can be a difficult concept to measure experimentally. The Derjaguin-Landau-Verwey-Overbeek (DLVO) theory describes this phenomenon quite well in terms of repulsive and attractive forces; however, experimental results except for cases of coagulation and flocculation can be difficult to compare to the theory. Through many experiments on the CPE, it has become evident that the separated bands do not always agree precisely with microcapillary electrophoresis measurements which are carried out under very dilute concentrations. It is felt that this anomaly of results may be an indication of this particle-particle interaction of electrical double layers. For instance, as one band of particles moves through a second band, due to the high concentration of particles possible in the CPE, the electrical double layers will overlap and interact, resulting in a force which may slow down the faster band or accelerate the slower band so that the band displacement does not reflect its true mobility. This interaction of double layers and factors affecting mobility will be the subject of this chapter.

A. DLVO Theory

The DLVO theory states that an ionic cloud and an electrical double layer exist around most colloid particles. The electrical double layer around a polystyrene latex particle arises from the

negative surface groups such as SO_4^- and COO^- groups which give the particle a net negative charge. Around the surface then are found a large number of positive counter ions which make up the double layer as shown in Figure 6.1. This double layer cloud is not fixed, but can expand or shrink as a function of the electrolyte concentration. The effect of the surface potential then falls off in an exponential manner with distance due to the shielding or neutralizing effect of the counter ions.

Now when two particles come into close proximity to each other their double layers will begin to interact due to the displacement of a number of the counter ions. This interaction results in a net repulsive force which, depending on electrolyte conditions, tends to keep the particles from coming together and sticking, thereby stabilizing the dispersion.

The basic equations relating the repulsive and attractive interaction forces for two sphere systems have been taken from Verwey and Overbeek[3]. Basically the potential energy is broken down into two terms, one repulsive due to the similar charges of the two spheres and the shielding effect of the dissociated ions surrounding the spheres, and the other attractive due to the Van der Waals interaction. Other forces may be present such as Born repulsion at very short distances and steric considerations due to long chain molecules, but these will not be considered here, since electrical effects are assumed to predominate.

From Verwey and Overbeek[3], the attractive potential may be represented in equation form as:

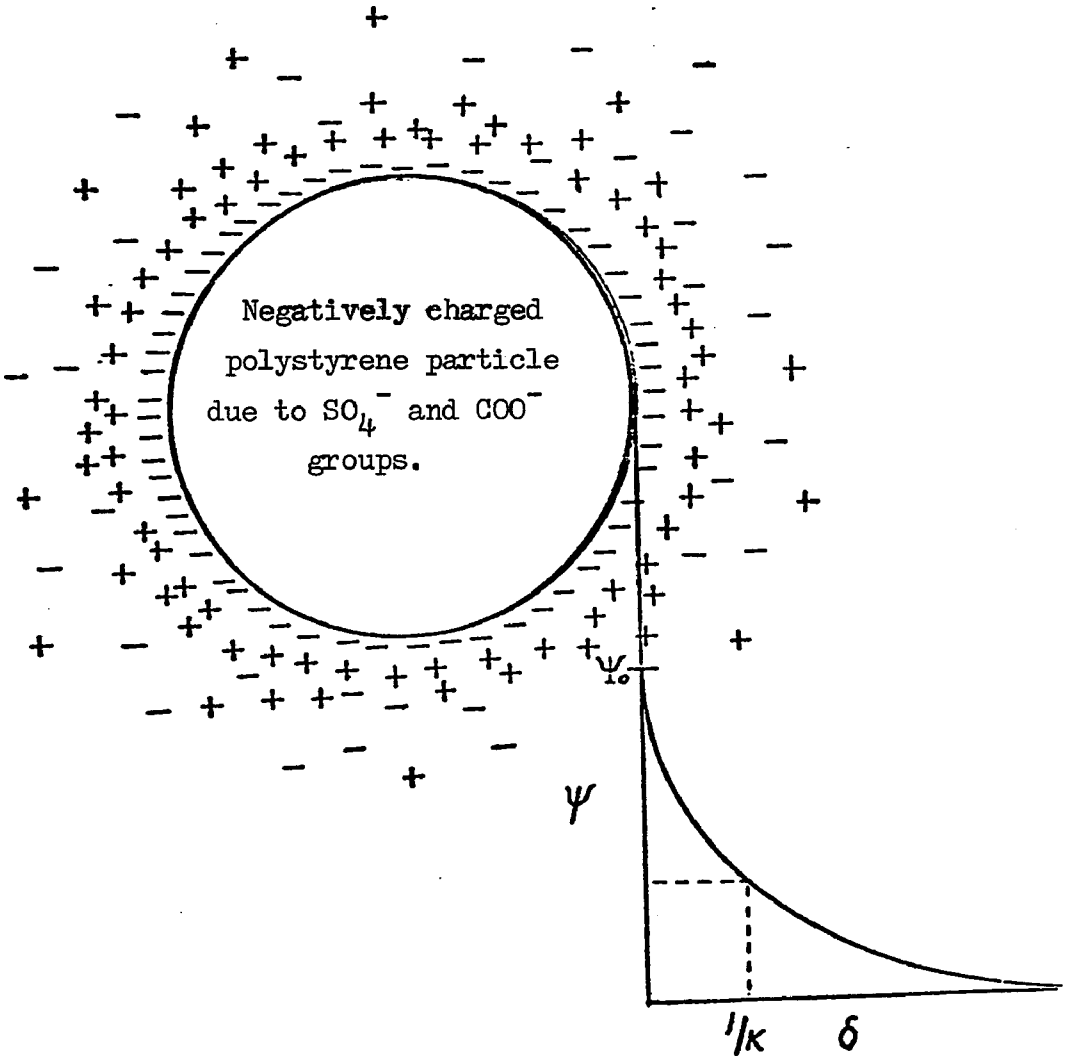

Figure 6.1. Typical Representation of the Ionic Double Layer Cloud and Potential Gradient Distribution.

$$V_A = \frac{-A_h}{6}\left(\frac{2}{s^2 - 4} + \frac{2}{s^2} + \ln \frac{s^2 - 4}{s^2} \right) \tag{6.1}$$

where A_h is the Hamaker constant and s is the ratio of R/a (R being the center-to-center distance of two particles and a the particle radius. Typical values of A_h for a polystyrene latex are in the range from 10^{-13} to 10^{-15} ergs and have been calculated by various authors. For the following calculations a value of 5×10^{-14} ergs was chosen as determined by Fowkes[29].

The repulsive potential of two spheres may be defined for two cases, depending on the value of τ which is equal to κa, the product of the reciprocal double layer thickness and the particle radius. The value of κ may be defined as:

$$\kappa^2 = \frac{8\pi ne^2v^2}{kT} \tag{6.2}$$

where n is the ion concentration, e is the electronic charge, v is the valency, k is Boltzmann's constant, and T is the temperature. For $\tau > 2.5$, corresponding to large particles and a thin double layer, the following equation may be used:

$$V_R = \frac{\epsilon a \psi_o^2}{2} \ln \left(1 + e^{-\tau(s - 2)} \right) \tag{6.3}$$

where ϵ is the dielectric constant of the medium and ψ_o is the surface potential in millivolts. On the other hand, if $\tau < 2.0$, which means small particles with extended double layers, the following equation may be used:

$$V_R = \frac{\epsilon a \psi_o^2 e^{-\tau(s - 2)}}{s} \beta \tag{6.4}$$

where β is a complex function of τ and s and depends on whether the system may be considered to have a constant surface potential or constant charge. Under low electrolyte conditions the assumption of constant charge is usually best. However, typical values for β lie in the range from 0.6 to 1.0 for either condition.

Similar equations have been derived by Oshima[27] for interactions between particles of different radii and surface charge density which are:

$$V_R = \frac{8\pi^2 a_1 a_2 (R - a_1)(R - a_2)}{\epsilon K^2 R\left[(a_1 + a_2)R - a_1^2 - a_2^2\right]}\left[\frac{C\sigma_1\sigma_2}{\bar{\alpha}_1\bar{\alpha}_2}\ln\left(\frac{1 + \sqrt{\bar{\alpha}_1\bar{\alpha}_2 A}}{1 - \sqrt{\bar{\alpha}_1\bar{\alpha}_2 A}}\right)\right.$$

$$\left. -\left(\frac{\sigma_1^2}{\bar{\alpha}_1} + \frac{\sigma_2^2}{\bar{\alpha}_2}\right)\ln\left(1 - \bar{\alpha}_1\bar{\alpha}_2 A\right)\right] \qquad (6.5)$$

where:

$$R = H_o + a_1 + a_2$$

$$\alpha_i = (1 + (\epsilon/\epsilon_i)2Ka_i)^{-1}$$

$$\bar{\alpha}_i = (1 - \alpha_i)/(1 + \alpha_i)$$

$$A = A_1 A_2 \qquad (6.6a\text{-}e)$$

$$A_i = a_j/(R - a_i)\exp(-KH_o)$$

$$C = \sqrt{A_1/A_2} + \sqrt{A_2/A_1}$$

In these equations, H_o is the surface-to-surface distance with a_1 and a_2 being the respective radii, and σ_1 and σ_2 are the respective surface charge densities. This equation is valid for the conditions where $\alpha_1 \ll 1$ and $\alpha_2 \ll 1$.

The attractive potential has then been described by Hamaker[28]

as:

$$V_A = -\frac{A_h}{6}\left[\frac{y}{x^2 + xy + x} + \frac{y}{x^2 + xy + x + y} + 2 \ln\left(\frac{x^2 + xy + x}{x^2 + xy + x + y}\right)\right] \qquad (6.7)$$

where:

$$x = H_o/2\, a_1$$
$$y = a_2/a_1 \qquad (6.8a\text{-}c)$$
$$a_1 < a_2$$

These two equations then yield the potential of interaction between two latexes of different size.

Applying equations 6.1 and 6.3 to the three latexes used in determining the particle-particle interactions, we obtain the results shown in Figure 6.2 for the three electrolyte levels of interest. These curves are only for interactions between particles of the same size. The three particles were the 0.234, 0.357, and 0.46 micron polystyrene latexes which had surface potentials of 96, 105, and 121 mV respectively. The curves show that increased surface charge and size increases the double layer, and also that decreasing the electrolyte significantly extends the double layer. As seen from the curves, the repulsive barrier is very steep and high. No primary attractive minimum is shown because it occurs very close to the particle surface at less than 1.0 Angstrom units in distance. This is because the surface charge is quite high for these latexes. For an electrolyte strength of 1×10^{-3} the double layer extends to

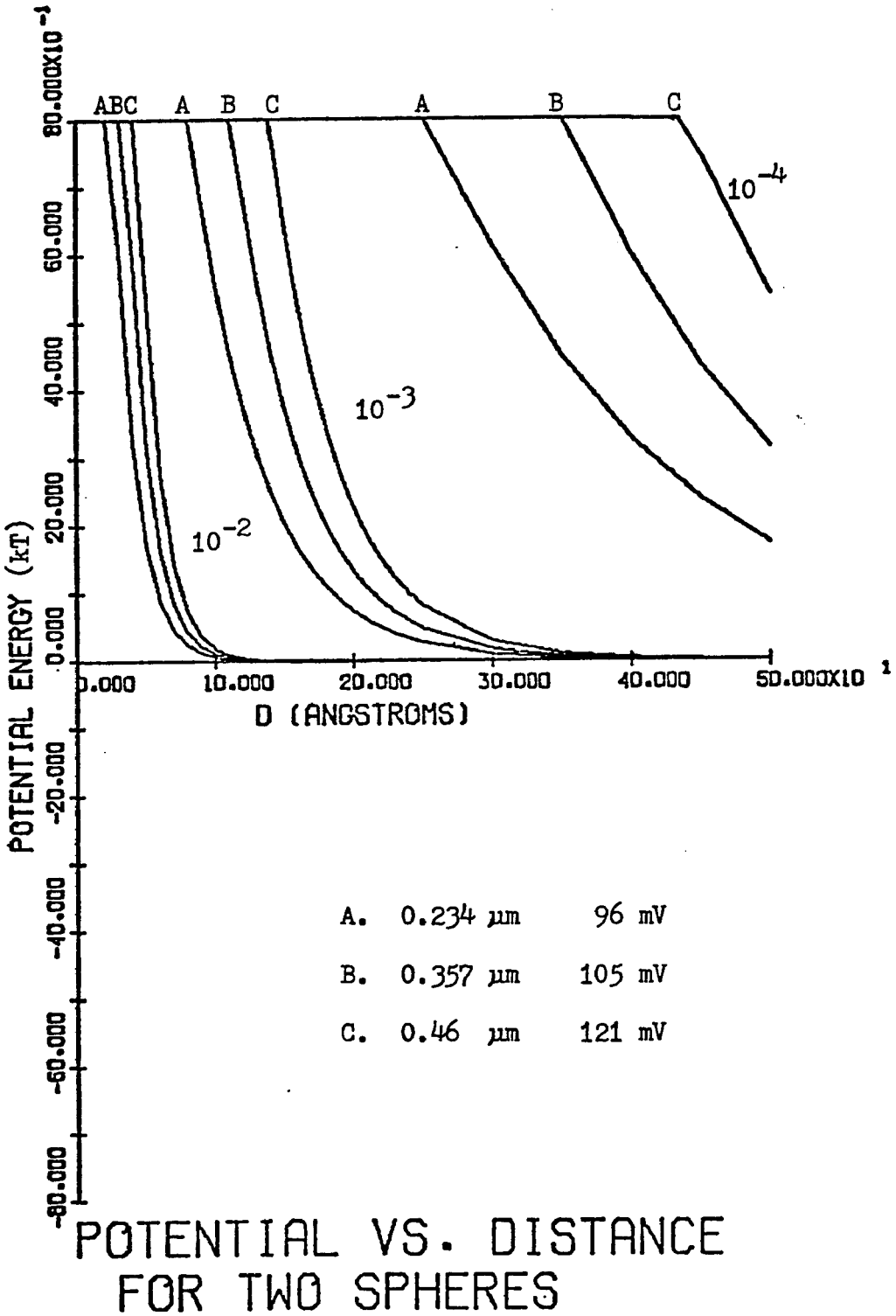

Figure 6.2. Potential Energy Curves Showing the Effect of Ionic Strength and Particle Size on Double Layer Extension

about 200 to 300 Angstroms which is about 15 to 20 percent of the particle radii. This then increases the effective particle volume by 60 to 70 percent.

B. Nature of the Interactions

The extended double layer, then, can be an important factor to consider as a band of faster particles moves through a band of slower particles. The polystyrene latexes used in this work exhibit electrophoretic mobilities that are a function of the size of the latex, where increased size results in increased mobility. Therefore, one may consider a moving field of particles, as depicted in Figure 6.3, where the arrows indicate the difference in velocity. The larger faster particles will impart a force on the smaller slower particles in the direction of movement depending on the angle of collision, and of course there is an equal and opposite force on the larger particles slowing them down. However the faster particle being larger will have more momentum and therefore will not decrease in velocity appreciably. This force will serve to increase the velocity of the slower particle for a short time until the slower particle has been displaced from the path of the faster particle. After the slower particle has been displaced, it will return to its normal velocity through the drag and electrophoretic forces. One can envisage this type of interaction happening many times where the sample band width is 3×10^{-2} to 5×10^{-2} cm. in diameter and the effective diameter of the particle is 3×10^{-5} to 5×10^{-5} cm., a factor of 1000 less. Of course, this should be

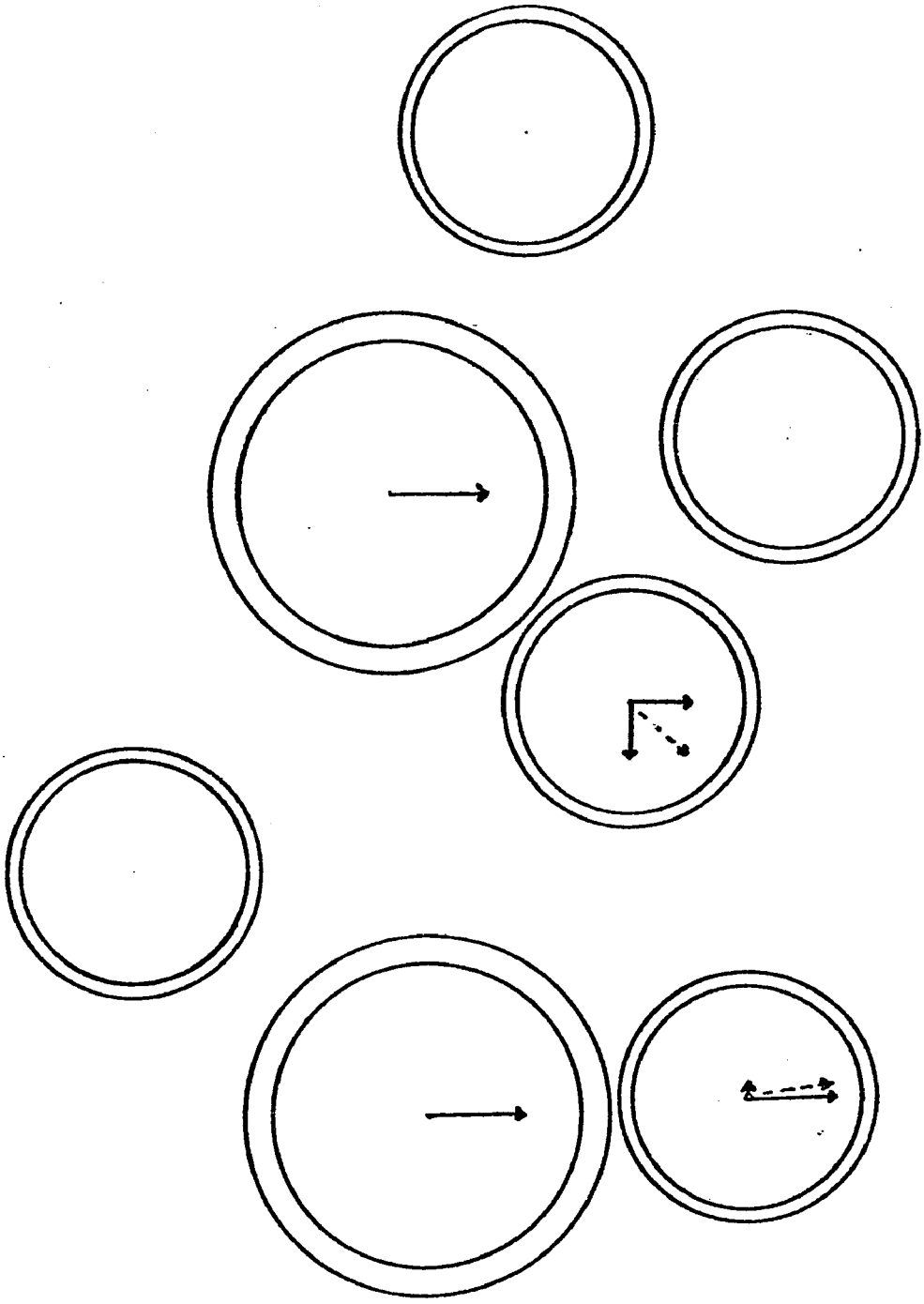

Figure 6.3. Representation of How Larger Particles Affect the Migration Velocity and Displacement of the Smaller Slower Particles.

directly relatable to the numbers of each particle species, and also to the effective size which depends on the particle diameter plus the double layer extension. Particle-particle interactions of this nature should be detectable in the scans of the separated bands, where the distance between bands decreases with increasing interaction.

C. Experimental Results

As previously mentioned, the three particles used in this study were the 0.234, 0.357 and 0.46 micron particles. These latexes were chosen because they are highly monodisperse and uniform, giving sharp well separated peaks. Also the sizes are not different by more than a factor of 2, so that on the basis of comparing weight percent, the number percent is not drastically different.

Initially, particle-particle interactions were investigated with the three latexes as they were prepared and stored. This may introduce some effects such as spreading of the bands due to different ionic conditions between the band and bulk curtain. Also, the amount of surfactant and nature of the surfaces is not well characterized which could lead to misinterpretation of results. To correct this, a second set of experiments was performed, this time using the serum replacement technique[26] to exchange the initial serum with a concentration of the barbital-sodium barbital buffer plus some sodium lauryl sulfate that was equivalent to the curtain electrolyte. The surfactant was added because some spreading of

the separated bands was observed when all the excess surfactant was washed off the latex. The effect of this surfactant addition on mobility will be discussed later. The trends of the second set of experiments were similar to the trends from the first experiments, therefore the difference in ionic conditions and other unknowns of the original serum did not significantly affect the results.

Table 6.1 and Table 6.2 show the results of the initial separations on the latexes without serum replacement. Table 6.1 gives the difference in migration distance between the two peaks, while Table 6.2 shows the absolute migration distance of the 0.46 micron latex particles. Each separation was recorded at three applied potentials of 25, 50 and 75 volts/cm. to minimize any error from a bad measurement, and to allow the progression of the separation to be followed at different stages. Also, all distances are actual distances reported in millimeters which were converted by a factor of 18.2 from the recorder scans. The three results, measured at the three voltage gradients, have been averaged into a single number per 25 volts/cm. by summing the three values and dividing by six. This method weights the results at the higher voltages more heavily. Two combinations of particles were investigated, the 0.357 and 0.46 micron particles which are fairly close in size and are separable, and the 0.234 and 0.46 micron particles which are more easily separable and differ in size by a factor of eight in volume. Data were recorded as a function of the weight percent of each latex, maintaining the total solids content between about one and thirty percent.

Table 6.1.

Peak-to-Peak Separation Distances[1] for "As Is" Latexes

% solids 0.357-0.46 μm	Volts/Centimeter 25	50	75	Avg/25
1-30	0.00	0.00	0.00	0.00
1-20	0.082	0.220	0.330	0.105
1-10	0.055	0.165	0.385	0.101
1-5	0.137	0.275	0.440	0.142
2-20	0.110	0.275	0.467	0.142
5-20	0.220	0.495	0.659	0.229
10-20	0.275	0.522	0.824	0.270
15-15	0.275	0.577	0.824	0.279
1-1	0.220	0.440	0.604	0.210
20-10	0.302	0.522	0.852	0.279
20-5	0.275	0.632	0.934	0.307
20-2	0.275	0.604	0.879	0.293
5-1	0.220	0.549	0.604	0.229
10-1	0.275	0.577	0.797	0.275
20-1	0.302	0.659	0.824	0.298
30-1	0.220	0.632	0.714	0.261
% solids 0.234-0.46 μm	25	50	60	Avg/25
1-20	0.275	0.659	0.934	0.312
15-15	0.385	0.604	0.907	0.316
1-1	0.385	0.852	1.181	0.403
20-1	0.495	0.907	1.154	0.426

[1] Distances in millimeters.

Table 6.2.

Absolute Migration Distance[1] of 0.46 μm Particle for "As Is" Latexes

% solids 0.357-0.46 μm	Volts/Centimeter 25	50	75	Avg/25	Slope	Int.
1-30	5.05	10.38	14.34	4.96	0.186	0.633
1-20	5.22	10.27	15.27	5.13	0.201	0.203
1-10	4.56	9.78	13.79	4.69	0.185	0.147
1-5	4.78	9.84	13.96	4.76	0.184	0.347
2-20	5.22	10.22	15.00	5.07	0.196	0.367
5-20	5.05	10.05	14.34	4.91	0.186	0.523
10-20	4.56	9.12	13.96	4.61	0.188	-0.187
15-15	5.32	11.15	15.88	5.39	0.211	0.223
1-1	4.94	9.45	14.01	4.73	0.181	0.397
20-10	4.62	9.78	14.29	4.78	0.193	-0.107
20-5	5.16	10.05	15.38	5.10	0.204	-0.023
20-2	5.32	10.93	15.55	5.30	0.205	0.370
5-1	4.84	10.38	14.78	5.00	0.199	0.060
10-1	5.00	10.05	14.62	4.95	0.192	0.270
20-1	5.49	11.21	15.66	5.39	0.203	0.617
30-1	5.38	10.71	14.73	5.14	0.187	0.923
%solids 0.234-0.46 μm	25	50	75	Avg/25	Slope	Int.
1-20	4.07	8.90	13.13	4.35	0.181	-0.360
15-15	4.67	10.44	14.45	4.93	0.196	1.410
1-1	4.56	9.23	13.68	4.58	0.182	0.037
20-1	4.23	9.18	13.24	4.44	0.180	-0.127

[1] Distances in millimeters.

The results of Table 6.1 are plotted in Figure 6.4. This figure shows the effect on separation distance as one particle is held constant at either one or twenty percent solids and the second particle varied in concentration from one percent up to thirty percent solids. These results show that there is some effect on the peak-to-peak separation distance when the concentration of the 0.46 micron particles is high relative to the concentration of the 0.357 micron particles. The same sort of trend also appears with the smaller 0.234 micron particles. However, there appears to be an initial increase followed by a decrease in the peak-to-peak separation where the 0.357 micron particles are concentrated and the 0.46 micron are at lower levels. This type of effect seems to indicate that the 0.46 micron particles, being larger in size and volume by a factor of 2.14, can push the smaller 0.357 micron particles farther or faster than they would normally migrate, if the concentration of the 0.46 micron particles is high which increases the probability of collisions. However, when the smaller 0.357 micron particles are in high concentration, the larger 0.46 micron particles can push through the field of smaller particles to migrate to their normal displacement distance. Also, when the 0.46 micron particles are in low concentration, the 0.357 micron particles are, as a whole, unaffected so that the separation distance is not appreciably affected. It should be remembered, that these are weight percents which do not reflect the larger numbers of the smaller particles.

The results in Table 6.2 show the effect of the relative weight percents of each species on the absolute migration distance of the 0.46

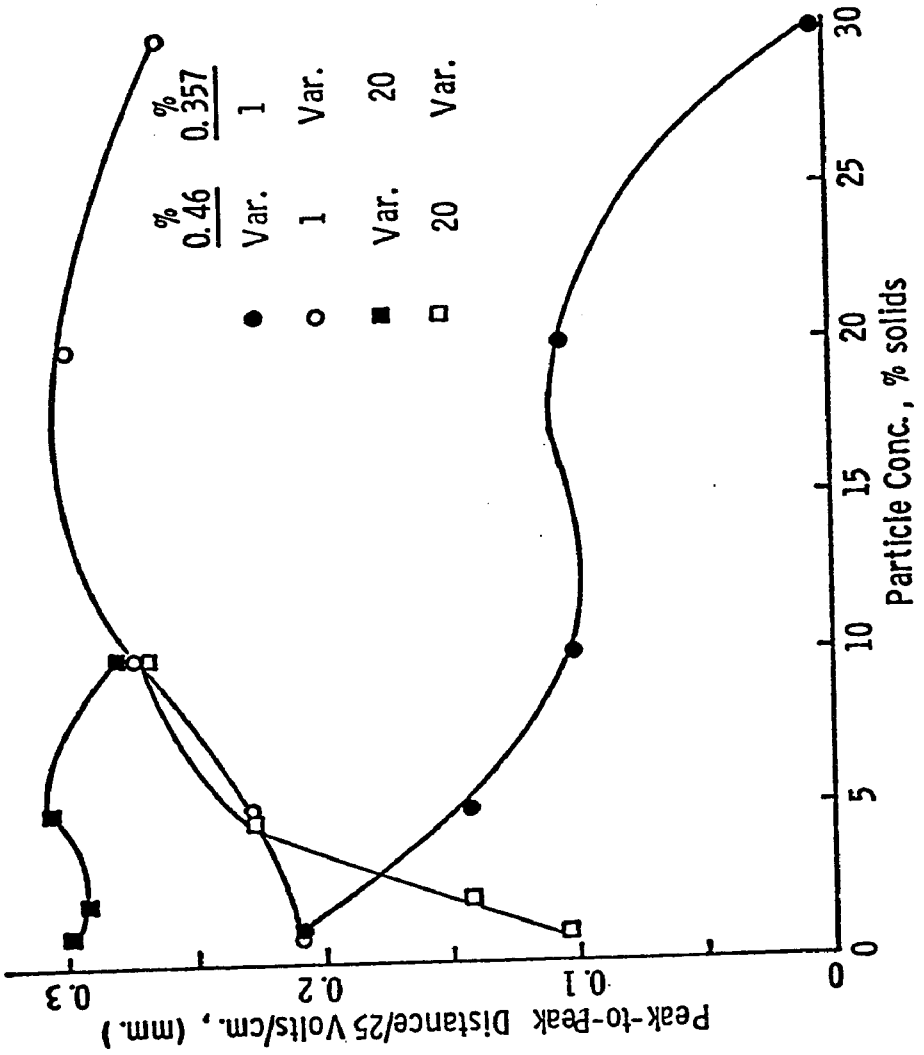

Figure 6.3. The Effect of Particle Size and Concentration on Peak-to-Peak Separation Distance for the Latexes not Subjected to Serum Replacement.

micron particles. Also, the calculated slope and intercept of the three data points for each entry are provided. The slope reflects the average migration distance per 25 volts/cm applied voltage while the intercept shows how far the reference peak, at 0 voltage, was from its calculated position. The data indicate some trends between the points where one solids concentration was held constant which is shown in Figure 6.5. This figure shows the migration distance for both one and twenty percent solids while the second particle concentration is varied from one up to thirty percent solids. The results when one of the latex samples is held constant at twenty percent solids shows that the migration distance decreases linearly with increasing particle concentration. These results suggest that at higher concentrations, particle-particle interactions are a sensitive function of particle concentration and this effect leads to a decrease in the migration distance of both the faster and slower moving particles. On the other hand, the migration distance results when one of the latex samples is held constant at one percent solids are somewhat erratic in that the migration distance increases to a maximum up to a concentration of twenty percent, followed by a decrease.

Since these initial results indicate that there is some effect on the migration distance and peak-to-peak separation distance as a function of the concentration of the two species, it is necessary to determine if there is any concentration effect when just one species is present. Table 6.3 shows the results from a number of runs which demonstrate this effect. The 0.46, 0.357, and 0.234 micron latexes have all been buffer exchanged with curtain buffer,

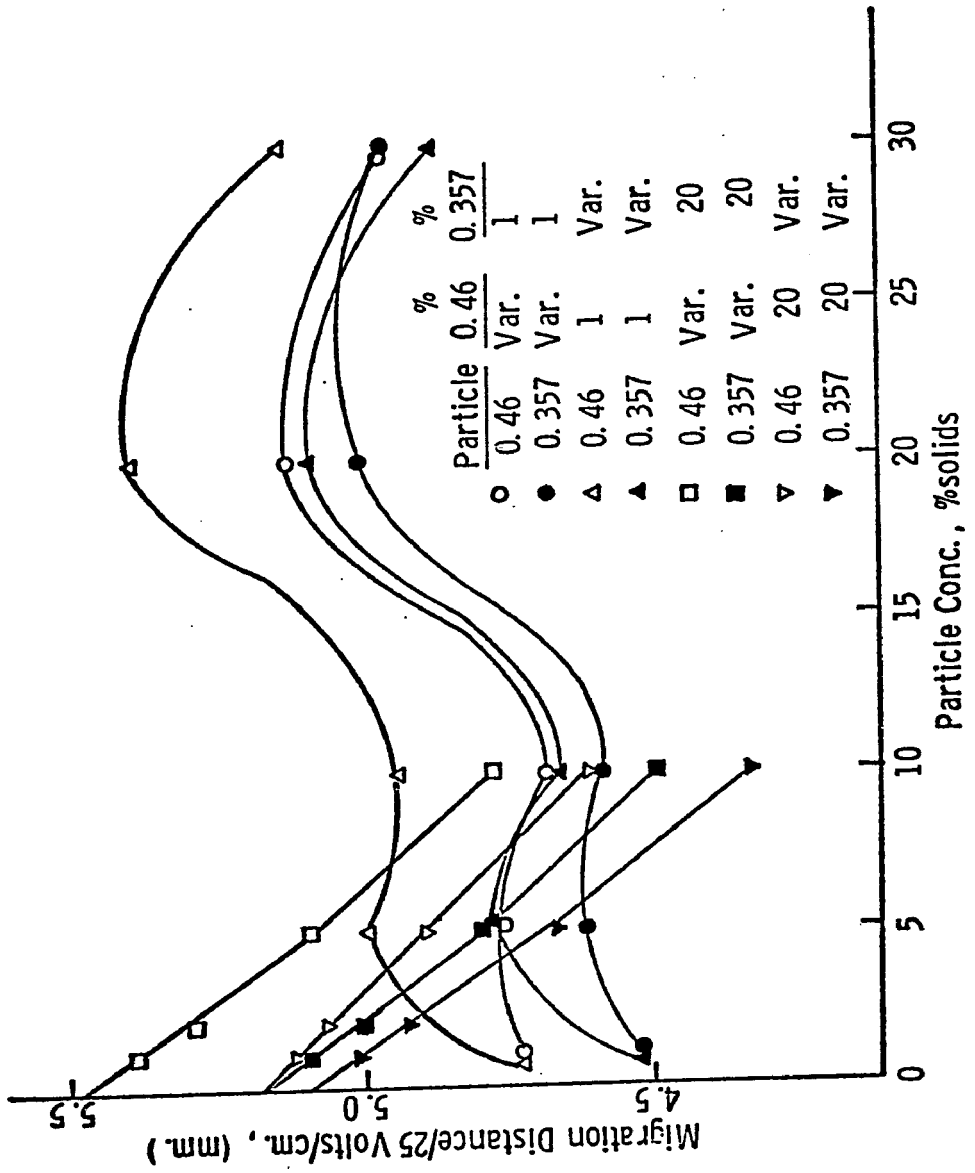

Figure 6.4. The Effect of Particle Size and Concentration on Migration Distance for the Latexes not Subjected to Serum Replacement.

Table 6.3.

Absolute Migration Distance as a Function of Concentration[1]

Conc.	Applied Voltage Gradient (Volts/cm) 20	40	60	80	Avg/20[2]	Avg/20[3]
		0.46 μm Polystyrene				
28.60	3.96	8.08	12.14	16.59	4.08	4.04
14.30	3.74	8.02	12.09	16.26	4.01	3.96
7.15	3.90	8.08	12.36	16.70	4.10	4.06
3.58	3.79	8.52	12.14	16.76	4.12	4.07
		0.357 μm Polystyrene				
17.25	3.57	7.75	11.59	16.04	3.90	3.83
8.63	3.90	7.69	12.25	16.04	3.99	3.96
4.32	3.41	7.58	11.37	16.04	3.84	3.75
2.16	3.68	8.08	11.65	15.99	3.94	3.90
		0.234 μm Polystyrene				
17.00	3.63	7.80	11.70	15.55	3.87	3.83
8.50	3.52	7.75	11.26	15.55	3.81	3.76
4.25	3.52	7.47	11.26	15.55	3.78	3.73
2.13	3.46	8.08	11.81	15.88	3.92	3.85
		0.23 μm Poly(vinyl toluene)				
40.0	3.24	7.42	11.37	15.05	3.71	3.63
20.0	4.29	7.31	12.03	15.60	3.93	3.97
10.0	4.12	7.47	10.49	14.45	3.65	3.74
5.0	3.08	7.91	12.20	15.22	3.84	3.72
2.0	3.57	7.20	9.84	13.68	3.43	3.52
1.0	4.23	6.98	10.82	15.05	3.71	3.77

[1] Distances in millimeters.

[2] Average calculated by totaling the four data points and dividing by 10.

[3] Average calculated by normalizing each data point to 20, then averaging the four values.

while the 0.23 micron poly(vinyl toluene) latex has not. In each case the concentration of latex was successively halved, to see if there was any effect on the absolute migration distance. The displacement was at four voltage gradients, 20, 40, 60 and 80 volts/cm., and as before averaged to one value per 20 volts/cm. Averaging was calculated in two ways, the first as before which gives increasing weight to the larger voltage gradients, and a second method which weights each entry equally. The two averaging methods agree within the limits of experimental error which is estimated at plus or minus 0.1 millimeter.

The averaged absolute migration distance values show some variation, but they are well within experimental error. Therefore, it may be concluded that there is little or no effect on the migration distance as a function of concentration for a single species. Figure 6.6 shows the least squares calculated displacement as a function of the voltage gradient for each particle from the data of Table 6.3. This gives an indication of the expected displacement between the peaks and also the absolute migration distances when two or more of the particles are present. However, these values may change somewhat if the electroosmosis of the curtain walls is affected by the particle and its accompanying ionic conditions with surfactant.

A second set of experiments was performed with the buffer exchanged latexes to determine particle-particle interaction. The results of these runs are listed in Table 6.4. Again the data was recorded at four voltage gradients, 20, 40, 60 and 80 volts/cm.

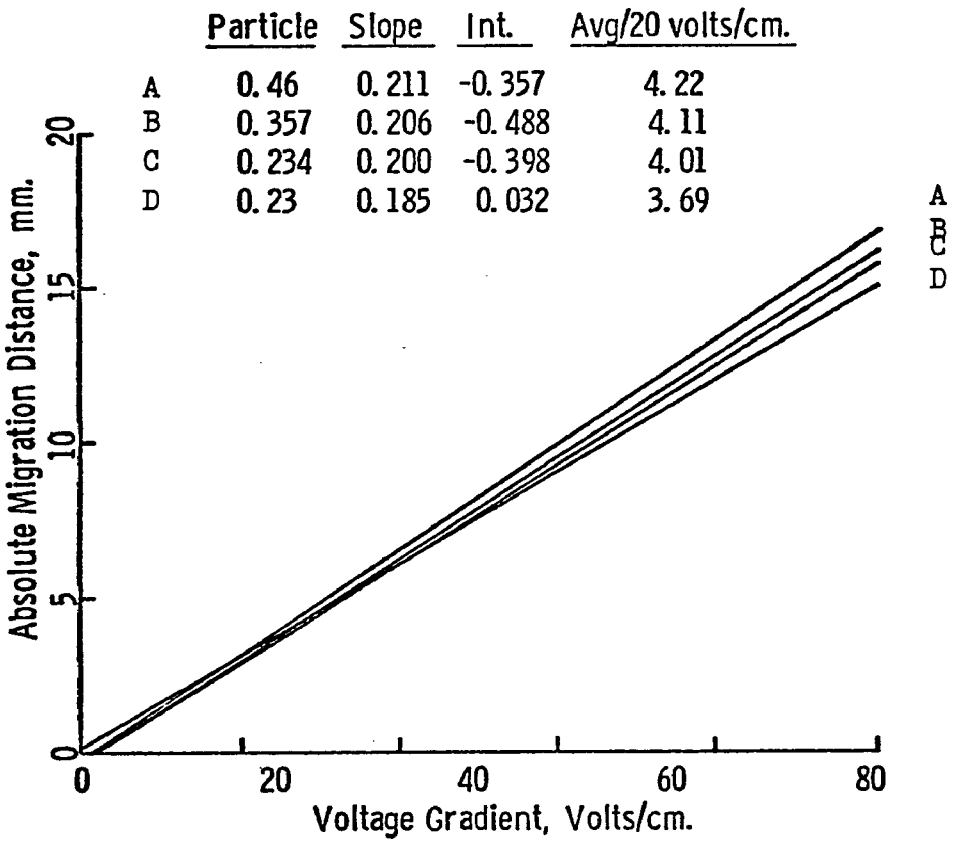

Figure 6.5. Least Squares Averaged Displacement Distances as a Function of the Potential Gradient for the Four Latexes.

Table 6.4.

Peak-to-Peak Separation Distance for Serum-Replaced Latexes[1]

Wt % Ratio 0.234–0.46 μm	Total Conc.	20	40	60	80	Avg/20	Migration Distance 0.46/20
5/95 (28.5/71.5)[2]	27.64	0.247	0.549	0.797	1.154	0.275	3.98
	13.82	0.275	0.604	0.797		0.280	4.23
	6.91	0.302	0.632	0.824		0.294	4.36
25/75 (71.7/28.3)	24.33	0.329	0.604	0.879	1.236	0.305	4.12
	12.16	0.329	0.659	0.879		0.310	4.22
	6.08	0.357	0.687	0.989		0.338	4.34
50/50 (88.4/11.6)	21.20	0.329	0.797	1.071	1.401	0.360	4.35
	10.60	0.385	0.797	1.044		0.371	4.38
	5.30	0.385	0.714	1.016		0.352	4.51
75/25 (95.8/4.2)	18.73	0.357 (0.357)	0.769 (0.659)	(1.071)		0.360	4.59 (4.08)
	9.36	0.439 (0.385)	0.797 (0.659)	(1.044)		0.369	4.59 (4.08)
	4.68	0.329 (0.385)	0.769 (0.687)	(1.099)		0.363	4.26 (4.16)
95/5 (99.3/0.7)	17.15	0.329	0.769	1.154		0.376	4.74
	8.58	0.412	0.824	1.099		0.390	4.47
	4.29	0.385	0.824	1.154		0.393	4.69

[1]Distances in millimeters.

[2]Number % Ratio.

but for many cases at 80 volts/cm. the 0.46 micron latex migrated just beyond the scanning capabilities, and therefore the peak-to-peak distance could not be recorded. The handling of the particle concentrations and ratios was done differently for these runs. Five ratios of the two latexes were prepared from the stock solutions after buffer exchange. Each mixture was then twice halved in total solids content. This shows more clearly the effect of the ratio of the larger particle to the smaller and also the effect of the total concentration on the interactions. Included also is the average absolute migration distance of the 0.46 micron particle. The net results for the 75/25 weight percent ratio of the 0.234 to 0.46 micron latexes was repeated due to a suspected abnormality in the displacement at 60 volts/cm. This may have resulted from small air bubbles which sometimes develop in the curtain. Therefore the bracketed values are from the repeat run. The peak-to-peak values of the repeat run agree with the previous run and the other data, however, the absolute migration distances are not in good agreement. This fact may have resulted from a different value of electroosmosis for the cell walls, since in the interim between the initial set of experiments and the repeat run another buffer system was investigated which may have altered the electroosmosis.

The trends in this data may be easily seen in Figure 6.7. This figure shows the average peak-to-peak separation distances versus the weight fraction of the 0.234 micron particle. At each ratio, a high, medium, and low total solids concentration was run, and these are represented by a circle, square, and triangle

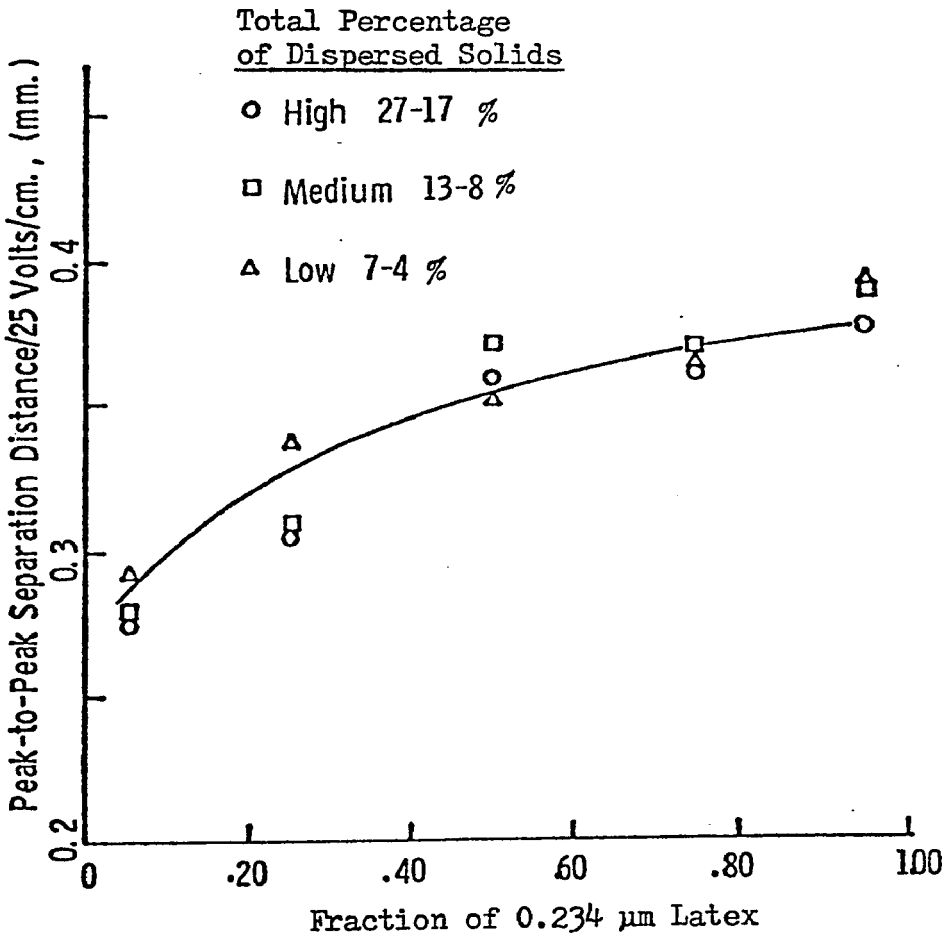

Figure 6.6. The Effect of Particle Size and Concentration on Peak-to-Peak Separation Distance for the Latexes Subjected to Serum Replacement.

respectively. The plot shows that when the ratio of the 0.234 to 0.46 micron particles is low, the peak-to-peak distance is significantly smaller than when the ratio is high, and the separation distance drops off more sharply as the ratio begins to favor the 0.46 micron particle. This is similar to the trends that were found in the initial experiments without serum replacement. However, there does not appear to be any slight drop off in separation distance at the extreme other end where the smaller particles far outnumber the larger ones, as was noted in the initial experiments. This may indicate an effect of the relative sizes. The 0.357 micron particles being only 2.14 times smaller can have a small effect at this end of the scale whereas the 0.234 micron particles being 8 times smaller have no effect in this region. Their momentum is not great enough to significantly displace the 0.46 micron particle from its line of electrophoretic migration. Also notable is the fact that as the total solids concentration decreases the separation distance increases in most cases, which is as expected. The separation distance between peaks should be related to the number of collisions between the particles of each species.

Therefore, the results of these particle-particle interactions suggest that electrophoretic mobility determination by continuous particle electrophoresis may be affected when the particle concentration is very high or the double layers very extended. Such considerations may be neglected if total solids concentrations are maintained below about five percent and ionic strengths are

maintained at a level where the double layer is small (less than 10%) compared to the particle radius. More research in this area, such as (1) varying the ionic concentration to change the double layer extension, (2) using more sizes of monodisperse latexes, and (3) using latexes of the same size but different mobilities, would be very helpful in determining exactly what effect the particle size, concentration, and charge, along with the electrolyte concentration have on the band separation distance. Possibly a statistical mathematical model could be developed to simulate the number of collisions and momentum of the particles to predict how the migration distance of a theoretical particle will be affected by the other particles which it encounters. These preliminary results suggest that this is one way to investigate these interactions and that the effect does indeed exist.

D. Surfactant Addition

Lastly, the effect of surfactant addition on the mobility of a buffer exchanged latex has been briefly investigated, mainly as a factor to decrease the band width. As a latex is subjected to serum replacement, eventually the surfactant will be washed out unless there is some continually being added. It has been observed that a latex that has been cleaned and buffer exchanged in this way will produce a broader band in the CPE, which can be narrowed by the addition of small amounts of surfactant. The addition of surfactant, however, also affects the apparent electrophoretic mobility as the bands are now displaced farther towards the positive

electrode. These results may be seen in Table 6.5 for the 0.46 and 0.357 micron latexes both at ten percent solids. Both had been buffer exchanged with the 1 x 10^{-3} barbital-sodium barbital buffer. The results show a trend toward greater mobility as more surfactant is added to the latex. This would be expected since the sodium lauryl sulfate is negatively charged and would contribute to the negative charge of the particles. Also of interest is the larger increase in the migration distance of the 0.46 micron particles as a function of the addition of the surfactant. This probably reflects the smaller total surface area of the 0.46 micron latex which would be closer to saturation than the smaller 0.357 micron particles with 66 percent more surface area for the same volume and solids content. However, if the two particle sizes were mixed, the surface charge density (expressed in number of surfactant molecules per unit area) should be the same regardless of the size of the particles and provided that the particles are of the same material, e.g. polystyrene. These results show that band displacement can be a sensitive function of the amount of surfactant addition. More research in this area could provide information on the adsorption and distribution of the surfactant in the latex dispersion.

Table 6.5.

Displacement Distance as a Function of

Surfactant Addition to Serum-Replaced Latexes[1]

Added Surfactant Concentration	Voltage Gradient (Volts/cm) 20	40	60	80	Avg/20
	10% 0.46 μm Polystyrene				
0.0	3.74	7.86	12.09	16.81	4.05
0.50×10^{-4}	4.01	8.46	11.76	17.03	4.13
1.25×10^{-4}	4.01	8.68	13.02	17.03	4.29
2.50×10^{-4}	4.34	9.23	13.24	17.03	4.47
	10% 0.357 μm Polystyrene				
0.0	3.68	7.86	11.53	15.44	3.85
0.50×10^{-4}	3.79	7.74	11.70	16.10	3.92
1.25×10^{-4}	3.79	8.08	11.70	15.99	3.95
2.50×10^{-4}	3.52	7.69	11.98	16.15	3.93

[1] Distances in millimeters.

Chapter VII

Conclusions

The two types of electrophoresis for separation and collection of fractions which have been investigated in this work have progressed a long way since their first inception. Both have been considered for space processing and both have certain advantages and disadvantages. Some of the major differences are:

Free-Fluid Electrophoresis;

1. Strictly a batch process, limited sample processing.
2. Relatively simple piece of equipment.
3. Resolution can be very good for all bands with a suitable low electroosmotic mobility coating.
4. Separation requires a relatively long period of time (about 0.5 to 1.0 hours).
5. Difficult to obtain separated fractions (freezing required), but once frozen, slicing can be done in very small increments.
6. Only applicable in microgravity conditions (space).

Continuous Particle Electrophoresis;

1. A continuous process, larger volume of sample processing.
2. Rather complicated and more difficult piece of equipment to operate.
3. Resolution is maximized for only a narrow range of mobilities not differing appreciably from the electroosmotic mobility.

4. Separation time is short (about 20 to 30 seconds).

5. Easy to collect separated bands, but resolution of bands limited physically by number and size of collection tubes.

6. Applicable both for earth and space processing.

On the other hand, both types of electrophoresis have some things in common also such as:

1. Similar particles, buffer systems, and voltage gradients may be employed in both.

2. Resolution depends on the sample amount and size relative to the column dimensions.

3. A need for specific electroosmotic mobility coatings to maximize resolution.

4. A dependence on the temperature profiles which develop from Joule heating of the suspending fluid.

The ASTP free-fluid electrophoresis experiment has shown that this form of electrophoresis is a viable method for fractionating small sample volumes. It successfully fractionated three species of fixed red blood cells according to electrophoretic mobility, and proved that the epoxy-silane plus methylcellulose coating was effective in reducing the value of electroosmosis along the walls to near zero. However, improvement is needed in the method of inserting and retrieving the sample from the column, in so far as the freezing process which was used resulted in some clumping of the cells and some handling errors. Other than this, the experimental photographic results agree well with the theory developed so far, in

that the band positions, shapes, and concentrations were in good agreement with theory.

Modeling of this system has revealed the important parameters and considerations for maximizing the resolution. Of primary importance for this type of system is the low, near-zero, value of electroosmosis. Such a coating allows an increase in the ratio of sample radius to column radius which increases the sample volume without serious overlapping distortions to the separated bands. Next in importance is the temperature gradient, of which both viscosity and dielectric constant are a function. These two variables affect the electrophoretic and electroosmotic mobility such that a temperature gradient has a distorting effect similar to electroosmosis. This may be counteracted by cooling and with a slightly positive value of electroosmosis. Lastly, the sample plug thickness has a small effect, which is minimal if this dimension is negligible in relation to the total migration distance. Therefore, with these considerations in mind the resolution can be made comparable to that obtainable in the CPE.

Continuous particle electrophoresis is an alternate method for separating and collecting samples. It is capable of handling samples over a large size range from dye molecules up to blood cells that may be five to ten microns in size. Also it can handle a large range of concentrations from less than one to more than thirty percent solids, and it can process samples of high density. This makes it a useful instrument for measuring electrophoretic mobilities

as well as collecting fractions. With a CPE it is possible to determine the electrophoretic mobility of certain samples under conditions that could not be accommodated in a microcapillary electrophoresis cell or electrophoretic mass transport analyzer. Absolute mobilities may be routinely measured by injecting a marker species of known mobility just prior to or along with the sample of interest. This allows the electroosmosis to be calculated so that the migration distance is an indication of the electrophoretic mobility. Also the separation distance between the marker and sample can indicate the electrophoretic mobility since the electroosmosis, being the same for both, cancels out of the calculations. Both methods may be used and agree well with microcapillary electrophoresis results. However, the second approach yields more reliable results since the peak-to-peak separation distance develops quickly and is easily reproducible while the absolute migration distance develops more slowly and is not always readily reproducible.

Resolution of different mobilities in the CPE may be detected very well; however, collection of separated fractions is not as well resolved due to the size limitations of the collection tubes. Using monodisperse latexes of varying sizes, two latexes differing in mobility by as little as 0.15 mobility unit have been separated and detected but not collected. This has occurred with a very thin sample injection stream, under optimum electrolyte conditions, at voltage gradients from 30 to 60 volts/cm. Collected fractions evaluated from electron micrographs show that the bands must be

well separated to obtain clean fractions. This is probably due to the coarseness of the collection system, the electroosmotic tailing of the bands, and some particle-particle interactions.

Modeling of this system on the computer has also led to interesting revelations about the effect of the various parameters. Again, electroosmosis is the main consideration since it manifests itself in all the other parameters. Maximum resolution is obtained when the electrophoretic and electroosmotic mobilities match. Obviously, if two or more different particles are present in the CPE, only one can have a matching mobility. The larger the difference the more crescent-shaped and elongated the bands become. The effect of electroosmosis may be minimized by keeping the sample injection stream very thin at the sacrifice of sample throughput rate, and by keeping the stream in the center of the column. If sample throughput rather than resolution is of prime importance, there may be an advantage to going to a rectangular injection port rather than a cylindrical port, since the rectangular port could be increased in size in one direction only. The dimension that may be increased depends on the electroosmotic and electrophoretic mobilities. If the electrophoretic and electroosmotic mobilities match, then the width in the direction of the colum wall could be increased without undue distortion. On the other hand, if the mobilities do not match, the thickness in the electrode direction would result in less distortion than increasing sample width.

If throughput is not the prime concern, but resolution is,

there may be special conditions when a low value of electroosmosis may give better resolution than matching electroosmotic and electrophoretic mobilities. For instance, if limited by a small migration distance, it is best to use that distance for electrophoretic migration rather than electroosmotic migration which does not contribute to the separation distance. However, in most cases where migration distance is not the limiting factor it is best to match mobilities. Therefore, the optimum conditions for any separation depend on a number of factors, primarily a suitable value of electroosmosis.

These considerations for maximizing the resolution do not only apply to the Beckman CPE on which this work was done, but also to other designs such as the SPAR CPE which is shorter, but has a thicker channel. The main difference is in the Joule heating and development of the temperature profiles. Where the Beckman CPE was designed for earth use, the SPAR CPE is strictly for space processing. The microgravity conditions of space obviate the tendency for convectional mixing, reducing the SPAR system to the same principles as the Beckman CPE. Therefore, the same model may be used to predict probable separations in the SPAR CPE. Comparison of the model to experimental separations in the Beckman CPE has shown good agreement as far as predicting the position, concentration, and spread of the bands.

Lastly, the CPE instrument can be a sensitive tool to investigate particle-particle interactions. Experimental evidence

indicates that the peak-to-peak distance between bands may change in response to the relative concentrations and size of the particles. This change results from one band of particles interacting with the second band through collisions, which cause the displacement to be more or less than normal. Larger particles in high concentration exert an influence on the migration distance of smaller particles since they are larger in mass and also in velocity. Therefore, they have a much greater momentum. However, smaller particles in high concentration do not influence the migration distance of the larger particles to the same extent. Rather the larger particles just push their way through so that their migration distance and corresponding separation is unaffected. The experiments as performed did not show the need to buffer exchange the latexes since results before and after were similar in the trends that were evident. Also, there is no discernible effect of concentration on the migration distance when only one particle species is injected into the CPE column.

DLVO theory calculations show that the double layers exert sufficient repulsive energies out to 200 to 300 angstroms for an ionic concentration of 1×10^{-3}. This is roughly fifteen percent of the particle radius. Therefore the double layers have only a small effect on the number of collisions and interaction at this ionic concentration. By decreasing the ionic concentration to 1×10^{-4} this effect should be magnified and be even more dramatic.

Surfactant addition to buffer exchanged latexes has a two-fold effect. First, it serves to prevent the bands from broadening

out upon passing through the CPE, and secondly, it increases the migration distance of the bands as a function of the surfactant concentration. This results from the negatively charged sodium lauryl sulfate molecules adsorbing onto the latex surface giving it a higher surface potential. More of an effect is seen for the larger latex because it has less surface area for the same volume of latex; therefore it is closer to saturation.

Overall the CPE has many possibilities both for collection of fractionated samples and as an analytical tool for determining mobilities, and the double layer effects surrounding the particle. Finally it should be emphasized that this work shows that the CPE is a powerful instrument for the electrophoretic separation of particles both for ground-based work and under microgravity conditions which offer the advantage of a combination of high throughput and greater resolution.

A P P E N D I C E S

Appendix A. Free-Fluid Electrophoresis Computer Program.

```
                PROGRAM PHORESE  (INPUT,OUTPUT,PLOT,TAPE99=PLOT)
  3             DIMENSION W(25),Z(25)
  3             DIMENSION FM1(192),FM2(192),PEAK(192),D(192)
  3             COMMON/DRAW/SHAPE(3,45),R(45),IMP
  3             DIMENSION DIS(45)
  3             COMMON//S1(10),S2(10),NA,NB,RATIO1,RATIO2,DIELECN,REV
               1ISN
  3             COMMON/VAR/XLU,RU,RA,THETA,IPRINT
  3             COMMON/SET/T1,T2,ALPHA,UOS,E
  3             COMMON/SUB/UMEAN(3),UVARL(3),UVARR(3),AREA(3),AB(3),ID
               1IST(3)
  3             COMMON/TAB/QUEST(3,20),IORDER(3),JC(3)
  3             COMMON/PT/US(165),VS(165),VSA(3,165)
  3             DATA WORD1,WORD2,WORD3/9H GAUSSIAN,9H TRIANGLE,9HPARA
               1BOLIC/
  3             DATA WORD4,WORD5/9H   SQUARE,9H   RANDOM/
  3             READ 100,JA,NA
 13             READ 101,(W(I),I=1,JA)
 26             READ 101,(Z(I),I=1,JA)
 41             NA1=NA+1
 43             CALL LINEGEN(S1,NA,NA1,JA, W,Z)
 47             READ 100,JB,NB
 57             READ 101,(W(I),I=1,JB)
 72             READ 101,(Z(I),I=1,JB)
105             NB1=NB+1
107             CALL LINEGEN(S2,NB,NB1,JB,W,Z)
113             READ 102,XLU,YLU,RU,RA,THETA,IPRINT
133             READ 103,UOS,T1,T2,E
147             READ 104,LOVE
155             PRINT 120
161             PRINT 110
165             PRINT 108
171             DO 1 I=1,LOVE
173             READ 105,UMEAN(I),UVARL(I),UVARR(I),AB(I),AREA(I),IDI
               1ST(I)
212             UEMAX=UMEAN(I)+UVARR(I)
215             UE=UMEAN(I)-UVARL(I)
217             IF(IDIST(I).EQ.1) WORD=WORD1
222             IF(IDIST(I).EQ.2) WORD=WORD2
226             IF(IDIST(I).EQ.3) WORD=WORD3
232             IF(IDIST(I).EQ.4) WORD=WORD4
236             IORDER(I)=0
240             IF(IDIST(I).NE.5) GO TO 4
242             WORD=WORD5
243             READ 106,JC(I)
251             K=JC(I)
253             READ 107,(W(J),J=1,K)
```

```
266           READ 107,(Z(J),J=1,K)
301           DO 5 J=1,K
303         5 QUEST(I,J)=Z(J)
312           CALL SEARCH(W,Z,K,IO)
315           IORDER(I)=IO
317         4 CONTINUE
317           PRINT 109,I,UEMAX,UE,UMEAN(I),AREA(I),WORD,IORDER(I)
341         1 CONTINUE
344           PRINT 110
347           PRINT 112,E
355           PRINT 114,UOS
363           PRINT 110
367           PRINT 116,THETA
375           PRINT 117,RA
403           PRINT 110
407           PRINT 115,T1,T2
417           PRINT 120
423           DO 2 N=1,161
425           US(N)=-1.0+(N-1)/10.0
432           IF(US(N).LT.0.0) US(N)=0.0
435           IF(US(N).GT.14.0) US(N)=14.0
442           DO 25 M=1,LOVE
444        25 VSA(M,N)=0.0
451         2 VS(N)=0.0
455           DIELEC1=ZAM(S1,NA,T1)
460           DIELEC2=ZAM(S1,NA,T2)
463           DIELECN=ZAM(S1,NA,298.0)
466           REVIS1=ZAM(S2,NB,T1)
471           REVIS2=ZAM(S2,NB,T2)
474           REVISN=ZAM(S2,NB,298.0)
477           RATIO1=(DIELEC1*REVISN)/(DIELECN*REVIS1)
502           RATIO2=(DIELEC2*REVISN)/(DIELECN*REVIS2)
505           READ 111,NUM,NFRAME,NSLIDE
517           ALPHA=0.0
520           TIMET=3.0*60.0/10000.0*NFRAME
523           CALL ACTUAL (TIMET,LOVE)
527           PRINT 110
533           READ 113,(FM2(I),I=1,NUM)
546           READ 113,(FM1(I),I=1,NUM)
561           SUMA=0.0
562           DO 7 I=1,NUM
564           PEAK(I)=FM2(I)-NSLIDE-FM1(I)
570           D(I)=(13.0+I*0.6394736842)*0.1
575           IF(PEAK(I).LT.0.0) PEAK(I)=0.0
600           SUMA=SUMA+PEAK(I)
603         7 CONTINUE
605           SUM=0.0
606           DO 3 N=1,161
607         3 SUM=SUM+VS(N)
613           FACTAR=1.485566E7/SUM
```

```
615           DO 6 N=1,161
616           DO 24 M=1,LOVE
617          24 VSA(M,N)=VSA(M,N)*FACTAR/1.7945E-2
626           6 VS(N)+VS(N)*FACTAR/1.7945E-2
633           UPGRADE=0.1/0.06394736842
634           FACTER=828.0/SUMA
636           DO 8 N=1,NUM
640           8 PEAK(N)=PEAK(N)*UPGRADE*FACTER
646           CALL NAMPLT
647           CALL FACTOR(0.9)
651           IF(IPRINT.NE.1) GO TO 22
653           CALL FACTOR(1.2)
655          22 CONTINUE
655           CALL PLOT(0.0,-0.5,-3)
660           FM1(NUM+1)=0.0
662           FM1(NUM+2)=25.0
664           FM2(NUM+1)=0.0
665           FM2(NUM+2)=25.0
667           D(NUM+1)=0.0
670           D(NUM+2)=2.54
672           PEAK(NUM+1)=0.0
673           PEAK(NUM+2)=25.0
675           US(162)=0.0
676           US(163)=2.54
677           VS(162)=0.0
700           VS(163)=2.5E7
701           R(IMP+1)=-1.0
703           R(IMP+2)=2.54
705           DIS(IMP+1)=0.0
707           DIS(IMP+2)=2.54
710           IF(PRINT.NE.5) GO TO 30
712           CALL FACTOR(1.1)
713           CALL AXIS(1.5,1.5,33H     THEORETICAL CONC. (CELLS/ML)
             1,33,4.0,90.0,0.0,2.5E7,20.0)
724           CALL AXIS1(1.5,1.5,13HDISTANCE (CM),-13,5.512,0.0,0.0,
             12.54,25.4)
735           CALL SYMBOL(2.8,0.75,0.125,26HCOMPUTED CELL DISPLACEME
             1NT,0.0,26)
741           CALL PLOT(1.5,1.5,-3)
744           CALL LINE(US,VS,161,1,0,0)
750           DO 26 I=1,LOVE
752           DO 27 J=1,161
753          27 VS(J)=VSA(I,J)
762           CALL PLOT(0.0,0.0,3)
764           CALL LINE(US,VS,161,1,0,0)
770          26 CONTINUE
773           CALL PLOT(0.0,2.5,-3)
775           DO 28 I=1,LOVE
777           DO 29 J=1,IMP
```

```
1000        29 DIS(J)=SHAPE(I,J)
1007           CALL LINE(DIS,R,IMP,1,0,0)
1013           CALL PLOT(0.0,0.0,3)
1016        28 CONTINUE
1021           CALL PLOT(-1.5,-4.0,-3)
1023        30 CONTINUE
1023           IF(IPRINT.EQ.5) GO TO 19
1025           IF(IPRINT.EQ.3) GO TO 18
1027           CALL AXIS1(1.5,1.5,13HLIGHT DENSITY,13,4.0,90.0,0.0,25.
              10,20.0)
1037           CALL AXIS1(1.5,1.5,13HDISTANCE (CM),-13,5.512,0.0,0.0,
              12.54,25.4)
1050           CALL AXIS1(7.012,1.5,33H     THEORETICAL CONC. (CELLS/
              1ML),-33,4.0,90.0,0.0,2.5E7,20.0)
1061           CALL SYMBOL(1.65,0.6,0.125,49HMICRO-DENSITOMETER SCAN A
              1ND COMPUTED DISPLACEMENT,0.0,49)
1065           CALL SYMBOL(5.5,5.0,0.15,5HFRAME,0.0,5)
1071           CALL NUMBER(6.125,5.0,0.15,NFRAME,0.0,2HI2)
1075           CALL PLOT(1.5,1.5,-3)
1100           CALL LINE(D,PEAK,NUM,1,0,0)
1104           CALL PLOT(0.0,0.0,3)
1107           CALL LINE(US,VS,161,1,0,0)
1113           CALL PLOT(-1.5,-1.5,-3)
1116           IF(IPRINT.NE.1) GO TO 21
1120           CALL PLOT(1.5,4.0,-3)
1123           DO 20 I=1,LOVE
1125           DO 17 J=1,IMP
1126        17 DIS(J)=SHAPE(I,J)
1135           CALL LINE(DIS,R,IMP,1,0,0)
1141           CALL PLOT(0.0,0.0,3)
1144        20 CONTINUE
1147           CALL PLOT(-1.5,-4.0,-3)
1151        21 CONTINUE
1151           IF(IPRINT.EQ.1) GO TO 18
1153           CALL AXIS1(1.5,6.5,13HLIGHT DENSITY,13,4.0,90.0,0.0,25.
              10,20.0)
1164           CALL AXIS1(1.5,6.5,13HDISTANCE (CM),-13,5.512,0.0,0.0,
              12.54,25.4)
1175           CALL SYMBOL(5.5,10.0,0.15,5HFRAME,0.0,5)
1201           CALL NUMBER(6.125,10.0,0.15,NFRAME,0.0,2HI2)
1205           DO 9 N=1,NUM
1207           FM1(N)=FM1(N)/1.5
1211         9 FM2(N)=FM2(N)/1.5
1215           CALL PLOT(1.5,6.5,-3)
1220           CALL LINE(D,FM1,NUM,1,0,0)
1224           CALL PLOT(0.0,0.0,3)
1227           CALL LINE(D,FM2,NUM,1,0,0)
1233           CALL PLOT(8.0,-6.5,-3)
1236        18 CONTINUE
```

```
1236          IF(IPRINT.LT.3) GO TO 19
1241          CALL FACTOR(1.0)
1242          CALL AXIS1(1.5,3.0,14HRELATIVE CONC.,14,5.0,90.0,0.0,2
             10.0,20.0)
1253          CALL AXIS1(1.5,3.0,24HELECTROPHORETIC MOBILITY,-24,7.8
             180,0.0,0.0,0.635,25.4)
1264          T1=298.0
1266          T2=298.0
1267          UOS=0.0
1270          THETA=0.0001
1271          TIMET=0.264
1273          DO 12 N=1,161
1274          DO 23 K=1,LOVE
1275       23 VSA(K,N)=0.0
1302       12 VS(N)=0.0
1306          CALL ACTUAL (TIMET,LOVE)
1310          CALL CONCENT (TIMET,LOVE)
1312          XMAX=0.0
1313          DO 10 N=1,161
1315          IF(VS(N).GT.XMAX) XMAX=VS(N)
1321       10 US(N)=US(N)/(E*TIMET)
1326          FACTUR=XMAX/100.0
1330          DO 11 N=1,161
1332       11 VS(N)=VS(N)/FACTUR
1336          US(162)=0.0
1337          US(163)=0.635
1341          VS(162)=0.0
1342          VS(163)=20.0
1343          CALL PLOT(1.5,3.0,-3)
1346          CALL LINE(US,VS,161,1,0,0)
1352          DO 13 L=1,LOVE
1354          DO 16 N=1,161
1355       16 VS(N)=VSA(L,N)/FACTUR
1364          CALL PLOT(0.0,0.0,3)
1367          CALL LINE(US,VS,161,1,0,0)
1373       13 CONTINUE
1376       19 CONTINUE
1376          CALL PLOT(10.0,-1.5,-3)
1401          CALL ENDPLT
1402      100 FORMAT(2I2)
1402      101 FORMAT(8E10.0)
1402      102 FORMAT(5(F8.3),I2)
1402      103 FORMAT(4(F8.3))
1402      104 FORMAT(3(I5))
1402      105 FORMAT(5(F8.3),2X,I1)
1402      106 FORMAT(I2)
1402      107 FORMAT(8E10.0)
1402      108 FORMAT(19X,4HLEAD,3X,5HTRAIL,4X,4HPEAK,4X,4HAREA,6X,5H
         1SHAPE,3X,5HORDER,/)
```

```
1402        109 FORMAT(1X,*PARTICLE NO,*,I2,4(F8.3),2X,A9,6X,I2)
1402        110 FORMAT(//)
1402        111 FORMAT(I3,2(1X,I2))
1402        112 FORMAT(5X,21HPOTENTIAL GRADIENT = ,F5.1,*VOLTS/CM*)
1402        113 FORMAT(20E4.0)
1402        114 FORMAT(5X,*UOS =*,F6.2,*MICRON CM/VOLT SEC*)
1402        115 FORMAT(5X,*WALL TEMPERATURE =*,F10.4,*DEGREES K*,/,5X,
                1*CENTER TEMPERATURE =*,F10.4,*DEGREES K*)
1402        116 FORMAT(5X,*THETA =*,F5.2,*CM*)
1402        117 FORMAT(5x,*SAMPLE RADIUS =*,F4.3)
1402        120 FORMAT(1X,/,*XXXXXXXXXXXXXXXXXXXXXXXXXXXXXXXXXXXXXXXXXX
               1XXXXXXXXXXXXXXXXXXXXXXXXXXX*,/)
1402             CALL EXIT
1403             END


                 SUBROUTINE ACTUAL (TIME,LOVE)
   5             DIMENSION DF(3,21),DR(3,21)
   5             COMMON/DRAW/ SHAPE(3,45),R(45),IMP
   5             COMMON//S1(10),S2(10),NA,NB,RATIO1,RATIO2,DIELECN,REVI
                1SN
   5             COMMON/VAR/XLU,YLU,RU,RA,THETA,IPRINT
   5             COMMON/SET/T1,T2,ALPHA,UOS,E
   5             COMMON/ZVAL/Z,KIMP
   5             COMMON/SUB/UMEAN(3),UVARL(3),UVARR(3),AREA(3),AB(3),ID
                1IST(3)
   5             FIN=1.0E10
   6             CEN=0.0
   7             RUT=RA
  10             KIMP=0
  11             IMAX=2.0*RUT/0.1+1.5
  15             RUM=CEN
  16             DO 4 K=1,2
  20             IF(K.EQ.2) RUM=RA
  23             T3=T2-(T2-T1)*ABS(RUM)**2
  31             DIELEC3=ZAM(S1,NA,T3)
  35             REVIS3=ZAM(S2,NB,T3)
  40             RATIO3=(DIELEC3*REVISN)/(DIELECN*REVIS3)
  43             POSIT=2.0*RUM**2-1.0
  46             DTFIN=((UMEAN(1)-UVARL(1))*RATIO3+UOS*POSIT*RATIO1)*E*
                1TIME-THETA
  60             IF(DTFIN.LT.FIN) FIN=DFIN
  63           4 CONTINUE
  65             SCALE=YLU+FIN-1.0
  70             ISCALE=SCALE
  71             Z=ISCALE
  72             DO 32 I=1,IMAX
  74             IF(RUT.GT.RA+0.01) GO TO 29
 101             IF(RUT.LT.-RA-0.01) GO TO 29
```

```
103           T3=T2-(T2-T1)*ABS(RUT)**2
111           DIELEC3=ZAM(S1,NA,T3)
115           REVIS3+ZAM(S2,NB,T3)
120           RATIO3=(DIELEC3*REVISN)/(DIELECN*REVIS3)
123           POSIT=2.0*RUT**2-1.0
126           IM=2*IMAX-I+1
131           DO 28 M=1,LOVE
134           DF(M,I)=((UMEAN(M)+UVARR(M))*RATIO3+UOS*POSIT*RATIO1)*
             1E*TIME+YLU
146           DR(M,I)=((UMEAN(M)-UVARL(M))*RATIO3+UOS*POSIT*RATIO1)*
             1E*TIME+YLU-THETA
162           SHAPE(M,I)=DF(M,I)
167           R(I)=RUT
171           SHAPE(M,IM)=DR(M,I)
175           R(IM)=RUT
177           K1=(DF(M,I)-Z)*10.0+6.0
204           IF(K1.GT.KIMP) KIMP=K1
207        28 CONTINUE
212        29 CONTINUE
212           RUT=RUT-0.1
214        32 CONTINUE
217           IMP=2*IMAX+1
220           DO 5 M=1,LOVE
222         5 SHAPE(M,IMP)=DF(M,1)
231           R(IMP)=R(1)
233           RETURN
233           END


              SUBROUTINE CONCENT(TIME,LOVE)
  5           DIMENSION P(20),Q(20),UGH(10),G(3),F(3)
  5           DIMENSION Y(250),SUM(4,250)
  5           COMMON//S1(10),S2(10),NA,NB,RATIO1,RATIO2,DIELECN,REVI
             1SN
  5           COMMON/VAR/XLU,YLU,RU,RA,THETA,IPRINT
  5           COMMON/SET/T1,T2,ALPHA,UOS,E
  5           COMMON/ZVAL/ Z,KIMP
  5           COMMON/SUB/UMEAN(3),UVARL(3),UVARR(3),AREA(3),AB(3),I
             1DIST(3)
  5           COMMON/TAB/QUEST(3,20),IORDER(3),JC(3)
  5           COMMON/PT/ US(165),VS(165),VSA(3,165)
  5           DATA PI/3.141692654/
  5           CEN=0.0
  6           IMAX=2.0*RU/0.05+1.1
 12           IF(KIMP.GT.131) KIMP=131
 15           DO 19 M=1,LOVE
 17           DO 1 J=1,KIMP
 20         1 SUM(M,J)=0.0
 25           RUT=RU
```

```
 27          DO 17 I=1,IMAX
 30          IF(RUT.GT.CEN+RA+0.01) GO TO 16
 36          IF(RUT.LT.CEN-RA-0.01) GO TO 16
 41          XMULT-2.0*PI*ABS(RUT)
 44          T3=T2-(T2-T1)*ABS(RUT)**2
 51          DIELEC3=ZAM(S1,NA,T3)
 55          REVIS3=ZAM(S2,NB,T3)
 60          RATIO3=(DIELEC3*REVISN)/(DIELECN*REVIS3)
 63          POSIT=2.0*RUT**2-1.0
 66          DT=(UMEAN(M)*RATIO3+UOS*POSIT*RATIO1)*E*TIME
 76          DL=UVARL(M)*E*RATIO3*TIME+THETA/2.0
103          DR=UVARR(M)*E*RATIO3*TIME+THETA/2.0
111          ATHE=DT*10.0
113          THE=(DT-DL)*10.0
115          LTHE=THE
116          XTHE=LTHE
117          DTHE=1.0-(THE-XTHE)
122          YUM=DL*10.0
124          WUM=DR*10.0
125          NYUM=YUM-DTHE
130          DIST=ABS(DL+DR)*10.0
132          LDIST=DIST
133          IF(LDIST.LT.1) LDIST=1
136          AC=AB(M)
140          MCOUNT=0
141          KTEL=IDIST(M)
142          GO TO (40,46,48,50,7) KTEL
152        7 NAC=IORDER(M)+1
155          NAC1=NAC+1
156          THE=DT*10.0
160          LTHE=THE
161          XTHE=LTHE
162          DTHE=1.0-(THE-XTHE)
165          JOY=JC(M)
167          PLUS=DIST/(JOY-1)
173          DO 6 K=1,JOY
174          P(K)=THE+(K-1)*PLUS
201          Q(K)=QUEST(M,K)
205        6 CONTINUE
207          CALL LINEGEN(UGH,NAC,NAC1,JOY,P,Q)
213          DO 8 K=1,LDIST
216          Y(K)=0.0
217          XNUM=THE+DTHE+K-1
224          Y(K)=ZAM(UGH,NAC,XNUM)
231        8 IF(Y(K).LT.0.0) Y(K)=0.0
241          GO TO 52
241       40 DOG1=1.0/YUM
243          DOG2=1.0/WUM
245          SAME=0.0
```

```
246             DO 41 K=1,40
247             XNUM=THE+DTHE+(1-K)
254             YK=AC*EXP(-(DOG1**2)*(XNUM-ATHE)**2)
263             IF(YK,LT.AC*0.01) GO TO 42
267             MCOUNT=MCOUNT+1
270          41 CONTINUE
272          42 DO 44 K=1,70
274             XNUM=XNUM+1
277             Y(K)=AC*EXP(-(DOG1**2)*(XNUM-ATHE)**2)
306             IF(Y(K).LT.SAME) GO TO 43
312             SAME=Y(K)
313             GO TO 44
313          43 Y(K)=AC*EXP(-(DOG2**2)*(XNUM-ATHE)**2)
323             IF(Y(K).LT.0.01*AC) GO TO 45
330          44 CONTINUE
332          45 LDIST=K
334             GO TO 52
334          46 SLOPER=AC/WUM
336             SLOPEL=AC/YUM
340             BL=AC-SLOPEL*ATHE
342             BR=AC+SLOPER*ATHE
344             DO 47 K=1,LDIST
346             XNUM=THE+DTHE+(K-1)
353             Y(K)=SLOPEL*XNUM+BL
356             IF(K.GT.NYUM) Y(K)=-SLOPER*XNUM+BR
364             IF(Y(K).GT.AC) Y(K)=AC
371          47 IF(Y(K).LT.0.0) Y(K)=0.0
377             GO TO 52
377          48 Q(1)=0.0
400             Q(2)=AB(M)
402             Q(3)=0.0
403             P(2)=ATHE
404             P(1)=ATHE-YUM
406             P(3)=ATHE+YUM
407             CALL LINEGEN(G,3,4,3,P,Q)
413             P(1)=ATHE-WUM
415             P(3)=ATHE+WUM
417             CALL LINEGEN(F,3,4,3,P,Q)
423             DO 49 K=1,LDIST
426             XNUM=THE+DTHE+(K-1)
433             Y(K)=ZAM(G,3,XNUM)
440             IF(K.GT.NYUM) Y(K)=ZAM(F,3,XNUM)
451          49 IF(Y(K).LT.0.0) Y(K)=0.0
457             GO TO 52
457          50 DO 51 K=1,LDIST
461          51 Y(K)=AC
465          52 CONTINUE
465             TOTAL=0.0
466             DO 10 K=1,LDIST
```

```
470          10 TOTAL=TOTAL+Y(K)
474             ADJUST=AREA(M)/TOTAL
477             DO 11 K=1,LDIST
500          11 Y(K)=Y(K)*ADJUST*XMULT
506             LIM1=1
507             LIM2=0
510             NWIDTH=THETA*10.0
512             IF(NWIDTH.LT.1) NWIDTH=1
515             NO=LDIST+NWIDTH-1
517             J=ABS(Z-DT+DL+THETA-YLU)*10.0-MCOUNT+2
532             DO 14 L=1,NO
533             IF(L.GT.NWIDTH) LIM1=LIM1+1
537             LIM2=LIM2+1
541             IF(LIM2.GT.LDIST) LIM2=LDIST
544             DO 13 K=LIM1,LIM2
546          13 SUM(M,J)=SUM(M,J)+Y(K)
555             J=J+1
557          14 CONTINUE
561          16 CONTINUE
561             RUT=RUT-0.05
563          17 CONTINUE
566             TOSUM=0.0
567             DO 9 J=1,KIMP
570           9 TOSUM=TOSUM+SUM(M,J)
576             ADJ=AREA(M)/TOSUM
601             DO 12 J=1,KIMP
602          12 SUM(M,J)=SUM(M,J)*ADJ
610          19 CONTINUE
613             LOVE1=LOVE+1
614             DO 20 K=1,KIMP
616             SUM(LOVE1,K)=0.0
621             DO 20 I=1,LOVE
622          20 SUM(LOVE1,K)=SUM(LOVE1,K)+SUM(I,K)
635             IF(ALPHA.EQ.1.0) GO TO 25
637             YK=0.0
640             DO 21 K=1,KIMP
642             XK=SUM(LOVE1,K)
645             IF(XK.GT.YK) YK=XK
650          21 CONTINUE
653             FACTOR=YK/100.0
655          25 CONTINUE
655             NOX=(Z+1.0)*10.0
661             DO 35 M=1,KIMP
662             MORE=NOX+M
664             IF(MORE.GT.161) MORE=161
667             DO 36 K=1,LOVE
671          36 VSA(K,MORE)=VSA(K,MORE)+SUM(K,M)/FACTOR
703             VS(MORE)=VS(MORE)+SUM(LOVE1,M)/FACTOR
710          35 CONTINUE
```

```
712             RETURN
713             END


                SUBROUTINE LINEGEN(S,NA,NA1,JA,X,Y)
 11             DIMENSION X(JA),Y(JA),S(NA)
 11             COMMON/NEED/ A(10,11)
 11             DO 3 I=1,NA
 12             DO 2 J=1,NA
 13             BNUM=0.0
 14             DO 1 K=1,JA
 16             BNUM=BNUM+X(K)**(I+J-2)
 25           1 CONTINUE
 27             A(I,J)=BNUM
 33           2 CONTINUE
 35           3 CONTINUE
 37             DO 5 L=1,NA
 40             CNUM=0.0
 41             DO 4 K=1,JA
 43             CNUM=CNUM+Y(K)*X(K)**(L-1)
 54           4 CONTINUE
 56             A(L,NA1)=CNUM
 61           5 CONTINUE
 63             CALL GAUSS(S,NA,NA1)
 64             RETURN
 65             END


                SUBROUTINE GAUSS (X,N,NP1)
  6             DIMENSION X(N)
  6             COMMON/NEED/ A(10,11)
  6             NM1=N-1
 10             DO 4 K=1,NM1
 11             KP1=K+1
 13             L=K
 14             DO 1 I=KP1,N
 16           1 IF(ABS(A(I,K)).GT.ABS(A(L,K))) L=I
 33             IF(L.EQ.K) GO TO 3
 35             DO 2 J=K,NP1
 36             TEMP=A(K,J)
 41             A(K,J)=A(L,J)
 46           2 A(L,J)=TEMP
 53           3 DO 4 I=KP1,N
 55             FACTOR=A(I,K)/A(K,K)
 62             DO 4 J=KP1,NP1
 64           4 A(I,J)=A(I,J)-FACTOR*A(K,J)
103             X(N)=A(N,NP1)/A(N,N)
111             I=NM1
112           5 IP1=I+1
```

```
114             SUM=0.0
115             DO 6 J=IP1,N
117           6 SUM=SUM+A(I,J)*X(J)
131             X(I)=(A(I,NP1)-SUM)/A(I,I)
140             I=I-1
141             IF(I.GE.1) GO TO 5
143             RETURN
143             END


                SUBROUTINE SEARCH(X,Y,J,IO)
  7             DIMENSION X(J),Y(J),S(10),XSUM(10)
  7             RSUM=1.0E100
 10             LOVE=6
 11             DO 3 N=2,LOVE
 13             NA=N
 13             NA1=NA+1
 15             NAM1=NA-1
 16             CALL LINEGEN(S,NA,NA1,J,X,Y)
 23             SUM=0.0
 24             DO 2 I=1,J
 30             YC=0.0
 31             XA=X(I)
 33             YC=ZAM(S,NA,XA)
 36             YE=Y(I)
 42             YA=YB-YC
 44             SUM=SUM+YA**2
 46           2 CONTINUE
 50             XSUM(NA)=SUM
 52             IF(XSUM(NA).LT.RSUM) RSUM=XSUM(NA)
 55           3 CONTINUE
 60             DO 4 I=2,LOVE
 61           4 IF(RSUM.EQ.XSUM(I)) GO TO 5
 66           5 IO=I-1
 70             RETURN
 70             END


                FUNCTION ZAM(S,N,T)
  6             DIMENSION S(N)
  6             YC=0.0
  7             DO 1 J=1,N
 10           1 YC=YC+S(J)*T**(J-1)
 22             ZAM=YC
 23             RETURN
 23             END
```

Appendix B. Continuous Particle Electrophoresis Computer Program

```
                PROGRAM PHORESE(INPUT,OUTPUT,PLOT,TAPE99=PLOT)
  3             DIMENSION DIS(85),ABC(8)
  3             DIMENSION W(50),Z(50),B(3),C(3),P(3)
  3             DIMENSION FM(400),D(400)
  3             DIMENSION US(630),VS(630),VSA(630)
  3             COMMON/VEL/ DISTAL(10),DISTAR(10),DISTAT(10)
  3             COMMON/SUB/UMEAN(10),UVARL(10),UVARR(10),AB(10),AREA(10)
               1,IDIST(10)
  3             COMMON/VAR/XLU,YLU,RU,RA,CEN,WIDTH,FLOW,INJECT,IPRINT
  3             COMMON/SET/T1,T2,ALPHA,XDATA
  3             COMMON/TAB/ QUEST(10,50),IORDER(10),JC(10)
  3             COMMON/ZVAL/ ZA,KIMP
  3             COMMON/PLT/ PTS(11,300)
  3             COMMON//S1(10),S2(10),NA,NB,RATIO1,DIELECN,REVISN
  3             COMMON/DRAW/ SHAPE(10,85),R(85),IMP
  3             DATA WORD1,WORD2,WORD3/9H GAUSSIAN,9H TRIANGLE,9HPARABOL
               1IC/
  3             DATA WORD4,WORD5/9H   SQUARE,9H   RANDOM/
  3             READ 100,JA,NA
 13             READ 101,(W(I),I=1,JA)
 26             READ 101,(Z(I),I=1,JA)
 41             NA1=NA+1
 43             CALL LINEGEN(S1,NA,NA1,JA,W,Z)
 47             READ 100,JB,NB
 57             READ 101,(W(I),I=1,JB)
 72             READ 101,(Z(I),I=1,JB)
105             NB1=NB+1
107             CALL LINEGEN(S2,NB,NB1,JB,W,Z)
113             READ 111,(ABC(I),I=1,8)
121             READ 102,XLU,XWU,HLEN,FLOW
135             READ 102,YLU,RU,RA,CEN,WIDTH,IPRINT,INJECT
157             READ 102,UOSRU,UOSFU,T1,T2,EU
175             READ 104,LOVE,JAX,LAX,XDATA
211             DO 1 I=1,LOVE
213             READ 102,UMEAN(I),UVARR(I),AB(I),AREA(I),IDIST(I)
232           1 CONTINUE
235             PRINT 120
240             PRINT 111,ABC
246             PRINT 110
252             PRINT 108
256             VO=FLOW/(XWU*XLU)*2.25/60.0
262             YST=YLU*10.0-1.0
265             C(1)=1.0E-15
266             C(2)=XLU/2.0
270             C(3)=XLU
271             B(1)=0.0
272             B(2)=VO
```

```
273           B(3)=0.0
274           CALL LINEGEN(P,3,4,3,C,B)
300           DO 3 I=1,LOVE
302           UEMAX=UMEAN(I)+UVARR(I)
304           UE=UMEAN(I)-UVARL(I)
306           IF(IDIST(I).EQ.1) WORD=WORD1
312           IF(IDIST(I).EQ.2) WORD=WORD2
316           IF(IDIST(I).EQ.3) WORD=WORD3
322           IF(IDIST(I).EQ.4) WORD=WORD4
326           IORDER(I)=0
330           IF(IDIST(I).NE.5) GO TO 4
332           WORD=WORD5
333           READ 100,JC(I)
341           K=JC(I)
343           READ 101,(W(J),J=1,K)
356           READ 101,(Z(J),J=1,K)
371           DO 2 J=1,K
373         2 QUEST(I,J)=Z(J)
402           CALL SEARCH (W,Z,K,IO)
405           IORDER(I)=IO
407         4 CONTINUE
407           PRINT 109,I,UEMAX,UE,UMEAN(I),AREA(I),WORD,IORDER(I)
431           DISTAT(I)=0.0
433           DISTAL(I)=0.0
434           DISTAR(I)=0.0
436         3 CONTINUE
440           DIELEC1=ZAM(S1,NA,T1)
443           DIELECN=ZAM(S1,NA,298.0)
446           REVIS1=ZAM(S2,NB,T1)
451           REVISN=ZAM(S2,NB,298.0)
454           RATIO1=(DIELEC1*REVISN)/(DIELECN*REVIS1)
457           WIDTH=WIDTH*0.075
461           PRINT 110
464           PRINT 114,UOSRU,UOSFU
474           PRINT 115,T1,T2
504           PRINT 110
510           PRINT 119,XLU,XWU,HLEN
522           PRINT 116,FLOW
530           PRINT 117,RA
536           PRINT 118,CEN
544           PRINT 120
550           DO 5 N=1,628
552           US(N)=YST+(N-1)/30.0
557           VSA(N)=0.0
561         5 VS(N)=0.0
564           ALPHA=0.0
565           READ 122,NUM
573           READ 123,(FM(I),I=1,NUM
606           DO 7 I=1,NUM
610         7 D(I)=YST+I*0.0549868421
```

```
616           D(NUM+1)=YST
620           D(NUM+2)=4.0
622           FM(NUM+1)=0.0
623           FM(NUM+2)=2.5
625           US(629)=YST
627           US(630)=4.0
630           VS(629)=0.0
631           VS(630)=2.5
632           VSA(629)=0.0
633           VSA(630)=2.5
634           IF(IPRINT.EQ.0) GO TO 17
635           CALL NAMPLT
636           IF(IPRINT.EQ.2) GO TO 17
640           CALL FACTOR(1.1)
642           CALL AXIS1(1.5,1.5,16H  RELATIVE CONC.,16,4.0,90.0,0.0,
             12.5,20.0)
653           CALL AXIS1(1.5,1.5,13HDISTANCE (MM),-13,5.5,0.0,YST,4.0
             1,20.0)
664           CALL SYMBOL(1.65,0.75,0.125,46HTHEORETICAL BAND SHAPE A
             1ND DISPLACEMENT IN CPE,0.0,46)
670           CALL PLOT(1.5,1.5,-3)
673         17 CONTINUE
673           DO 10 KO=1,JAX
675           IF(KO.EQ.1) GO TO 11
677           H=HLEN
700           READ 107,EU,NPLT
710           DO 8 L=1,LOVE
712           DISTAT(L)=H*EU/VELOC(P,H,EU,UMEAN(L),UOSRU,UOSFU,VO,YLU)
726           DISTAL(L)=H*EU/VELOC(P,H,EU,UMEAN(L)-UVARL(L),UOSRU,UOSF
             1U,VO,YLU)
743           DISTAR(L)=H*EU/VELOC(P,H,EU,UMEAN(L)+UVARR(L),UOSRU,UOSF
             1U,VO,YLU)
760           8 CONTINUE
762         11 CONTINUE
762           CALL ACTUAL(UOSRU,UOSFU,LOVE)
765           ALPHA=ALPHA+1.0
767           IF(IPRINT.EQ.0.OR.IPRINT.EQ.2) GO TO 18
776           IF(IPRINT.EQ.1.AND.NPLT.EQ.0) GO TO 18
1004          R(IMP+1)=-0.75
1006          R(IMP+2)=4.0
1010          DIS(IMP+1)=YST
1012          DIS(IMP+2)=4.0
1013          CALL PLOT(0.0,4.5,-3)
1016          DO 28 I=1,LOVE
1020          DO 29 J=1,IMP
1021        29 DIS(J)=SHAPE(I,J)
1030          CALL LINE(DIS,R,IMP,1,0,0)
1034          CALL PLOT(0.0,0.0,3)
1037        28 CONTINUE
1042          CALL PLOT(0.0,-4.5,-3)
```

```
1044      18 CONTINUE
1044         PRINT 110
1050         PRINT112,EU
1056         CALL CONCENT (UOSRU,UOSFU,LOVE)
1061         IF(IPRINT.EQ.0) GO TO 10
1062         IF(IPRINT.EQ.1.AND.NPLT.EQ.0) GO TO 10
1070         IF(ALPHA.GT.1.0) GO TO 22
1073         YK=0.0
1073         LOVE1=LOVE+1
1075         DO 21 K=1,KIMP
1077         XK=PTS(LOVE1,K)
1103         IF(XK.GT.YK) YK=XK
1106      21 CONTINUE
1111         FACTER=YK/10.0
1113      22 CONTINUE
1113         IF(ALPHA.NE.2.0) GO TO 23
1115         FTNEW=0.0
1116         DO 34 M=1,LOVE
1120      34 FTNEW=FTNEW+AREA(M)/100.0
1125         WHOA=0.2/RA
1127         IF(INJECT.NE.2) GO TO 16
1131         WHOA=0.2/WIDTH*0.075
1133      16 CONTINUE
1133         FACTER=FACTER/FTNEW/WHOA
1136      23 CONTINUE
1136         NOX=(ZA-YST)*30.0
1142         IF(IPRINT.EQ.2) GO TO 19
1144         DO 36 K=1,LOVE
1145         DO 32 M=1,KIMP
1146         MORE=NOX+M
1150         IF(MORE.GT.628) MORE=628
1153         VSA(MORE)=PTS(K,M)/FACTER
1161      32 CONTINUE
1163         VSA(MORE+1)=0.0
1164         VSA(MORE+2)=2.5
1166         TEMP1=US(MORE+1)
1170         TEMP2=US(MORE+2)
1171         US(MORE+1)=YST
1173         US(MORE+2)=4.0
1175         CALL LINE(US,VSA,MORE,1,0,0,)
1201         CALL PLOT(0.0,0.0,3)
1204         US(MORE+1)=TEMP1
1206         US(MORE+2)=TEMP2
1210         KIMP2=KIMP+2
1212         DO 31 M=1,KIMP2
1214         MORE=NOX+M
1216      31 VSA(MORE)=0.0
1222      36 CONTINUE
1224      19 CONTINUE
1224         DO 35 M=1,KIMP
```

```
1226          MORE=NOX+M
1230          IF(MORE.GT.628) MORE=628
1233          VS(MORE)=VS(MORE)+PTS(LOVE1,M)/FACTER
1242       35 CONTINUE
1244       10 CONTINUE
1247          IF(IPRINT.EQ.0) GO TO 42
1250          SUM=0.0
1251          DO 12 N=1,628
1252       12 SUM=VS(N)*0.03333333333+SUM
1256          SUMA=0.0
1257          DO 13 N=1,NUM
1261       13 SUMA=SUMA+FM(N)*0.0549868421
1266          DO 14 N=1,NUM
1270       14 FM(N)=FM(N)*SUM/SUMA
1276          IF(IPRINT.EQ.2) GO TO 15
1300          CALL PLOT(0.0,4.5,3)
1302          CALL PLOT(5.5,4.5,2)
1305          CALL PLOT(5.5,4.875,3)
1310          CALL PLOT(0.0,4.875,2)
1313          CALL SYMBOL(1.5,5.0,0.125,19HBAND CROSS-SECTIONS,0.0,19)
1317          CALL LINE(US,VS,628,1,0,0)
1323          CALL PLOT(10.0,-1.5,-3)
1326       15 CONTINUE
1326          IF(IPRINT.EQ.1) GO TO 6
1330          CALL FACTOR(0.9)
1332          CALL PLOT(0.0,-0.5,-3)
1335          CALL AXIS1(1.5,1.5,13HLIGHT DENSITY,13,4.0,90.0,0.0,2.5
             1,20.0)
1346          CALL AXIS1(1.5,1.5,13HDISTANCE (MM),-13,5.5,0.0,YST,4.0
             1,20.0)
1357          CALL SYMBOL(1.35,0.65,0.125,54HLIGHT DENSITY SCAN AND T
             1HEORETICAL DISPLACEMENT ON CPE,0.0,54)
1363          CALL PLOT(1.5,1.5,-3)
1366          CALL LINE(D,FM,NUM,1,0,0)
1372          CALL PLOT(-1.5,-1.5,-3)
1375          CALL AXIS1(1.5,6.25,17HTHEORETICAL CONC.,17,4.0,90.0,0.
             10,2.5,20.0)
1406          CALL AXIS1(1.5,6.25,13HDISTANCE (MM),-13,5.5,0.0,YST,4.
             10,20.0)
1417          CALL PLOT(1.5,6.25,-3)
1422          CALL LINE(US,VS,628,1,0,0)
1426          CALL PLOT(10.0,-6.25,-3)
1431        6 CONTINUE
1431          CALL ENDPLT
1432       42 CONTINUE
1432      100 FORMAT(2I2)
1432      101 FORMAT(8E10.0)
1432      102 FORMAT(5(F8.3),2(I2))
1432      104 FORMAT(3I5,E5.0)
1432      107 FORMAT(E5.0,4X,I1)
```

```
1432      108 FORMAT(19X,4HLEAD,3X,5HTRAIL,4X,4HPEAK,4X,4HAREA,6X,5HS
             1HAPE,3X,5HORDER,/)
1432      109 FORMAT(1X,*PARTICLE NO.*,I2,4(F8.3),2X,A9,6X,I2)
1432      110 FORMAT(//)
1432      111 FORMAT(8A10)
1432      112 FORMAT(5X,21HPOTENTIAL GRADIENT = ,F5.1,*VOLTS/CM*)
1432      113 FORMAT(5X,*LOWER*)
1432      114 FORMAT(5X,*UOS FRONT WALL =*,F6.2,*MICRON CM/VOLT SEC*,
             1/,5X,*UOS REAR WALL =*,F6.2,*MICRON CM/VOLT SEC*)
1432      115 FORMAT(5X,*WALL TEMPERATURE =*,F7.1,* DEGREES K*,/,5X,*
             1CENTER TEMPERATURE =*,F7.1,* DEGREES K*)
1432      116 FORMAT(5X,*CURTAIN FLOW RATE =*,F5.1,* CC?MIN*)
1432      117 FORMAT(5X,*SAMPLE INJECTION RATIO =*,F5.3)
1432      118 FORMAT(5X,*DEPTH OF CENTER STREAM = *,F5.3)
1432      119 FORMAT(5X,*CURTAIN WIDTH =*,F6.2,* CM*,/,5X,*CURTAIN TH
             1ICKNESS =*,F5.2,* CM*,/,5X,*ELECTRODE LENGTH =*,F5.1,*
             2CM*)
1432      120 FORMAT(1X,/,*XXXXXXXXXXXXXXXXXXXXXXXXXXXXXXXXXXXXXXXXX
             1XXXXXXXXXXXXXXXXXXXXXXXXXXX*,/)
1432      122 FORMAT(5I3)
1432      123 FORMAT(20E4.0)
1432          CALL EXIT
1432          END



          SUBROUTINE ACTUAL(UOSR,UOSF,LOVE)
        6 DIMENSION DF(10,41),DR(10,41),DTF(3)
        6 COMMON/VEL/ DISTAL(10),DISTAR(10),DISTAT(10)
        6 COMMON/SUB/UMEAN(10),UVARL(10),UVARR(10),AB(10),AREA(10
          1),IDIST(10)
        6 COMMON/VAR/XLU,YLU,RU,CEN,WIDTH,FLOW,INJECT,IPRINT
        6 COMMON/SET/T1,T2,ALPHA,XDATA
        6 COMMON/ZVAL/Z,KIMP
        6 COMMON//S1(10),S2(10),NA,NB,RATIO1,DIELECN,REVISN
        6 COMMON/DRAW/SHAPE(10,85),R(85),IMP
        6 FIN=1.0E10
        7 RUT=RU
       11 KIMP=0
       12 IMAX=2.0*RUT/0.05*XDATA+1.5
       17 RUM=0.0
       20 DISTAN=DISTAT(1)
       21 DO 4 K=1,3
       23 IF(K.EQ.1) RUM=CEN+RA
       27 IF(K.EQ.2) RUM=CEN
       33 IF(K.EQ.3) RUM=CEN-RA
       37 T3=T2-(T2-T1)*ABS(RUM)**2
       45 DIELEC3=ZAM(S1,NA,T3)
       51 REVIS3=ZAM(S2,NB,T3)
       54 RATIO3=(DIELEC3*REVISN)/(DIELECN*REVIS3)
       57 POSIT=1.0-ABD(RUM)**2
```

```
 62          IF(INJECT.EQ.2) GO TO 1
 66          WIDTH=SQRT(ABS(RA**2-ABS(RUM-CEN)**2))*0.075
 77        1 CONTINUE
 77          DTFIN=DISTAN*(0.5*RATIO1*(UOSR/(1-ABS(RUM))+UOSF/(1+ABS
            1(RUM))+(UMEAN(1)-UVARL(1))*RATIO3/POSIT-0.75*RATIO1*(UO
            2SF+UOSR))*.0001-WIDTH
127          IF(DTFIN.LT.FIN) FIN=DTFIN
132        4 CONTINUE
134          SCALE=YLU+FIN-0.02
137          ISCALE=SCALE*100.0
141          XSCALE=ISCALE
142          Z=XSCALE/10.0
144          J=0
145          DO 32 I=1,IMAX
146          IF(RUT.GT.CEN+RA+0.01) GO TO 29
154          IF(RUT.LT.CEN-RA-0.01) GO TO 29
157          J=J+1
160          T3=T2-(T2-T1)*ABS(RUT)**2
166          DIELEC3=ZAM(S1,NA,T3)
172          REVIS3=ZAM(S2,NB,T3)
175          IF(INJECT.EQ.2) GO TO 20
201          WIDTH=SQRT(ABS(RA**2-ABS(RUT-CEN)**2))*0.075
212       20 CONTINUE
212          RATIO3=(DIELEC3*REVISN)/(DIELECN*REVIS3)
216          POSIT=1.0-ABS(RUT)**2
221          DO 28 M=1,LOVE
224          UOSIN=RATIO1*(0.5*(UOSR/(1.0-RUT)+UOSF/(1.0+RUT))-0.75*
            1(UOSF+UOSR))
237          DF(M,I)=DISTAR(M)*((UMEAN(M)+UVARR(M))*RATIO3/POSIT+UOS
            1IN)*0.0001+WIDTH+YLU
253          DR(M,I)=DISTAL(M)*((UMEAN(M)-UVARL(M))*RATIO3/POSIT+UOS
            1IN)*0.0001-WIDTH+YLU
267          K1=(DF(M,I)-Z/10.0)*300.0+6.0
277          IF(K1.GT.KIMP) KIMP=K1
302          SHAPE(M,J)=DF(M,I)*10.0
311          IM=4.0*RA/0.05+3.5-J
317          R(J)=RUT*0.75
321          R(IM)=RUT*0.75
323          SHAPE(M,IM)=DR(M,I)*10.0
331       28 CONTINUE
333       29 CONTINUE
333          RUT=RUT-0.05/XDATA
336       32 CONTINUE
341          IMP=4.0*RA/0.05+3.5
345          DO 5 M=1,LOVE
346        5 SHAPE(M,IMP)=SHAPE(M,1)
355          R(IMP)=R(1)
357          RETURN
357          END
```

```
      SUBROUTINE CONCENT(UOSR,UOSF,LOVE)
    6 DIMENSION P(50),Q(50),UGH(20),G(3),F(3)
    6 DIMENSION Y(250)
    6 COMMON/VEL/ DISTAL(10),DISTAR(10),DISTAT(10)
    6 COMMON/SUB/UMEAN(10),UVARL(10),UVARR(10),AB(10),AREA(10
     1),IDIST(10)
    6 COMMON/VAR/XLU,YLU,RU,RA,CEN,WIDTH,FLOW,INFECT,IPRINT
    6 COMMON/SET/T1,T2,ALPHA,XDATA
    6 COMMON/TAB/QUEST(10,50),IORDER(10),JC(10)
    6 COMMON/PLT/SUM(11,300)
    6 COMMON//S1,(10),S2,(10),NA,NB,RATIO1,DIELECN,REVISN
    6 COMMON/ZVAL/Z,KIMP
    6 IMAX=2.0*RU/0.025*XDATA+1.5
   13 DO 19 M=1,LOVE
   14 DO 1 J=1,KIMP
   15 1 SUM(M,J)=0.0
   23 RUT=RU
   25 DO 17 I=1,IMAX
   26 IF(RUT.GT.CEN+RA+0.01) GO TO 16
   34 IF(RUT.LT.CEN-RA-0.01) GO TO 16
   37 T3=T2-(T2-T1)*ABS(RUT)**2
   44 DIELEC3=ZAM(S1,NA,T3)
   50 REVIS3=ZAM(S1,NB,T3)
   53 RATIO3=(DIELEC3*REVISN)/(DIELECN*REVIS3)
   56 IF(INJECT.EQ.2) GO TO 2
   62 WIDTH=SQRT(ABS(RA**2-ABS(RUT-CEN)**2))*0.075
   73 2 CONTINUE
   73 POSIT=1.0-ABS(RUT)**2
   76 UOSIN=RATIO1*(0.5*(UOSR/(1.0-RUT)+UOSF/(1.0+RUT))-0.75*
     1(UOSF+UOSR))
  112 DT=DISTAT(M)*(UOSIN+UMEAN(M)*RATIO3/POSIT)*0.0001
  120 DL=DISTAL(M)*(UOSIN+(UMEAN(M)-UVARL(M))*RATIO3/POSIT)*0
     1.0001
  126 DR=DISTAR(M)*(UOSIN+(UMEAN(M)+UVARR(M))*RATIO3/POSIT)*0
     1.0001
  135 ATHE=DT*300.0
  137 THE=DL*300.0-1.0
  141 LTHE=THE
  142 XTHE=LTHE
  143 DTHE=1.0-(THE_XTHE)
  146 YUM=(DT-DL)*300.0+1.0
  151 WUM=(DR-DT)*300.0+1.0
  154 NYUM=YUM-DTHE
  156 DIST=ABS(DR-DL)*300.0+2.0
  163 LDIST=DIST
  164 IF(LDIST.LT.1) LDIST=1
  167 AC=AB(M)
  171 MCOUNT=0
  172 IF(ALPHA.EQ.1.0) GO TO 50
  174 KTEL=IDIST(M)
  175 GO TO (40,46,48,50,7) KTEL
```

```
205       7 NAC=IORDER(M)+1
210         NAC1=NAC+1
211         THE=DT*300.0
213         LTHE=THE
214         XTHE=LTHE
215         DTHE=1.0-(THE-XTHE)
220         JOY=JC(M)
222         PLUS=DIST/(JOY-1)
226         DO 6 K=1,JOY
227         P(K)=THE+(K-1)*PLUS
234         Q(K)=QUEST(M,K)
240       6 CONTINUE
242         CALL LINEGEN(UGH,NAC,NAC1,JOY,P,Q)
246         DO 8 K=1,LDIST
252         Y(K)=0.0
253         XNUM= THE+DTHE+K-1
260         Y(K)=ZAM(UGH,NAC,XNUM)
265       8 IF(Y(K).LT.0.0) Y(K)=0.0
275         GO TO 52
275      40 DOG1=1.0/YUM
277         DOG2=1.0/WUM
301         SAME=0.0
302         DO 41 K=1,40
303         XNUM=THE+DTHE+(1-K)
310         YK=AC*EXP(-(DOG1**2)*(XNUM-ATHE)**2)
317         IF(YK.LT.AC*0.01) GO TO 42
323         MCOUNT=MCOUNT+1
325      41 CONTINUE
327      42 DO 44 K=1,70
331         XNUM=XNUM+1
334         Y(K)=AC*EXP(-(DOG1**2)*(XNUM-ATHE)**2)
343         IF(Y(K).LT.SAME) GO TO 43
347         SAME=Y(K)
350         GO TO 44
351      43 Y(K)=AC*EXP(-(DOG2**2)*(XNUM-ATHE)**2)
361         IF (Y(K).LT.0.01*AC) GO TO 45
366      44 CONTINUE
370      45 LDIST=K
372         GO TO 52
372      46 SLOPER=AC/WUM
374         SLOPEL=AC/YUM
376         BL=AC-SLOPEL*ATHE
400         BR=AC+SLOPER*ATHE
402         DO 47 K=1,LDIST
404         XNUM=THE+DTHE+(K-1)
411         Y(K)=SLOPEL*XNUM+BL
414         IF(K.GT.NYUM) Y(K)=-SLOPER*XNUM+BR
422         IF(Y(K).GT.AC) Y(K)=AC
427      47 IF(Y(K).LT.0.0) Y(K)=0.0
435         GO TO 52
```

```
435      48 Q(1)=0.0
436         Q(2)=AB(M)
440         Q(3)=0.0
441         P(2)=ATHE
442         P(1)=ATHE-YUM
444         P(3)=ATHE+YUM
445         CALL LINEGEN(G,3,4,3,P,Q)
451         P(1)=ATHE-WUM
453         P(3)=ATHE+WUM
455         CALL LINEGEN(F,3,4,3,P,Q)
461         DO 49 K=1,LDIST
465         XNUM=THE+DTHE+(K-1)
472         Y(K)=ZAM(G,3,XNUM)
477         IF(K.GT.NYUM) Y(K)=ZAM(F,3,XNUM)
512      49 IF(Y(K).LT.0.0) Y(K)=0.0
520         GO TO 52
520      50 DO 51 K=1,LDIST
522      51 Y(K)=AC
526      52 CONTINUE
526         TOTAL=0.0
527         DO 10 K=1,LDIST
531      10 TOTAL=TOTAL+Y(K)
535         ADJUST=AREA(M)/TOTAL
540         DO 11 K=1,LDIST
541      11 Y(K)=Y(K)*ADJUST
546         LIM1=1
547         LIM2=0
550         NWIDTH=2.0*WIDTH*300.0
553         IF(NWIDTH.LT.1) NWIDTH=1
556         NO=LDIST+NWIDTH-1
560         J=ABS(Z/10.0-DL+WIDTH-YLU)*300.0-MCOUNT+1
573         DO 14 L=1,NO
574         IF(L.GT.NWIDTH) LIM1=LIM1+1
600         LIM2=LIM2+1
602         IF(LIM2.GT.LDIST) LIM2=LDIST
605         DO 13 K=LIM1,LIM2
607      13 SUM(M,J)=SUM(M,J)+Y(K)
617         J=J+1
621      14 CONTINUE
623      16 CONTINUE
623         RUT=RUT-0.025/XDATA
626      17 CONTINUE
631         TOSUM=0.0
632         DO 9 J=1,KIMP
633       9 TOSUM=TOSUM+SUM(M,J)
642         ADJ=AREA(M)/TOSUM
645         DO 12 J=1,KIMP
646      12 SUM(M.J)=SUM(M,J)*ADJ
655      19 CONTINUE
660         LOVE1=LOVE+1
661         DO 20 K=1,KIMP
```

```
663          SUM(LOVE1,K)=0.0
667          DO 20 I=1,LOVE
670       20 SUM(LOVE1,K)=SUM(LOVE1,K)+SUM(I,K)
704          IF(ALPHA.EQ.1.0) GO TO 21
706          CALL RESOLVE(LOVE)
710       21 CONTINUE
710          RETURN
711          END



             SUBROUTINE RESOLVE(LOVE)
  3          COMMON/PLT/ SUM(11,300)
  3          COMMON/ZVAL/ ZA,KIMP
  3          DIMENSION TAREA(10),NAM(10),NEM(10),NOM(10),OVLPA(10),O
            1VLPB(10),PERPU(10)
  3          DO 1 I=1,LOVE
  5          TAREA(I)=0.0
  6          ITOG=0
  7          DO 3 J=1,KIMP
 11          TAREA(I)=TAREA(I)+SUM(I,J)
 16          IF(ITOG.GE.1) GO TO 2
 20          IF(SUM(I,J).GT.0.0) ITOG=1
 26          NAM(I)=J
 30          GO TO 4
 30        2 CONTINUE
 30          IF(SUM(I,J).NE.0.0) NOM(I)=J
 36        4 CONTINUE
 36        3 CONTINUE
 41          LIMA=NAM(I)
 43          LIMB=NOM(I)
 44          VALUE=0.0
 45          DO 5 J=LIMA,LIMB
 47        5 IF(SUM(I,J).GT.VALUE) VALUE=SUM(I,J)
 62          NO=0
 63          DO 6 J=LIMA,LIMB
 65          IF(SUM(I,J).NE.VALUE) GO TO 6
 71          NEM(I)=J
 72          NO=NO+1
 74        6 CONTINUE
 77          NU=NO/2
100          NEM(I)=NEM(I)-NU
102          IF(2*NU.NE.NO) GO TO 1
104          IF(IABS(NEM(I)-NAM(I)).LT.IABS(NEM(I)-NOM(I))) NEM(I)=N
            1EM(I)+1
113        1 CONTINUE
116          DO7 I=2,LOVE
117          TIT=0.0
120          TAT=0.0
121          IF(NAM(I).GT.NOM(I-1)) GO TO 9
124          LIMA=NAM(I)
```

```
125         LIMB=NOM(I-1)
126         DO 8 J=LIMA,LIMB
130         TIT=TIT+SUM(I-1,J)
135       8 TAT=TAT+SUM(I,J)
143       9 CONTINUE
143         OVLPA(I-1)=TIT/TAREA(I-1)*100.0
147         OVLPB(I)=TAT/TAREA(I)*100.0
152       7 CONTINUE
154         OVLPA(LOVE)=0.0
155         OVLPB(1)=0.0
156         DO 10 I=1,LOVE
157         PERPU(I)=100.0-OVLPA(I)-OVLPB(I)
163      10 IF(PERPU(I).LT.0.0) PERPU(I)=0.0
170         PRINT 100
174         PRINT 101
200         DO 11 I=1,LOVE
203         XNAM=ZA+(NAM(I)-1)/30.0
211         XNEM=ZA+(NEM(I)-1)/30.0
216         XNOM=ZA+(NOM(I)-1)/30.0
223         SPAN=ABS(XNAM-XNOM)
225         IF(I.EQ.LOVE) GO TO 12
227         XNOT=IABS(NEM(I)-NEM(I+1))/30.0
234         PRINT 102,I,XNAM,XNEM,XNOM,SPAN,PERPU(I),OVLPB(I),OVLPA
           1(I),XNOT
261       12 CONTINUE
261         IF(I.NE.LOVE) GO TO 13
264         PRINT 102,I,XNAM,XNEM,XNOM,SPAN,PERPU(I),OVLPB(I),OVLPA
           1(I)
307       13 CONTINUE
307       11 CONTINUE
313         PRINT 103
316      100 FORMAT(//,50X,*BAND RESOLUTION PARAMETERS*,//)
316      101 FORMAT(4X,*PARTICLE*,7X,*TRAIL*,24X,*LEAD*,22X,*PERCENT
           1*,7X,*OVERLAP*,7X,*OVERLAP*,5X,*PEAK TO PEAK*,/,5X,*NUM
           2BER*,9X,*EDGE*,10X,*PEAK*,10X,*EDGE*,10,*SPAN*,10X,*PUR
           3E*,10X,*LEFT*,9X,*RIGHT*,8X,*DISTANCE*,/)
316      102 FORMAT(7X,I2,2X,4(7X,F7.3),3(8X,F6.2),/,116X,F7.3)
316      103 FORMAT(/////)
316         RETURN
317         END



            FUNCTION VELOC (P,H,E,UMEAN,UOSR,UOSF,VO,YLU)
13          DIMENSION P(3)
13          V=VO*0.8
15        1 DT=(H*E/V)*(UMEAN-0.25*(UOSR+UOSF))*0.0001+YLU
24          VAV=(P(1)*(DT-YLU)+P(2)/2.0*(DT**2-YLU**2)+P(3)/3.0*(DT
           1**3-YLU**3))/(DT-YLU)
44          IF(ABS(VAV-V)/V).LT.0.001) GO TO 2
51          V=VAV
```

```
52          GO TO 1
53        2 VELOC=VAV
55          RETURN
55          END
```

Bibliography

1. Krumrine, P. H., M.S. Thesis, Lehigh University, (1976).

2. Strickler, A. and Sacks, T., Annals of the New York Academy of Sciences, 209, pp. 497-514, (1973).

3. Verwey, E. J. W., and Overbeek, J. Th. G., "Theory of the Stability of Lyophobic Colloids", Elsevier, Amsterdam, (1948).

4. Derjaguin, B. V. and Landau, L., Acta Physicochim. U.S.S.R., 14, p. 633, (1941).

5. Derjaguin, B. V., Transactions of the Faraday Society, 36, p. 203, (1940).

6. Wiersema, P. H., Thesis, University of Utrecht, (1964).

7. Wiersema, P. H., Loeb, A. L., and Overbeek, J. Th. G., Journal of Colloid and Interface Science, 22, p. 78, (1966).

8. McKannan, E. C., Krupnick, A. C., Griffin, R. N., and McCreight, L. R., "Electrophoresis Separations in Space -- Apollo 14", NASA Technical Memorandum TMX-64611, (1971).

9. Micale, F. J., and Vanderhoff, J. W., "Electrophoresis Analysis for Apollo 16", Progress Report, Contract NAS8-28654, (1972).

10. Snyder, R. S., Bier, M., Griffin, R. N., Johson, A. J., Leidheiser, H., Micale, F. J., Vanderhoff, J. W., Ross, S., van Oss, C. J., Separation and Purification Methods, 2(2), pp. 259-282, (1973).

11. Vanderhoff, J. W., and Micale, F. J., "Electrophoresis Experiment for Space", Final Report, Contract NAS8-28654, April (1976).

12. Knox, R. J., "Electrophoretic Characterization of Aldehyde-Fixed Red Blood Cells, Kidney Cells, Lymphocytes,and Chamber Coatings", Report No. NASA CR-2755, October (1976).

13. Vanderhoff, J. W., Micale, F. J., and Krumrine, P. H., Separation and Purification Methods, 6(1), pp. 61-87, (1977).

14. Hannig, K., Wirth, U. H., "Electrophoresis Experiment-EPE-MAO-14 Within the Apollo Soyuz Test Project (ASTP)", October (1975).

15. Hannig, K., Z. Anal. Chem., 181, pp. 244-254, (1961).

16. Hannig, K., Hoppe-Seyler's Z. Physiol. Chem., 388, pp. 211-227, (1964).

17. Hannig, K., Wirth, H., Meyer, B. H., and Zeiller, K., Hoppe-Seyler's Z. Physiol. Chem., Bd. 356, pp. 1209-1223, August (1975).

18. Zeiller, K., Losër, R., Pascher, G., and Hannig, K., Hoppe-Seyler's Z. Physiol. Chem., Bd. 356, pp. 1225-1244, August (1975).

19. Strickler, A., Kaplan, A., and Vigh, E., Microchemical Journal, Vol. 10, No. 1-4, pp. 529-544, January (1966).

20. Strickler, A., Sacks, T., Preparative Biochemistry, 3(3), pp. 269-277, (1973).

21. McCann, G. D., Vanderhoff, J. W., Strickler, A., and Sacks, T., Separation and Purification Methods, 2(1), pp. 153-198, (1973).

22. Strickler, A., Separation Science, 2, p. 335, (1967).

23. Micale, F. J., Krumrine, P. H., and Vanderhoff, J. W., Colloid and Interface Science, Vol. IV, pp. 247-258, (1976).

24. Saville, D. H., and Ostrach, S., "Fluid Mechanics of Continuous Flow Electrophoresis -- Final Report", Contract No. NAS-8-31349 Code 361, April (1978).

25. Seaman, G. V. F., University of Oregon Health Sciences Center, personal correspondence, July 1977.

26. Ahmed, S., El-Aasser, M. S., Poehlein, G. W., Pauli, G.H., and Vanderhoff, J. W., Journal of Colloid and Interface Science, to be published.

27. Oshima, H., Colloid and Polymer Science, Vol. 253, No. 2, pp. 158-163, (1975).

28. Hamaker, H. C., Physica, 4, p. 1058, (1937).

29. Fowkes, F. M., Lehigh University, personal communication.

30. Mie, G., Ann. Physik, 25, p. 377, (1908).

VITA

Paul Henry Krumrine III was born on November 28, 1951 in Hanover, Penna. to Paul and Evelyn Krumrine Jr. He attended the Littlestown School System for twelve years, from which he graduated in 1969, as the Salutarian. He also received the A. G. Ealy Award for scholarship and football abilities.

In September of 1969, he entered Lehigh University in Bethlehem, Penna. Majoring in Chemical Engineering, he received a Bachelor of Science degree in 1973. In the fall of that year he again returned to Lehigh University as a research assistant working on a grant from NASA, concerned with various forms of electrophoresis. In 1976, Mr. Krumrine received a Master of Science degree in Chemical Engineering, followed by a Doctor of Philosophy degree in October of 1978.

From this work two publications have been written entitled "Electrophoretic Mobility Measurements by Continuous Particle Electrophoresis" and "Low-Electroosmotic-Mobility Coatings for ASTP Free-Fluid Electrophoretic Separations". Another paper entitled "Analysis of the ASTP Electrophoretic Separations in Space" has been presented, and two more papers entitled "Applicability of DLVO Theory to the Formation of Ordered Arrays of Monodisperse Latex Particles" and "Latex Particle Interactions in Electrophoretic Separations" are being prepared.